

CONFERENCES AND SYMPOSIA

PACS numbers: **03.75. – b**, 03.75.Hh, 05.30.Jp, **07.07. – a**, **32.30. – r**, 32.30.Jc, **33.20. – t**, **36.40. – c**, **37.20. + j**, 42.82.Cr, **61.43. – j**, **63.20. – e**, **63.50. – x**, 67.25.dw, 71.35.Lk, **71.36. + c**, **78.30. – j**, **78.47. – p**, **78.55. – m**, **81.07. – b**, 87.85.fk, **87.64. – t**, 95.30.Ky, **97.10. – q**

On the 40th anniversary of the Institute of Spectroscopy of the Russian Academy of Sciences

(Scientific session of the Physical Sciences Division of the Russian Academy of Sciences, 8 October 2008)

V I Balykin; A N Ryabtsev, S S Churilov; Yu E Lozovik; E A Vinogradov, B N Mavrin, N N Novikova, V A Yakovlev; B S Dumesh, A V Potapov, L A Surin; A V Naumov, Yu G Vainer; O N Kompanets, Yu M Yevdokimov

DOI: 10.3367/UFNe.0179.200903h.0297

A scientific session of the Physical Sciences Division of the Russian Academy of Sciences dedicated to the 40th anniversary of the Institute of Spectroscopy, RAS (ISAN) was held at ISAN on 8 October 2008. The following reports were presented at the session:

(1) **Balykin V I** (ISAN) "Atom optics and nanotechnology";

(2) **Ryabtsev A N, Churilov S S** (ISAN) "Spectroscopy of ionized atoms for astrophysics and nanotechnology";

(3) **Lozovik Yu E** (ISAN) "Strong correlations and new phases in a system of excitons and polaritons. A polariton laser";

(4) **Vinogradov E A, Mavrin B N, Novikova N N, Yakovlev V A** (ISAN) "Inverted optical phonons in ion-covalent crystals";

(5) **Mal'shukov A G** (ISAN) "Spin transport in semiconductor microstructures";

(6) **Dumesh B S, Potapov A V, Surin L A** (ISAN) "Spectroscopy of small helium clusters and 'nanoscopic' superfluidity: $He_N - CO$, $N = 2 - 20$...";

(7) **Naumov A V, Vainer Yu G** (ISAN) "Single molecules as spectral nanoprobes for the diagnostics of dynamic processes in solid media";

(8) **Kompanets O N** (ISAN), **Yevdokimov Yu M** (Engelhardt Institute of Molecular Biology, RAS) "Optical biosensors of genotoxicants based on DNA nanoconstructions and portable dichrometer."

A brief presentation of these reports, with the exception of report 5, is given below.

Uspekhi Fizicheskikh Nauk **178** (3) 297 – 334 (2009)
DOI: 10.3367/UFNr.0179.200903h.0297
Translated by K A Ragozin, V I Kisin, E N Gorin; edited by A M Semikhatov

PACS numbers: **03.75. – b**, **37.20. + j**, **81.07. – b**
DOI: 10.3367/UFNe.0179.200903i.0297

Atom optics and nanotechnology

V I Balykin

1. Introduction

Atom optics (along with electron, ion, and neutron optics) is the optics of material particles and deals with the problems of forming ensembles and beams of neutral atoms and of controlling them, as well as with application issues. Atom optics became a discipline in its own right in the mid-1980s as an outcome of research on the interaction of laser radiation pressure forces with atoms executing translational motion. Despite its weakness in the case of ordinary light sources, the effect of light pressure was experimentally discovered by P Lebedev in Russia back in the late 19th century and was later confirmed by E Nichols and G Hull in the USA. The experimental proof that momentum is transferred from a photon to a free atom is credited to Frisch (1933), who observed the deflection of an atomic sodium beam under irradiation.

The advent of lasers provided researchers with a fundamentally new light source possessing a high spectral brightness, monochromaticity, and a high radiation directionality. When laser radiation came into use, light pressure ceased to be a barely observable effect and became an efficient means of influencing atomic motion. The progress in atom optics [1 – 3] is closely related to the development of laser cooling and neutral atom localization techniques [4 – 8]. The laser cooling of atoms and their spatial localization enable forming atomic ensembles and beams with desired parameters. Laser cooling allows decreasing the atomic temperature to only a millionth of a degree above absolute zero. At such temperatures, the de Broglie wavelength becomes comparable to the wavelength of light and the wave properties of atoms show up markedly. The localization of neutral atoms opens up the opportunity to operate both with single atoms localized to nanometer-scale precision [9, 10] and with macroscopic ensembles of cold atoms having a high phase density [11].

Laser methods of neutral atom cooling, which allowed a substantial increase of the de Broglie wavelength, gave birth to atom wave optics [12]. Using different configurations of laser light fields and mechanical micro- and nanostructures (zone plates, multislit stops, etc.), it has been possible to make coherent atomic beamsplitters, atom interferometers, waveguides, and, lastly, an analogue of the optical laser — the atom laser.

The potentials of atom optics are much broader than the potentials of the optics of other types of material particles (electrons and neutrons) due to the internal structure of atoms. For a temperature close to absolute zero, when the de Broglie wavelength becomes comparable to the interatomic distance, the behavior of an atomic ensemble becomes appreciably dependent on an internal quantum atomic characteristic, spin.

A striking difference between the behavior of fermions and bosons is observed at very low temperatures. In 1924, Bose and Einstein predicted the effect of condensation for Bose particles, known as the Bose–Einstein condensation. Atoms in a Bose–Einstein condensate (BEC) make up a new type of 'coherent matter.' The first atomic condensates were obtained by several groups of American physicists by laser and evaporative cooling techniques in 1995 [11]. A magnetic trap that retains BEC atoms is an analogue of the optical resonator for photons in an optical laser. The atoms may be 'released' from the magnetic trap in a certain direction and, like photons passing through a semitransparent mirror of the optical laser resonator, form a coherent directional beam similar to a laser beam. This device is referred to as an atom laser.

The keen interest in atom lasers stems from the prospect of harnessing coherent atomic beams in precision measuring instruments and sophisticated technologies in the preparation of atomic and molecular micro- and nanostructures [9, 10].

2. Methods of constructing the elements of atom optics

Although similar mathematical foundations underlie atom and light optics, their 'technical means' are different. Producing the tools of light optics relies on the techniques of grinding and polishing the surfaces of different reflective and transparent materials of the desired shape. In atom optics, the principal technical means are electromagnetic fields. The use of diverse configurations of laser light fields, static electric and magnetic fields, and material structures, including micro- and nanostructures, has enabled constructing the basic elements of atom optics that are analogous to the elements of conventional optics: atom lenses, mirrors, deflectors and modulators of atomic beams, coherent atomic beamsplitters, atom interferometers, and waveguides.

2.1 Material structures

In his classic monograph [13], Ramsey considered the specular reflection and diffraction of a molecular beam from the surface of a solid. For the specular reflection to occur, the following two conditions must be satisfied.

(1) The projection of the average height of surface irregularities on the molecular beam direction must be shorter than the de Broglie wavelength of the molecules. If δ is the average height of surface irregularities and φ is the grazing angle of beam incidence, this requirement can be expressed as

$$\delta \sin \varphi < \lambda_{\mathrm{dB}} . \qquad (1)$$

(2) The average on-surface residence time for molecules must be short. In this case, the quantum state of the reflected molecule is the same as for the incident one. The irregularities of mechanically well-polished surfaces are typically of the order of 10^{-5} cm, while the de Broglie wavelength of a hydrogen molecule at the temperature 300 K is of the order of 10^{-8} cm. Consequently, in accordance with inequality (1), the angle for the specular reflection to occur is $\varphi < 10^{-3}$ rad.

More than 50 year ago, Knauer and Stern [14] observed a 5% reflection of a hydrogen molecular beam from polished bronze for the grazing incidence angle $\varphi = 10^{-3}$ rad. Crystal cleavage surfaces are much smoother. Thermal vibrations of a crystal lattice limit the surface smoothness at the level of 10^{-8} cm. In this case, an atomic beam experiences specular reflection at the incidence angles $20^\circ - 30^\circ$. This was borne out in experiments [15] with He atoms and an LiF crystal. The temperature dependence of the specular reflection angle exhibits a strongly pronounced feature, which indicates a passage from the specular reflection of atoms to the diffuse one and testifies to the effect of thermal vibrations on the smoothness of the crystal surface. Experiments on the reflection of atoms from the surface of a condensed medium continue to attract the attention of researchers. We mention experiments involving the reflection of ^{4}He atoms from the surface of liquid ^{4}He [16] and of thermal Cs atoms from a polished glass surface [17].

The first experiment involving the observation of atomic diffraction by a crystal cleavage surface, which operated like a two-dimensional plane lattice, was performed by Stern [18]; a comprehensive investigation of this effect was set forth in Ref. [19]. Atomic diffraction by an artificial periodic structure (grooves in a membrane) with a much longer grating period was observed in Ref. [20].

The effect of the quantum reflection of ^{4}He and ^{3}He atomic beams from the surface of liquid helium in a vacuum was validly employed to focus atoms using a curved surface [21] and to focus He atoms using a zone plate [22].

Atom interferometry based on microstructures was realized in two elegant devices: Young's two-slit atom interferometer [23] and Michelson's atom interferometer [24].

2.2 Static electric and magnetic fields

Some elements of atom and molecule optics reliant on the interaction of spatially nonuniform magnetic and electric fields with the magnetic or electric dipole moments of particles have long been known and profitably used in experimental physics [13].

In the presence of a magnetic or electric field, an atom or a molecule shifts, with the displacement depending on the initial quantum state of the particle and the field magnitude (the Zeeman and Stark effects). In the adiabatic approximation (the fields change little in space and time, while the particles move relatively slowly), the internal state of the particles follows variations in the field strength or, to state it in different terms, the particles reside in the same quantum sublevel, whose energy W depends on the field strength.

In the adiabatic approximation, the center-of-mass motion of a neutral particle of mass M obeys the Schrödinger

equation for the wave function $\Psi(\mathbf{r}, t)$:

$$i\hbar \frac{\partial \Psi_i(\mathbf{r}, t)}{\partial t} = \left(-\frac{\hbar^2}{2M} \nabla^2 + W_i(\mathbf{r}) \right) \Psi_i(\mathbf{r}, t) , \quad (2)$$

where $W_i(\mathbf{r}, t)$ is the internal energy of the particle in the quantum state i at a point $\mathbf{r}$, which depends on the electric $\mathbf{E}(\mathbf{r})$ or magnetic $\mathbf{H}(\mathbf{r})$ field strength.

Magnetic interaction. For an atom or a molecule with a permanent magnetic moment $\boldsymbol{\mu}$ in an external magnetic field $\mathbf{H}$, the effective potential energy W is expressed as

$$W = -\boldsymbol{\mu}\mathbf{H} = -\mu_{\text{eff}} H , \quad (3)$$

where μ_{eff} is the projection of $\boldsymbol{\mu}$ in the $\mathbf{H}$ direction. The force F acting on the atom or molecule with a potential energy W is

$$\mathbf{F} = -\nabla W = -\frac{\partial W}{\partial H} \nabla H = \mu_{\text{eff}} \Delta H . \quad (4)$$

It follows from relations (2)–(4) that a particle in a nonuniform magnetic field experiences a force aligned with the field strength gradient.

The authors of Refs [25–28] proposed the idea of using a nonuniform magnetic field to focus the beams of molecules emitted from a source at different angles.

The focusing properties of magnetic lenses depend on the magnetic sublevels of an atom. This was used by Ramsey and his collaborators to make the hydrogen maser [29]. Hydrogen atoms residing in the state $F = 1$, $M = 0$ were focused on a small opening in the wall of a storage bottle and were accumulated in it, while the atoms in the ground state $F = 0$ were defocused.

Electric interaction. Because the energy of atoms or molecules in an electric field depends on the field strength, by analogy with expressions (3) and (4), an atom (a molecule) may be regarded as having the effective dipole moment

$$\mu_{\text{eff}} = -\frac{dW}{dE} . \quad (5)$$

The force acting on the atom (the molecule) in a nonuniform electric field is defined by an expression similar to (4):

$$\mathbf{F} = \mu_{\text{eff}} \nabla E = \mu_{\text{eff}} \frac{\partial E}{\partial z} , \quad (6)$$

where the direction of the field strength gradient is chosen to coincide with the z axis.

Paul and his collaborators [30] developed fields for focusing a beam of polar molecules. Townes, Basov, and Prokhorov resorted to the electric focusing of a beam of molecules residing in a specific (excited) state to make the NH_3 maser [31, 32].

Hexapolar electric fields have not only the focusing property but also selectivity relative to the quantum state of a molecule (μ_{eff} depends on the molecule quantum numbers J, K, and M). This property was validly used in experiments in molecular dynamics with the beam of molecules in a certain quantum state, including experiments on the orientation of molecules.

2.3 Laser fields

Atoms and molecules without a static magnetic or electric dipole moment cannot change their mechanical trajectory in a static magnetic or electric field. However, an atom embedded in a quasiresonance laser field has a high-frequency polarizability and, when the laser field strength is spatially nonuniform, the atom experiences a gradient (dipole) force [33]. For instance, the gradient force in a standing laser wave [34] may give rise to the channeling of atoms in their motion at small angles to the wavefront [35, 36] or even to their trapping by a three-dimensional standing light wave (which received the name 'optical lattice') [37, 38].

The gradient force was profitably used by Ashkin and his collaborators for focusing an atomic beam [39] and controlling the motion of microparticles [40].

Controlling atoms by light fields is underlain by the recoil effect. In the optical domain of the spectrum, the recoil effect experienced by an atom in the emission or absorption of light is quite small. High-intensity laser radiation tuned to resonance with some allowed dipole transition of the atom may give rise to the reemission of one million photons per second and may therefore have a significant effect on the velocity and trajectory of atomic motion. Hänsch and Schawlow [41] proposed the use of the resonance force arising from the spontaneous reradiation of photons, much like it was suggested for cooling ions in an electromagnetic trap [42].

Since that time, a new avenue in the development of atom physics has emerged reliant on the effects of resonance laser light–atom interaction with the use of the wealth of well-known effects of atomic physics: recoil, Doppler, Stark, Zeeman, and Raman scattering (RS) effects. This new avenue has led to the elaboration of highly efficient methods of laser cooling and the trapping of atoms (Fig. 1), which laid the groundwork for the formation of atom optics and the physics of degenerate quantum gases (BEC, Fermi-degenerate gases, etc.), as well for the making of the main tools of atom optics — atom lasers, atom interferometers, etc.

Gradient and spontaneous forces underlie numerous experiments in controlling atomic motion by means of light. Elements for which the laser cooling of atomic beams has been carried out are marked by circles in the periodic table shown in Fig. 2.

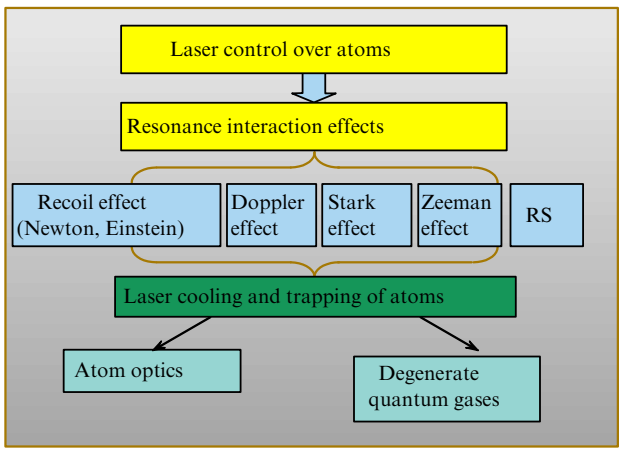

Figure 1. Diagrammatic illustration of the role played by the effects of atomic physics (recoil, Doppler, Stark, Zeeman, and Raman scattering effects) in the development of methods of laser cooling and trapping atoms and of atom optics.

3. Atom-optical nanotechnology

Atom optics holds good promise to make a contribution to nanotechnology, specifically to the investigation and fabrication of nanostructures. Neutral atoms, which are manipu-

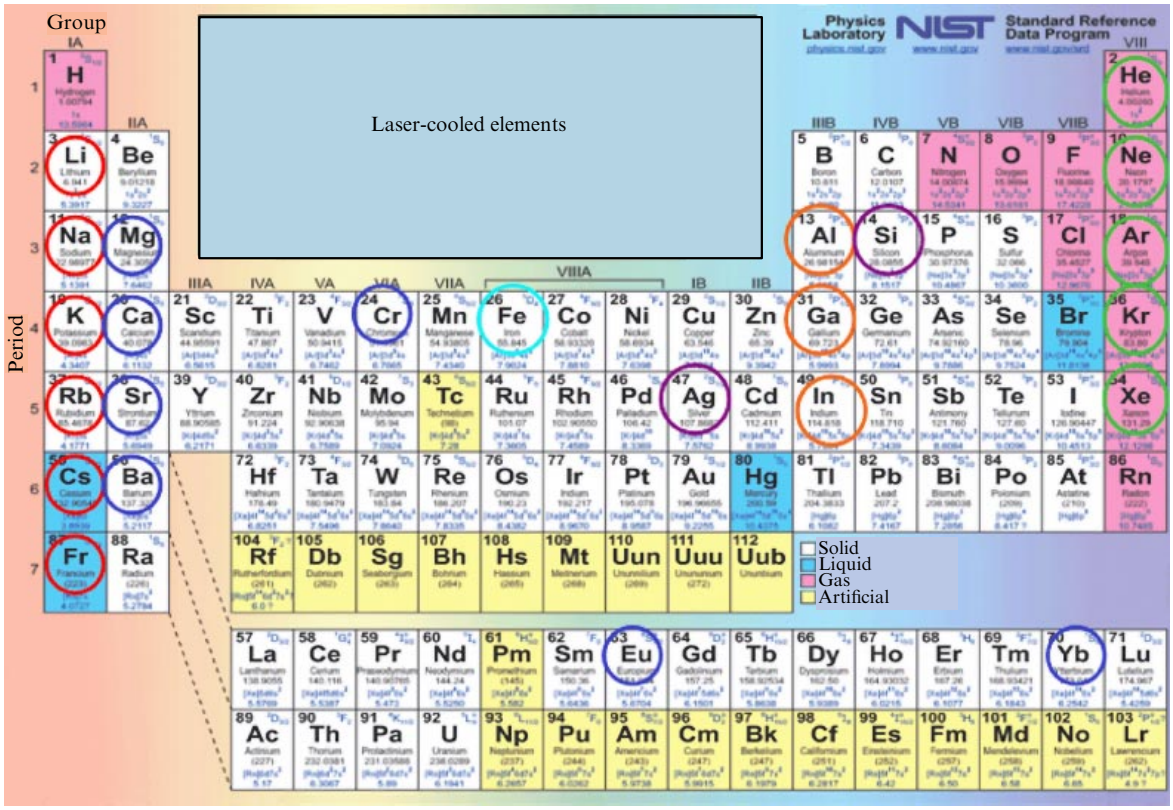

Figure 2. Elements (marked by circles) of the periodic table for which laser cooling of atomic beams has been carried out.

lated by means of different techniques of atom optics, offer certain advantages over other particles (ions or photons). First, neutral atoms have a short de Broglie wavelength λ_{dB} in comparison with photon wavelengths. Second, neutral atoms do not experience the Coulomb repulsion. Third, the methods of laser-assisted atom cooling enable controlling the longitudinal and transverse atomic velocities, collimating atomic beams, and increasing their phase density. (The latter signifies that the Helmholtz – Lagrange law and Liouville's theorem on the conservation of phase space volume, which substantially limits the capabilities of photon and ion optics, do not apply to atom optics.) All this permits controlling the parameters of atomic beams with the help of laser light, which is important in designing atomic and molecular nanostructures by the methods of atom optics.

The methods of atom optics are of special interest for nanolithography, which is referred to as atom-optical nanolithography. Nanolithography is quite often associated with the attainment of a high transistor number density on a chip, described by Moore's law (1965). Recent years have seen the successful advancement of optical lithography techniques using extreme vacuum ultraviolet (VUV) radiation and of lithographic techniques using electron and ion beams and X-ray radiation. These techniques permit producing nanostructures with a resolution of several nanometers. Meanwhile, extensive search for alternative lithographic techniques is underway. The following techniques are known today: (i) scanning nanoprobe, (ii) imprinting, and (iii) 'self-assembling' of nanostructures. The atom-optical methods discussed below should be considered from the standpoint of the search for the nanolithography techniques of the future.

Atom-optical lithography is represented by two main techniques: (i) direct deposition of atoms on a surface; (ii) lithography with the aid of excited (metastable) atoms and chemically active atoms (alkaline metals). Nanofabrication on a surface was realized in one-dimensional (1D) and two-dimensional (2D) versions in the form of regular and more complex structures. Demonstration experiments have been carried out for many atoms (metastable rare-gas atoms, nonmagnetic and magnetic atoms).

In what follows, we briefly consider the main achievements made in this area over the last 10 – 15 years, i.e., since the first successful experiments [43, 44]. This area in the development of nanotechnology is recognized to be quite promising, as is evidenced by the publication of numerous reviews [10, 45 – 49].

3.1 Direct deposition nanolithography

The direct deposition of laser-focused atomic beams was clearly demonstrated in experiments with a grid of 'photon lenses' in the form of standing waves [43 – 48, 50, 59]. This configuration of the light field permits obtaining a large number of periodically arranged nanostructures. Basically, many atoms having the corresponding quantum transitions may be used for atomic nanofabrication. The laser cooling of atoms may be effected due to cyclic quantum transitions, allowing the atoms to spontaneously reradiate the absorbed photons many times. Furthermore, the quantum transitions should have a wavelength at which available continuous-wave (CW) lasers operate.

A typical experimental layout suitable for many atoms is shown in Fig. 3. Even after passing through collimating apertures, the divergence of an atomic beam emerging from a thermal source is too high to attain a nanometer-scale resolution. In this case, the main feature of atom optics is first used: the capability of decreasing the transverse velocity

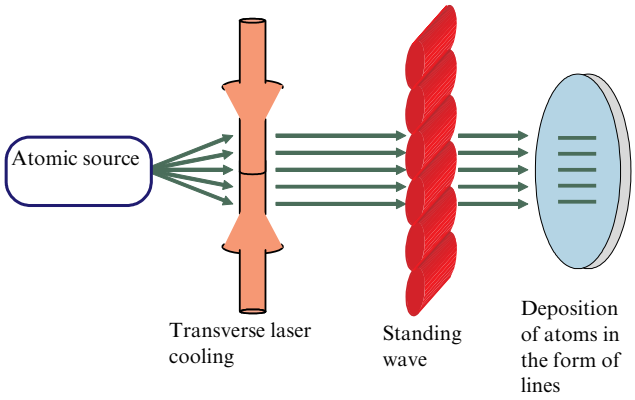

Figure 3. Direct-write nanolithography scheme. Two laser beams are used for the transverse cooling of an atomic beam. A standing light wave forms cylindrical photon lenses for focusing the atoms. The atoms are deposited on a surface to form parallel lines due to their focusing in the standing wave nodes, thereby forming a periodic nanostructure grating.

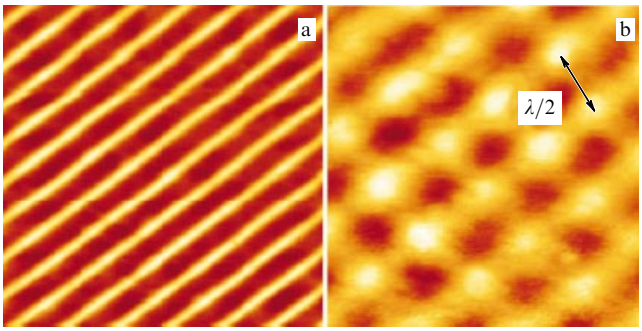

Figure 4. Images of chromium nanostructures fabricated by focusing with one-dimensional (a) and two-dimensional (b) photon lenses. The period of chromium lines and points is equal to $\lambda/2 - 213$ nm. The images were obtained with the aid of atomic force microscopy [52].

(temperature) of atoms by their transverse cooling (collimation), which was first demonstrated for an atomic sodium beam [51]. The barrier inherent in light optics due to the Helmholtz–Lagrange law is thus overcome in atom optics. The highly collimated atomic beam next passes through a high-intensity standing wave, whose frequency is shifted by several hundred MHz to the blue side of the spectrum relative to the atomic resonance frequency, with the result that the gradient force draws the atoms to the nodes of the standing wave, i.e. to the region where the potential energy of atoms in the light field is minimal. For atoms with a magnetic structure ($J \neq 0$), it is necessary to control the population of magnetic sublevels and afford the population of the state $|M| = J$ by optical pumping with circularly polarized light.

The first experiment following the scheme in Fig. 3 was performed with sodium atoms [43], which were deposited in the form of a grating of nanolines on a silicon substrate. The grating period was $\lambda/2 = 294.5$ nm, where λ is the wavelength of a dye laser tuned to the $3\,^2S_{1/2}$ $(F = 2)$–$3\,^3P_{3/2}$ $(F = 3)$ transition of the D_2 line (589 nm) of Na having the saturation intensity 6.3 mW cm^{-2} and the natural linewidth 10 MHz. The resultant gratings, which are unstable in the air, were studied in a vacuum also with the aid of light. The grating was initially recorded using the diffraction of shorter-wavelength laser radiation from this grating and then by scanning tunnel microscopy. The gratings of atomic Cs nanolines were produced similarly [50, 59].

It was not long before even more convincing experiments were performed Cr atoms [44, 52]. The advantage of using Cr atoms is that the Cr nanostructures fabricated in a vacuum survive in the air due to the formation of a very thin oxide film on them (about 1 nm in thickness). This permits investigating such nanostructures in the air with the help of an atomic force microscope. The experiments in Refs [44, 52], used transverse cooling of the atomic beam with the longitudinal temperature 1550–1650 °C by polarization gradient cooling [53, 54], which enabled obtaining a collimated beam with a divergence of only 0.1 mrad. Figure 4a shows images of chromium nanostructures in the form of lines. The halfwidth of the chromium nanolines was equal to 50 nm, and the height (22 nm in Fig. 4a) depended on the exposure time (several tens of minutes). The resultant background is, in particular, due to Cr isotopes that were out of resonance with the laser radiation. By using two mutually orthogonal standing waves, it was possible to fabricate a 2D grating of 'photon microlenses' and fabricate a two-dimensional nanostructure on the surface (Fig. 4b) [52, 55]. The same technique was used to obtain nanostructures with the minimal dimension of only 15 nm [56].

These pioneering experiments provided the foundation for subsequent experiments with other light field configurations, atoms, and substrates.

A standing light wave is perfectly suited for fabricating 1D periodic structures (line gratings) and 2D periodic structures (gratings of points). By varying the wavelength, it is possible to control the grating period ($\lambda/2$). By varying the polarization in the standing wave (for instance, by using two counterpropagating waves with orthogonal linear polarizations), it is possible to obtain the period $\lambda/8$ [54]. Owing to the complex interaction of all magnetic sublevels of ground-state Cr atoms with the light polarized this way, the optical potential varies in space with the period $\lambda/8 = 53.2$ nm. However, this simultaneously decreases the modulation depth of the resultant array of atomic nanolines.

The interference of three laser beams intersecting at an angle of 120° can also be used. In this case, the two-dimensional picture has a hexagonal symmetry, which may be additionally controlled by varying the detuning Δ of the field frequency relative to the atomic resonance frequency, drawing atoms to either the nodes ($\Delta > 0$) or the antinodes ($\Delta < 0$) of the interference pattern [57]. In another experiment, a decagonal quasiperiodic structure of ^{52}Cr atoms with the surface area 0.2×0.2 mm was fabricated with the aid of five laser beams intersecting at 72° [58].

The complexity of structures depends on the configuration of the light field produced by the superposition of many laser beams. Complex configurations may be obtained by holographic reconstruction of the light field [59]. The use of holographic techniques holds much promise due to the high angular and spectral selectivity of the holographic 'mirror.' In particular, one hologram may retain holographic images for two different wavelengths, which conceptually permits producing the field for two different atoms in one experimental setup with different configurations of the light field.

Also important for practical purposes is the fabrication of 3D structures. So far, this field has not been adequately developed. However, 3D structure formation has been successfully demonstrated using a combination of Cr atoms and MgF_2 material [52]. In the experiment reported in Ref. [52], the atoms of ^{52}Cr experienced resonance interac-

tion with a standing light wave, which permitted a laterally modulated density of MgF_2 doped with Cr atoms, while MgF_2 was deposited without experiencing an appreciable influence from laser radiation (large detuning of the laser frequency). It is believed that using combinations of atoms of groups III and IV with laser fields at the corresponding two resonance frequencies will allow fabricating laterally modulated heterostructures, which is of interest in constructing metamaterials.

A beam of magnetic Fe atoms became the next experimental subject, and a more difficult one at that [60, 61]. Shorter wavelength radiation ($\lambda = 372$ nm) is required to effect resonance excitation in this case. Furthermore, laser cooling is more difficult to realize because the Fe atom does not have a perfectly closed cyclic transition. An excited Fe atom returns to a metastable state instead of the initial state with the probability 1/243 and moves out of resonance with the radiation. Nevertheless, it was possible to fabricate the gratings of 50-nm-wide nanolines with the regular period 186 nm [62] in these experiments. Such highly regular ferromagnetic nanogratings may be used in experiments in spintronics and with nanomagnets. The use of shorter wavelength lasers will enable the pursuance of nanofabrication experiments with other magnetic atoms, ^{58}Ni (323.4 nm) and ^{59}Co (240.5 nm).

Successful experiments were carried out with atoms of rare-earth element Yb [63]. The prospects of experiments with the potentially important atoms ^{27}Al (309.4 nm), ^{69}Ga (294.4 nm), and ^{115,113}In (325.7 nm), which necessitate CW lasers in the poorly mastered UV range, were considered in [64].

For nanofabrication purposes, only several simple configurations, such as a standing light wave, and their combinations have been used so far, and hence there is much room for future research.

3.2 Nanolithography of a resist

Conventional lithographic techniques involve a resist (a thin film on a substrate), in particular, a photoresist sensitive to UV or VUV radiation. The same method may be used for nanolithography with a light mask (see Fig. 3). The light mask produces a spatially nonuniform distribution of excited (metastable) or chemically active atoms, which modify the resist. The subsequent etching of the exposed resist is performed by standard lithographic techniques. Suited for this approach to nanofabrication are substrates of any material that lend themselves to etching, including important magnetic materials like Ni and Fe. Nanofabrication techniques involving excited (metastable) rare-gas atoms (He*, Ne*, Ar*) and chemically active atoms of alkaline metals (Na, Cs) were demonstrated.

Metastable rare-gas atoms. The first resist used in nanolithography was a self-organizing monolayer (1.5 nm thick) of dodecanthiol on a gold-coated substrate [54]. The molecules of the highly ordered monolayer make up a hydrophobic surface, which protects the substrate from chemical etching in an aqueous solution. Metastable atoms with a high internal energy (up to 20 eV for He*) or chemically active atoms disrupt the local ordering of the organic molecules, making subsequent local etching possible. This technique, which relies on a light atom-excitation mask, was demonstrated for a standing light wave [55]. Nanostructures of the size 65 nm determined by the wave nature of atoms were obtained in experiments [65].

Instead of the local disruption of a self-organizing molecular resist film, the disruption in the film of background oil molecules deposited on the resist surface by an oil pump in the course of experiments can be used. The spatial structure of local disruption in this background film may be transferred onto the substrate for subsequent etching by the ion beam [64, 66].

Chemically active atoms of alkaline elements. Such atoms can be focused by means of the gradient force of the light field of both continuous and pulsed lasers; due to their high chemical activity, these atoms can modify surfaces on a nanometer scale.

3.3 Atomic nanopen lithography

The transportation of atoms through a hollow fiber waveguide [67] and their focusing in the near field of a nanoaperture [68] are the heart of the idea of an atom-optical 'pen,' which is schematically shown in Fig. 5. A hollow fiber or a screen with a nanoaperture may be translated laterally with a cantilever, which has been validly used for nanofabrication by the direct deposition technique [69]. The laser cooling, collimation, and focusing of an atomic beam may be effected in a tapering (bugle-like) hollow optical waveguide [70]. The use of an atom pen may become a universal way of 'nanowriting' [48, 71], although there are evident limitations on the productivity of this process due to the slow scanning procedure.

Conceptually, nanowriting may also be effected by a spatial scan of the de Broglie atomic wave by laser light. Such an atomic scanner has already been demonstrated in experiment [72].

3.4 Atom pinhole camera

An experimental approach to atom optics based on the idea of constructing images of an object with the aid of a pinhole camera, which is well known in light optics, was first

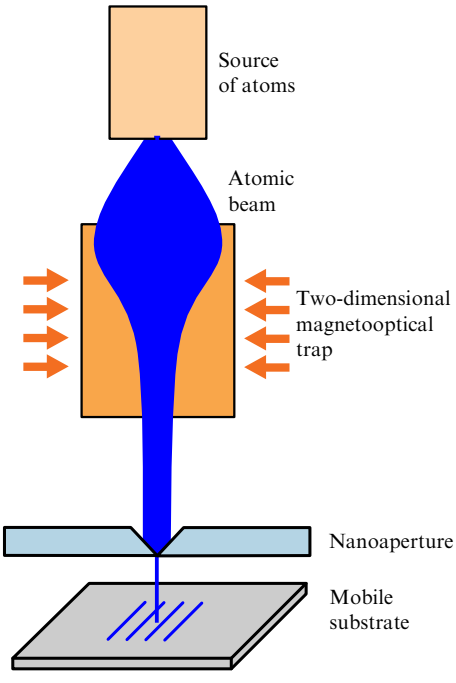

Figure 5. Schematic of an atom-optical pen for 'nanowriting' atomic structures [48, 71].

experimentally realized in Ref. [71]. Pinhole cameras are also used in modern experimental physics when the focusing potential is difficult to organize [73, 74].

A consideration of the optics of an atom pinhole camera shows [71, 75] that the realization of such a camera requires a screen of nanometer thickness with an opening a nanometer in diameter. The layout (Fig. 6a) of the atom pinhole camera comprises an atomic beam, a mask, an opening a nanometer in diameter, and a substrate on which nanostructures are fabricated. The atoms transmitted through the opening in the mask, as in optics, form 'a luminous object' with the desired geometry. The parameters of the atom pinhole camera are selected in such a way as to maximize the camera resolution and to fabricate as large a nanostructure array on the surface as possible, which is achieved by using an array of nanoopenings. It has been shown that the optimal focal distance is $f_{\rm opt} \approx 10-20$ μm when thermal atomic beams with typical de Broglie wavelengths of the order of 10^{-3} nm and an opening 20 nm in diameter are used. These considerations determine the choice of the distance l between the nanoopening and the substrate: $l = f_{\rm opt}$. For a given distance l, the nanoopening–mask distance determines the 'demagnification' of the object of the atom pinhole camera and hence the size of the mask itself.

The above considerations show that the optimal nanoopening–mask distance is in the range $L = 1-10$ cm. In this case, the 'demagnification power' $N = L/l$ of the atom pinhole camera is equal to 10^3-10^4. In this geometry of the atom pinhole camera, the characteristic mask dimensions are in the micrometer range and the characteristic dimensions of the structures fabricated on the surface are in the nanometer range; hence, the atom pinhole camera affords transformation of microworld objects to objects of the nanoworld. Another important implication of the 'dimension geometry' of the atom pinhole camera is the opportunity of using not one nanoopening but a large array of nanoopenings in one device. In this case, each nanoopening produces an image of its own, which does not overlap with the neighboring ones, and it is therefore possible to realize a multiple atom pinhole camera. Such an atom pinhole camera opens up the door to simultaneous fabrication of a large number of identical nanostructures. We note that the aberration of inclined beams does not appreciably limit the resolution of a multiple atom pinhole camera even for a large number of nanoopenings (up to 10^6).

An atom pinhole camera was realized in the geometry considered above and was used to fabricate nanostructures of different metal atoms on the surface of an insulator.

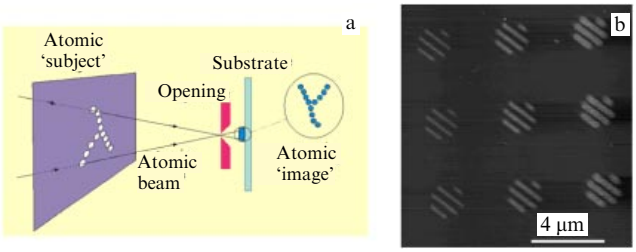

Figure 6. (a) Schematic representation of an atom pinhole camera. (b) Image of In atomic nanostructures on a silicon substrate. The mask was a metal screen with a grating of a series of strips of different widths: 40, 100, and 250 μm. The nanostructures reproduce the mask geometry with a specified demagnification coefficient equal to 3000 [75].

Figure 6b shows the image of the nanostructure of In atoms obtained with an atomic force microscope (from the Veeco Company). The mask was a metal screen with a grating of a series of strips of different widths (40, 100, and 250 μm) made by laser cutting. The distance between the strips in the mask was 1 mm. The nanoopening diameter was $s = 200$ nm. The nanostructures shown in Fig. 6b reproduce the mask geometry with a specified demagnification coefficient equal to 3000. It can be seen from the figure that the strips forming the nanostructure are different in height, because each of the strips is made up of atoms transmitted through mask slits of different widths. This circumstance may be of significance in the fabrication of nanostructures with a complex three-dimensional geometry. The shape of nanostructures is determined by the arrangement of openings in the mask, while the heights of individual nanostructure elements are determined by the diameters of the corresponding openings.

To find the ultimate parameters of the atom pinhole camera, measurements were made in the experiment in Ref. [75] on nanostructure fabrication through varying the nanoopening diameters over a wide range: from 250 to 20 nm. This allowed operating the atom pinhole camera both in the mode of geometrical optics and in the mode of wave optics. In the latter case, the effect of atom diffraction through nanoopenings becomes significant.

4. Summary

We have discussed approaches to nanotechnology based on atom optics techniques. In atom optics, the internal and external degrees of freedom of individual atoms are controlled by laser fields with nanometer accuracy, which allows fabricating structures with nanometer accuracy on a surface.

Acknowledgements. This work was supported in part by the Russian Foundation for Basic Research grants Nos 08-02-00653-a, 08-02-00871-a, and 08-02-12045-ofi.

References

1. Balykin V I, Letokhov V S *Phys. Today* **4** (4) 23 (1989)
2. Balykin V I, Letokhov V S *Usp. Fiz. Nauk* **160** (1) 141 (1990) [*Sov. Phys. Usp.* **33** 79 (1990)]
3. Balykin V I, Letokhov V S *Atom Optics with Laser Light* (Chur: Harwood Acad. Publ., 1995)
4. Balykin V I, Letokhov V S, Minogin V G *Usp. Fiz. Nauk* **147** 117 (1985) [*Sov. Phys. Usp.* **28** 803 (1985)]
5. Minogin V G, Letokhov V S *Davlenie Lazernogo Izlucheniya na Atomy* (Laser Light Pressure on Atoms) (Moscow: Nauka, 1986) [Translated into English (New York: Gordon and Breach Sci. Publ., 1987)]
6. Kazantsev A P, Surdutovich G I, Yakovlev V O *Mekhanicheskoe Deistvie Sveta na Atomy* (Mechanical Action of Light on Atoms) (Moscow: Nauka, 1991)
7. Metcalf H J, van der Straten P *Laser Cooling and Trapping* (New York: Springer, 1999)
8. Balykin V I, Minogin V G, Letokhov V S *Rep. Prog. Phys.* **63** 1429 (2000)
9. Balykin V, Klimov V, Letokhov V *Opt. Photon. News* **16** 33 (2005)
10. Balykin V I, Klimov V V, Letokhov V S, in *Handbook of Theoretical and Computational Nanotechnology* Vol. 7 (Eds M Rieth, W Schommers) (Stevenson Ranch, Calif.: Am. Sci. Publ., 2006) p. 1
11. Cornell E A, Wieman C E *Rev. Mod. Phys.* **74** 875 (2002); Ketterle W *Rev. Mod. Phys.* **74** 1131 (2002)
12. Meystre P *Atom Optics* (New York: AIP Press/Springer, 2001)
13. Ramsey N *Molecular Beams* (Oxford: Clarendon Press, 1956)
14. Knauer F, Stern O *Z. Phys.* **53** 779 (1929)
15. Estermann L, Stern O *Z. Phys.* **61** 95 (1930)

16. Nayak V U, Edwards D O, Masuhara N *Phys. Rev. Lett.* **50** 990 (1983)
17. Anderson A et al. *Phys. Rev. A* **34** 3513 (1986)
18. Stern O *Naturwissenschaften* **17** 391 (1929)
19. Frish R, Stern O *Z. Phys.* **84** 430 (1933)
20. Keith D W et al. *Phys. Rev. Lett.* **61** 1580 (1988)
21. Berkhout J J et al. *Phys. Rev. Lett.* **63** 1689 (1989)
22. Carnal O, Faulstich A, Mlynek J *App. Phys. B* **53** 88 (1991)
23. Carnal O, Mlynek J *Phys. Rev. Lett.* **66** 2689 (1991)
24. Keith D W et al. *Phys. Rev. Lett.* **66** 2693 (1991)
25. Friedburg H, Paul W *Naturwissenschaften* **37** 20 (1950)
26. Friedburg H, Paul W *Naturwissenschaften* **38** 159 (1951)
27. Korsunskii M I, Fogel' Ya M *Zh. Eksp. Teor. Fiz.* **21** 25 (1951); **21** 38 (1951)
28. Vanthier R *C.R. Acad. Sci.* **228** 1113 (1949)
29. Goldenberg H M, Kleppner D, Ramsey N F *Phys. Rev. Lett.* **5** 361 (1960)
30. Bennewitz H G, Paul W, Schlier Ch *Z. Phys.* **141** 6 (1955)
31. Gordon J P, Zeiger H J, Townes C H *Phys. Rev.* **99** 1264 (1955)
32. Basov N G, Prokhorov A M *Zh. Eksp. Teor. Fiz.* **28** 249 (1955) [*Sov. Phys. JETP* **1** 184 (1955)]
33. Askar'yan G A *Zh. Eksp. Teor. Fiz.* **42** 1567 (1962) [*Sov. Phys. JETP* **15** 1088 (1962)]
34. Letokhov V S *Pis'ma Zh. Eksp. Teor. Fiz.* **7** 348 (1968) [*JETP Lett.* **7** 272 (1968)]
35. Salomon C et al. *Phys. Rev. Lett.* **59** 1659 (1987)
36. Balykin V I et al. *Opt. Lett.* **13** 958 (1988)
37. Chu S et al. *Phys. Rev. Lett.* **55** 48 (1985)
38. Meacher D R *Contemp. Phys.* **39** 329 (1998)
39. Bjorkholm J E et al. *Phys. Rev. Lett.* **41** 1361 (1978)
40. Ashkin A, Dziedzic J M *Science* **235** 1517 (1987)
41. Hänsch T W, Schawlow A L *Opt. Commun.* **13** 68 (1975)
42. Wineland D J, Dehmelt H *Bull. Am. Phys. Soc.* **20** 637 (1975)
43. Prentiss M et al. *Appl. Phys. Lett.* **60** 1027 (1992); Timp G et al. *Phys. Rev. Lett.* **69** 1636 (1992)
44. McClelland J J et al. *Science* **262** 877 (1993)
45. Bradley C C et al. *Appl. Surf.* **141** 210 (1999)
46. McClelland J J, Prentiss M, in *Nanotechnology* (Ed. G Timp) (New York: AIP Press/Springer, 1999) Ch. 10
47. Oberthaler M K, Pfau T *J. Phys. Condens. Matter* **15** R233 (2003)
48. Meschede D, Metcalf H *J. Appl. Phys. D.: Appl. Phys.* **36** R17 (2003)
49. McClelland J J et al. *Sci. Technol. Adv. Mater.* **5** 575 (2004)
50. Mützel M, Haubrich D, Meschede D *Appl. Phys. B* **70** 689 (2000)
51. Balykin V I et al. *Zh. Eksp. Teor. Fiz.* **90** 458 (1986) [*Sov. Phys. JETP* **63** 264 (1986)]
52. Schulze Th et al. *Appl. Phys. Lett.* **78** 1781 (2000); Schulze Th et al. *Appl. Phys. B* **70** 671 (2001)
53. Cohen-Tannoudji C, Phillips W *Phys. Today* **43** (10) 33 (1992)
54. Gupta R et al. *Appl. Phys. Lett.* **67** 1378 (1995); *Phys. Rev. Lett.* **76** 4689 (1996)
55. Berggren K K et al. *Science* **269** 1255 (1995)
56. Behringer R E, Natarajan V, Timp G *Opt. Lett.* **22** 114 (1997)
57. Drodofsky U et al. *Appl. Phys. B* **65** 755 (1997)
58. Jurdik E et al. *Phys. Rev. B* **69** 201102 (2004)
59. Mützel M et al. *Appl. Phys. B* **77** 1 (2003)
60. te Sligte E et al. *Microel. Eng.* **67 – 68** 664 (2003)
61. Myszkiewicz G et al. *Appl. Phys. Lett.* **85** 3842 (2004)
62. te Sligte E et al. *Appl. Phys. Lett.* **85** 4493 (2004)
63. Ohmukai R, Urabe S, Watanabe M *Sci. Technol. Adv. Mater.* **5** 585 (2004)
64. Rehse S J, McGowan R W, Lee S A *Appl. Phys. B* **70** 657 (2000)
65. Johnson K S et al. *Appl. Phys. Lett.* **69** 2773 (1996)
66. Rehse S J et al. *Appl. Phys. Lett.* **71** 1427 (1997)
67. Balykin V I *Adv. Atom. Mol. Opt. Phys.* **41** 181 (1999)
68. Balykin V I, Klimov V V, Letokhov V S *J. Physique II* **4** 1981 (1994)
69. Lüthi R et al. *Appl. Phys. Lett.* **75** 1314 (1999)
70. Subbotin M V, Balykin V I, Laryushin D V, Letokhov V S *Opt. Commun.* **139** 107 (1997)
71. Balykin V I et al. *Pis'ma Zh. Eksp. Teor. Fiz.* **84** 544 (2006) [*JETP Lett.* **84** 466 (2006)]
72. Oberst H, Kasashima S, Balykin V I, Shimisu F *Phys. Rev. A* **68** 013606 (2003)
73. Bradley C C, Anderson W R, McClelland J J, Celotta R J *Appl. Surf. Sci.* **141** 210 (1999)
74. Li Y T et al. *Phys. Rev. E* **69** 036405 (2004)
75. Melentiev P N et al. *Nano Lett.* (2009) (submitted)

PACS numbers: **32.30. – r**, 32.30.Jc, 42.82.Cr, 95.30.Ky, **97.10. – q**
DOI: 10.3367/UFNe.0179.200903j.0305

Spectroscopy of ionized atoms for astrophysics and nanotechnology

A N Ryabtsev, S S Churilov

1. Introduction

Spectroscopy of ionized atoms is an important tool in the solution of scientific and technological problems in different fields of physics. The results of investigations of ion spectra were and are used in solar and stellar research, for the diagnostics of laboratory plasma sources, including the controlled thermonuclear fusion problem, and for high-resolution optical microscopy and lithography. The Department of Atomic Spectroscopy of the Institute of Spectroscopy, RAS (ISAN) has been pursuing research in the majority of these areas since the inception of the institute. The Department now has a unique experimental, theoretical, and methodological basis sufficient for analyzing the most complex ion spectra and validly applying the data acquired. In this report, we consider two relatively distant areas of application of the spectroscopy of ionized atoms: investigations into the atmospheres of peculiar magnetic stars and the development of efficient optical lithography sources in the far vacuum ultraviolet (VUV) domain.

A group of stars relatively close in properties, whose spectra exhibit high-intensity absorption lines of heavy elements, which are quite weak or not recorded at all in the spectra of the main-sequence stars, have long been the particular concern of astrophysicists. Absorption lines of rare-earth ions, and sometimes of heavier elements up to Pt, Bi, and U, are recorded in the stellar atmospheres of this group. The masses of these stars range from 2 to 5 solar masses, their surface temperatures lie between 7000 – 18000 K, and most of them have high magnetic fields up to 10 – 30 kGs, strong atmospheric turbulence, and pulsating intensities in their absorption spectra. These objects are known as peculiar magnetic stars and are often referred to as Ap stars in the literature. The atoms of rare-earth elements in the atmospheres of these stars are primarily in the first and second ionization stages, whose spectra have not been adequately studied [1 – 3]. In many spectra, especially in the spectra of doubly ionized atoms, only several tens (out of several thousand possible) lines lying in the visible range (transitions between low levels) have been identified. The transition probabilities (line strengths) calculated for doubly ionized rare-earth atoms and stored in DREAM (Database on Rare Earths at Mons University) [3] are restricted to the transition probabilities between a small number of the known energy levels. Determining the composition and parameters of the atmospheres of Ap stars, defining relevant processes more precisely, and accounting for the emergence of their special features requires data, as comprehensive as possible, about the corresponding ion spectra, which are practically the only source of information about these objects. In Section 2, we

describe investigations into the spectra of doubly ionized atoms Nd III and Eu III and the application of the findings of this research to the diagnostics of Ap stars.

Another topical application area of investigations into complex ion spectra is projection optical lithography in the extreme VUV domain. At present, integrated microcircuits are produced using the radiation of excimer ArF lasers ($\lambda = 193$ nm). To further upgrade the microcircuit parameters (increase the number of active elements in microprocessors and improve the internal performance, memory space, etc.) requires advancing to the shorter-wavelength range. Moving to the extreme VUV range will allow bringing the spatial resolution of optical lithography to 10 nm, which will undoubtedly result in a new leap in the development of microelectronics, up to its possible renaming to 'nanoelectronics.' The last several years have seen the vigorous development of a high-efficiency lithography source at the wavelength $\lambda = 13.5$ nm coinciding with the reflection band of Mo/Si mirrors. Plasma sources like vacuum sparks and laser-produced plasmas containing tin ions are believed to hold the greatest promise. These ions have a very intense emission peak near $\lambda = 13.5$ nm, which consists of a very large array of 4–4 transitions in several ions with an open 4d subshell (see, e.g., Refs [4, 5]). But the spectroscopic data on these transitions, which are extremely important for optimizing lithographic source parameters, have been practically nonexistent. In Section 3, we outline the results of tin ion spectra investigations with an eye to the development of a source for 13.5 nm lithography.

2. Investigation of the spectra of doubly ionized rare-earth elements for astrophysics

Nd III ion. The available data on the Nd III spectrum have been highly disembodied and partly contradictory [1, 6, 7]. This disagreement led to substantial complications in the analysis of the chemical composition of Ap stars [8]. Our group, jointly with the Institute of Astronomy, RAS, carried out an independent analysis of the Nd III spectrum with the use of the spectrum of the HD 217522 Ap star in the visible range. This star has a relatively low magnetic field ($B_s < 2$ kGs), and therefore the line profiles in its spectrum are hardly distorted by the Zeeman splitting and their wavelengths in the visible range are measured with high precision ($\sim 5 \times 10^{-4}$ nm) [9]. The energies and transition probabilities for the Nd III spectrum were calculated by the Hartree–Fock technique with the use of Cowan's code package [10]. In these calculations, we took the strong interaction between the electron configurations $4f^4 + 4f^3 6p + 4f^2 5d^2$ and $4f^3 5d + 4f^3 6s + 4f^2 5d6p$ into account (hereinafter, we omit the completely filled electron subshells in the notation for configurations). As far as possible, the interaction integrals were scaled with the inclusion of the data resulting from the analysis of the spectra of other doubly ionized atoms of rare-earth elements. More than 70 spectral lines were identified and about 40 energy levels of the $4f^4$ and $4f^3 5d$ configurations were determined in the course of this analysis. The classified transitions are shown with the darker color in Fig. 1, which shows the total calculated spectrum of the $4f^4 - 4f^3(5d + 6s) - 4f^3 6p$ transitions in Nd III. It can be seen that the identified transitions are only a very small part of the Nd III spectrum. However, even with the help of such an incomplete analysis, it was possible to confidently determine the density of neodymium in the

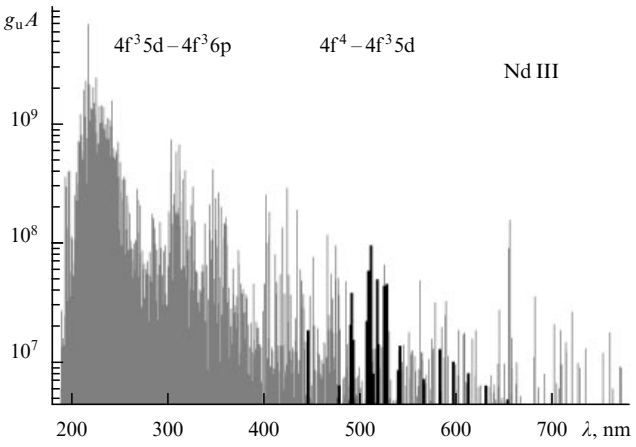

Figure 1. The calculated $4f^4 - 4f^3 5d - 4f^3 6p$ transition spectrum in Nd III. The line intensities are given in units of $g_u A$, where A is the radiative transition probability in [s^{-1}] and g_u is the statistical weight of the upper transition level. The darker color indicates the classified transitions.

atmosphere of the star HD 144897, in which all the rare-earth elements from La to Lu, with the exception of unstable Pm, were discovered in [8]. A portion of the spectrum of this star with Nd III lines and the result of its parametric modeling are depicted in Fig. 2. The newly obtained data on the Nd III spectrum allowed calculating the absorption spectrum of the stellar atmosphere with high precision. The observed structures of the Zeeman line splitting corresponding to the magnetic intensity of the HD 144897 star also confirm the validity of the Nd III spectrum analysis conducted.

Eu III ion. An analysis of the very complicated spectrum of Eu III is critical to the investigation of stellar atmospheres, because Europium is most abundant in the atmospheres of hot Ap stars, where it is found primarily in the second ionization stage (Eu III) [11, 12]. The spectrum of Eu III has been studied much better than that of Nd III: a list of its 890 lines has been published, one-third of them being classified as transitions between the levels $4f^7$, $4f^6(^7F)5d$, $4f^6(^7F)6s$, and $4f^6(^7F)6p$ [13]. But the transition probabilities calculated from the Eu III spectrum identification data turned out to be 2–3 orders of magnitude lower than those

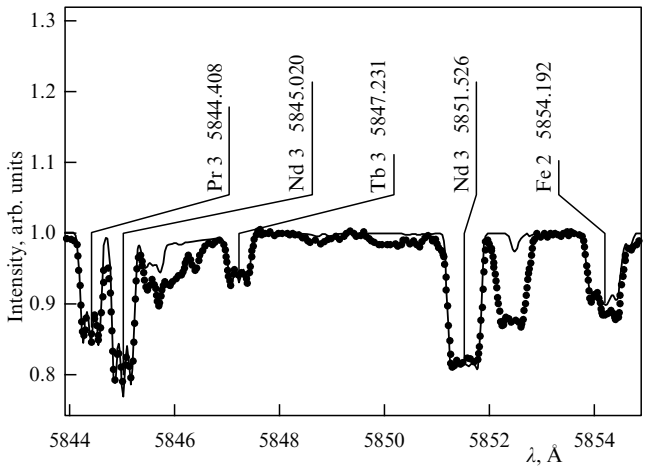

Figure 2. Portion of the atmospheric absorption spectrum of the HD 144897 peculiar magnetic star (points) and the result of its simulation (continuous line). Borrowed from Ref. [8].

Table 1. Densities, $\log(N/N_{\rm tot})$, of rare-earth elements in the atmospheres of several Ap stars and the Sun measured from the spectra of different ions. Measurement errors are given in parentheses. (Borrowed from Ref. [8].)

Ion	HD 144897	HD 170973	HD 116458	Sun
Ce II	−6.69(20)	−6.87	−7.34	−10.46
Ce III	−6.64(18)			
Pr II	−6.60(14)	−7.19	−7.30	−11.33
Pr III	−6.69(14)	−6.87	−7.32	
Nd II	−6.45(12)	−6.48		−10.59
Nd III	−6.45(20)	−6.63	−7.26	
Sm II	−6.98(21)	−7.07		−11.03
Sm III	−6.92(20)			
Eu II	**−7.75(20)**	**−7.77**	**−7.94**	**−11.52**
Eu III	**−6.32(23)**		**−6.90**	
Cd II	−6.95(18)	−7.17	−7.47	−10.92
Cd III	−6.60(14)			
Tb II	−7.83(10)			−11.76
Tb III	−7.92(22)	−7.96		
Dy II	−7.12(22)	−7.17		−10.90
Dy III	−6.99(39)	−7.13		
Er II	−7.55(14)	−7.54		−11,11
Er III	−7.21(14)	−7.79		
Tm II	−8.12(20)			−12.04
Tm III	−7.70(20)			

that would be expected from the lifetime measurements for some Eu III levels [14] and from astrophysical data [15].

The densities of several rare-earth elements in the atmospheres of three Ap stars, which were determined from the second and third spectra under the assumption of a local thermodynamic equilibrium, are collected in Table 1 [8]. It can be seen that the densities measured from the lines of different multiplicity ions are consistent, to within the uncertainty of measurements, for all the elements, with the exception of Europium. The densities of Europium derived from the spectra of Eu II and Eu III diverge by more than an order of magnitude. To solve this problem, new Eu III spectrum calculations were undertaken using the generalized least-square method (see, e.g., Refs [16, 17]) with the scaling of Hartree – Fock integrals and the inclusion of the effects of interaction with highly excited configurations.

The radial integrals were scaled with the inclusion of the data obtained in the analysis of the spectra of other doubly ionized lanthanides with the level lifetimes known from experiments. Along with the $4f^7$, $4f^6 5d$, $4f^6 6s$, and $4f^6 6p$ configurations under investigation, the doubly excited $4f^5 5d^2$, $4f^5 5d6s$, $4f^5 6s^2$, $4f^5 5d6p$, and $4f^5 6s6p$ configurations, which interact with them, were also included in the calculations. The transition probabilities calculated in this way are in good agreement with the measured level lifetime data and with the probabilities stored in DREAM [3]. In this case, the discrepancy between the Europium densities derived from the spectra of Eu II and Eu III became two times smaller. The residual difference may well be attributed to the deviation of level populations from the equilibrium values in Ap stellar atmospheres [18].

The calculations also resulted in the classification of 90 new spectral lines and the determination of more than

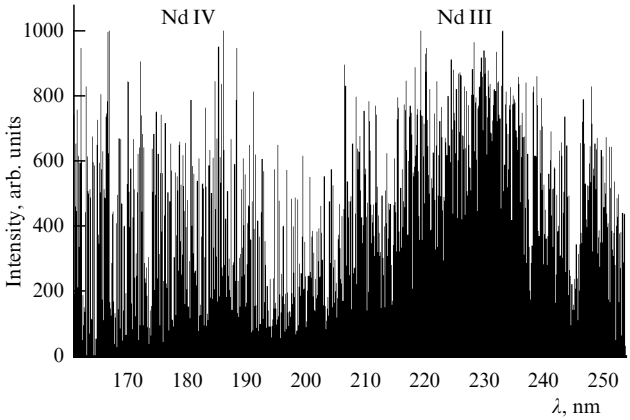

Figure 3. High-resolution spectrum of neodymium ions from a low-voltage spark plasma recorded with ISAN's VUV spectrograph.

30 new energy levels in the spectrum of Eu III [19]. The list of calculated transition probabilities for the 200 – 1000 nm wavelength range now contains 1145 lines arising from transitions between the known levels and 23,800 lines arising from transitions between all levels with energies lower than 90,000 $\rm cm^{-1}$. The results of these identifications and calculations were entered into the Vienna Atomic Line Database (VALD).

We note that the results outlined in this section were derived from the spectrograms recorded in the visible spectral range. However, the strongest transitions of doubly ionized atoms of rare-earth elements lie in the VUV spectral domain (see, e.g., Fig. 1). Investigating the VUV spectra of rare-earth ions would permit obtaining a wealth of reliable information about the processes occurring in the atmospheres of hot stars.

Planned for 2010 is the launch of the World Space Observatory (WSO), which will accommodate a high-resolution spectrometer WSO/UV for the 102 – 310-nm wavelength range. Recording the spectra of peculiar magnetic stars will inevitably bring up the question about the availability of laboratory data on the spectra of doubly and triply ionized heavy atoms. These data may be obtained using the normal-incidence VUV ISAN spectrograph, which outperforms the WSO/UV spectrometer. For example, Fig. 3 shows a spectrum of neodymium ions in the 160 – 250 nm wavelength range, which was recorded with a resolution of 200000 with ISAN's spectrograph. Standing out in the spectrum are line arrays arising from the $4f^3 5d - 4f^3 6p$ transitions in Nd III (cf. Fig. 1) and the resonance $4f^3 - 4f^2(5d + 6s)$ transitions in Nd IV. Presently, an analysis is being made of neodymium and ytterbium spectra below 250 nm, which were recorded in circumstances where the excitation of doubly and triply ionized atoms was dominant.

3. Investigation of tin ion spectra for extreme VUV lithography

As noted in the Introduction, developing a high-efficiency optical 13.5 nm lithography source requires comprehensive investigations into the spectra of multiply charged tin ions. According to preliminary calculations, the $4d^m - (4p^5 4f^{m+1} + 4d^{m-1} 4f)$ transitions ($m = 1 - 5$) in the spectra of Sn X – Sn XIV produce an intense radiation peak near the wavelength 13.5 nm. These transitions contain a multitude of closely located lines, and hence only a spectrally

unresolved structure of the 13.5 nm peak had been observed in the spectra recorded previously (see, e.g., Ref. [5]).

These 4–4 type transitions, which lie aside the main peak in the $\lambda > 16$ nm domain, were studied only for low-multiplicity ions: Sn VI [20] and Sn VII [21]. In the 13–14 nm wavelength range, only the four strongest 4–4 transition lines were classified in the simplest Sn XIV spectrum ($m = 1$) [22]. The spectra of analogous transitions in the nearest members of the corresponding isoelectronic sequences were not known either. That is why the 4–4 transitions were investigated via extrapolation along the 'isonuclear' sequence of tin ions with different multiplicities. The spectra were calculated by the Hartree–Fock method with the use of Cowan's code package [10] and the inclusion of $4d^m$, $4d^{m-1}nl$ ($n = 5, 6$; l = s, p, d, f), $4p^5 4d^{m+1}$, and $4p^5 4d^m 5s$ configurations.

The spectra were excited in a low-inductance vacuum spark with the peak discharge current $I = 10-25$ kA and recorded with a DFS-26 grazing-incidence spectrograph equipped with a holographic grating (3600 grooves/mm). The resolving power of this instrument is equal to about 20000 in the $\lambda = 13-14$ nm region, which enabled the structure of the strongest 4–4 transitions to be spectrally resolved. Figure 4 shows the spectra of tin ions acquired for the discharge currents 15 and 20 kA. Each spectrum consists of approximately 1000 strong lines, which stand out against a quasicontinuous background made up of a multitude of less intense lines. The calculated positions of highest-intensity transitions in different tin spectra are indicated in Fig. 4a. We can see that the spectral lines of different ions can be selected

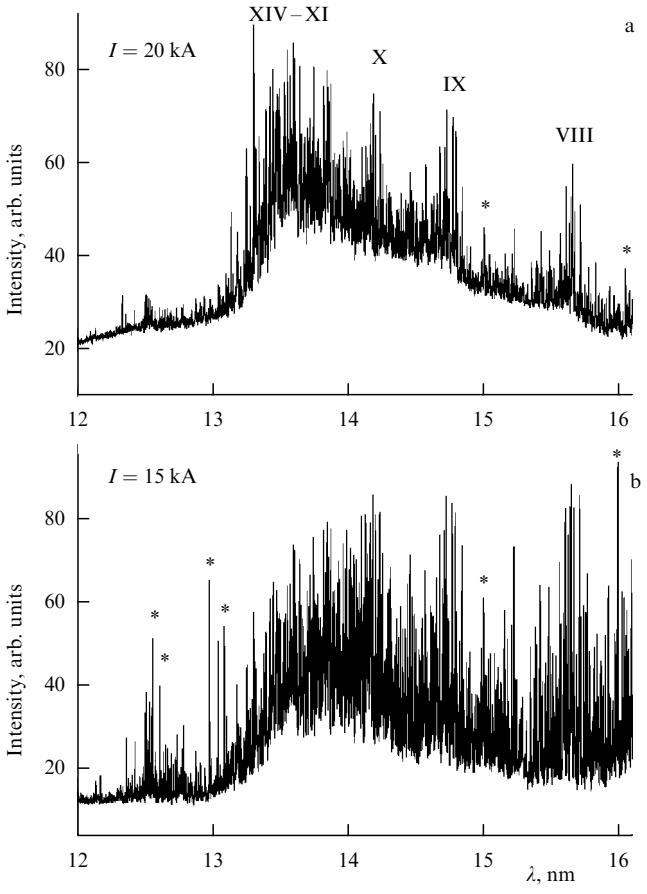

Figure 4. Extreme VUV spectra of tin ions excited in a low-inductance vacuum spark plasma. (Borrowed from Ref. [26].) Asterisks indicate oxygen and aluminum impurity ion lines.

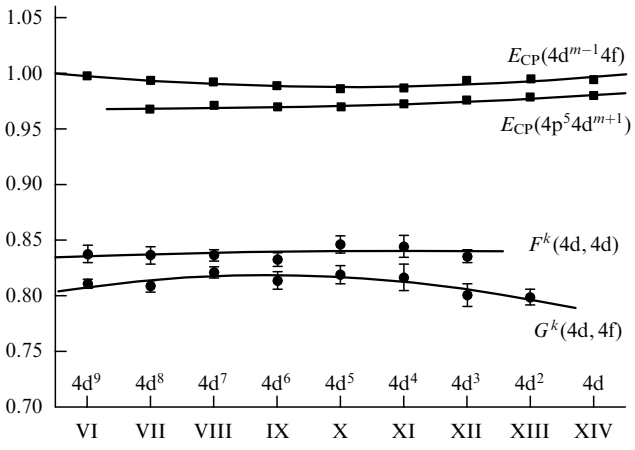

Figure 5. Variation of the scaling factors for the energy parameters of the $4d^{m-1}4f$ and $4p^5 4d^{m+1}$ configurations along the isonuclear sequence of tin ions.

according to the dependence of their intensities on the discharge current. In particular, on decreasing the current from 20 to 15 kA, the Sn VIII line intensities increase substantially, while the Sn XIII–XIV lines decrease. This fact was taken into account in the classification of the spectra.

The spectra were analyzed in several steps. Initially, the $4d^7 - (4p^5 4d^8 + 4d^6 4f)$ transitions were investigated in the spectrum of Sn VIII with the known structure of the ground configuration $4d^7$ [23]. In the semiempirical processing of the data acquired, it was noted that the scaling factors (the ratios between the semiempirical energy parameters and their Hartree–Fock values) were practically constant along the isonuclear sequence Sn VI–VIII [24]. That is why at the next stages, the spectra were analyzed by means of extrapolation of the scaling factors to their values for higher-charged ions. We thus classified the 4–4 transitions in the relatively simple spectra of Sn XIII and Sc XIV [25], and then investigated the higher-complexity spectra of Sn IX–Sn XII [26]. In the latter spectra, it has been possible to classify only the most intense transitions; however, even this incomplete analysis permitted determining the semiempirical values of the main parameters with sufficient precision. Figure 5 shows the scaling factors for the average energies (E_{CP}) and Slater parameters determined by the analysis of the excited configurations $4f^{m-1}4f$ and $4p^5 4d^{m+1}$ for the spectra of the isonuclear sequence Sn VI–XIV. The dependence of each factor on the nuclear charge is approximated by second-degree polynomials, up to uncertainties in the determination of the parameters (the uncertainty in E_{CP} does not exceed the size of the corresponding symbol in Figure 5).

This analysis resulted in the classification of about 440 spectral lines in the 12.5–16 nm wavelength range, which belong to $4d^m - (4d^{m-1}4f + 4p^5 4d^{m+1})$ transitions in the spectra of Sn VIII–XIV ($m = 1-7$). Of prime interest for VUV lithography is the 2% wavelength interval near $\lambda = 13.5$ nm (13.5 ± 0.135 nm); this is precisely the interval that coincides with the reflection band of Mo/Si mirrors.

Figure 6 shows a portion of the spectrum of a vacuum spark (20 kV) in the 2% wavelength interval with reference of the most intense lines to their ionization stages. The spectrum of tin ions in the interval used for 13.5 nm lithography primarily consists of transitions in Sn XI–Sn XIII. Hence, we can draw a preliminary conclusion: obtaining an efficient

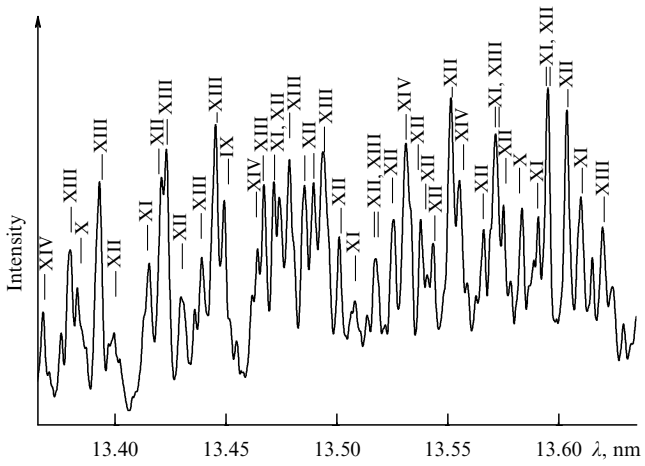

Figure 6. Classification of the spectral lines of tin in the 2% interval about the 13.5-nm wavelength by their ionization stages. (Borrowed from Ref. [26].)

radiation source in the interval $\lambda = 13.5 \pm 0.135$ nm requires producing a plasma with a prevalence of the ions Sn^{+10} – Sn^{+12}.

Similar investigations of the spectra of indium ions with the nuclear charge $Z_C = 49$ performed in parallel confirmed the main results of tin spectrum analysis ($Z_C = 50$). It was noted that the 4–4 transition spectra for different ionization degrees gradually separate in wavelength as the nuclear charge decreases. This is favorable to a more reliable classification of transitions in each specific ion. Presently underway in the Department of Atomic Spectroscopy of ISAN is an investigation of the 4–4 transition spectra in Pd, Ag, and Cd ions ($Z_C = 46-48$) intended to verify the results of our analysis of tin ionic spectra. Nevertheless, even now the data obtained are advantageously used as the spectroscopic foundation for modeling, development, and optimization of 13.5 nm lithography radiation sources based on tin ions.

Acknowledgements. This research was supported by the 6th Framework Program of the European Community (project IST-1-507754-IP), the Russian Foundation for Basic Research grants Nos 05-02-08224-ofi and 07-02-00244-a, and partly by the Optical Spectroscopy and Frequency Standards Program of the Physical Sciences Division, RAS.

References

1. Martin W C, Zalubas R, Hagan L, Natl. Stand. Ref. Data Ser. Natl. Bureau Stand. NSRDS-NBS 60 (Washington: National Bureau of Standards, 1978)
2. BIBL: Bibliography database on atomic spectra, http://das101.isan.troitsk.ru/bibl.htm
3. Biemont E, Palmeri P, Quinet P *Astrophys. Space Sci.* **269** 635 (1999); D.R.E.A.M. Database on Rare Earths at Mons University, http://w3.umh.ac.be/~astro/dream.shtml
4. Tolstikhina I Yu, Churilov S S, Ryabtsev A N, Koshelev K N, in *EUV Sources for Lithography* Vol. PM149 (Ed. V Bakshi) (Bellingham, Wash.: SPIE Press, 2006) p.113
5. Svendsen W, O'Sullivan G *Phys. Rev. A* **50** 3710 (1994)
6. Crosswhite H, Private communication (1976)
7. Aldenius M, Master Thesis (Lund: Depart. of Physics, Univ. of Lund, 2001)
8. Ryabchikova T, Ryabtsev A, Kochukhov O, Bagnulo S *Astron. Astrophys.* **456** 329 (2006)
9. Kochukov O, Ryabchikova T, Piskunov N *Astron. Astrophys.* **415** L13 (2004)
10. Cowan R D *The Theory of Atomic Structure and Spectra* (Berkeley: Univ. of California Press, 1981)
11. Wahlgren G M *Phys. Scripta* **T100** 22 (2002)
12. Biemont E, Quinet P *Phys. Scripta* **T105** 38 (2003)
13. Sugar J, Spector N *J. Opt. Soc. Am.* **64** 1484 (1974)
14. Den Hartog E A, Wickliffe M E, Lawler J E *Astrophys. J. Suppl.* **141** 255 (2002)
15. Ryabchikova T et al. *Astron. Astrophys.* **343** 229 (1999)
16. Wyart J F *J. Opt. Soc. Am.* **68** 197 (1978)
17. Wyart J F, Buache-Arnold Cl *Phys. Scripta* **22** 583 (1980)
18. Mashonkina L, Ryabchikova T, Ryabtsev A *Astron. Astrophys.* **441** 309 (2005)
19. Wyart J-F, Tchang-Brillet W-Ü L, Churilov S S, Ryabtsev A N *Astron. Astrophys.* **483** 339 (2008)
20. Churilov S S, Kildiyarova R R, Ryabtsev A N, Kramida A E, Joshi Y N *Phys. Scripta* **50** 463 (1994)
21. Azarov V I, Joshi Y N, Churilov S S, Ryabtsev A N *Phys. Scripta* **50** 642 (1994)
22. Sugar J, Kaufman V, Rowan W L *J. Opt. Soc. Am. B* **9** 1959 (1992)
23. Azarov V I, Joshi Y N *J. Phys. B* **26** 3495 (1993)
24. Churilov S S, Ryabtsev A N *Opt. Spektrosk.* **100** 721 (2006) [*Opt. Spectrosc.* **100** 660 (2006)]
25. Churilov S S, Ryabtsev A N *Opt. Spektrosk.* **101** 181 (2006) [*Opt. Spectrosc.* **101** 169 (2006)]
26. Churilov S S, Ryabtsev A N *Phys. Scripta* **73** 614 (2006)

PACS numbers: 03.75.Hh, 71.35.Lk, **71.36.+c**
DOI: 10.3367/UFNe.0179.200903k.0309

Strong correlations and new phases in a system of excitons and polaritons. A polariton laser

Yu E Lozovik

One of the most beautiful phenomena in many-particle physics — Bose–Einstein condensation (BEC) in a system of particles with nonzero mass m obeying the Bose statistics — was predicted by Einstein already in 1925 soon after the publication of Bose's paper on the thermodynamically equilibrium distribution of photons. Einstein showed that at a temperature T below the critical value

$$T_c = \frac{3.31\hbar^2}{m} n^{2/3} \quad (1)$$

(where n is the concentration of particles), the integral of the distribution function over all momenta decreases to below the total number of particles; in order to resolve this paradox, he assumed that all 'missing' particles lie in the one and only state with the lowest energy (and zero momentum). If $T \leqslant T_c$, the thermal de Broglie wavelength is of the order of the average distance between particles or is larger than it, such that the BEC occurs only in the quantum mode for a system of particles. If $T \to 0$, all particles in a system of noninteracting particles form the condensate.

After P Kapitza discovered the superfluidity of ^{4}He, F London suggested that superfluidity may stem from BEC. This was a brave hypothesis because BEC was then predicted only for noninteracting particles, while the interaction in condensed ^{4}He is strong. The BEC theory was generalized to the case of interacting particles only later (see [1–3] and the references therein). It was found that the interaction 'exhausts' the Bose condensate such that not more than 9% of particles in ^{4}He stay in the condensate even at $T \to 0$. This was shown by first-principle quantum Monte Carlo calcula-

tions and by evaluations based on experiments with neutron scattering in liquid ^{4}He at temperatures lower than the temperature of transition to the superfluid state. In reality, the number of atoms in the condensate was calculated in these experiments as a result of subtraction of two large numbers, i.e., the total number of particles and the number of above-condensate particles. This procedure is equivalent to determining a captain's weight by weighing a ship with the captain on board and subtracting the weight of the ship and is hardly conclusive in view of the accuracy achieved in the experiment. Consequently, to experimentally observe Bose condensation, it was necessary to pass to a system of weakly interacting atoms in which condensate exhaustion due to interaction is negligible, that is, to start using Bose gases at a low concentration of particles and hence, as follows from formula (1), at ultralow temperatures (in the range of nanokelvins). This dictated the need to develop a spectacular technology of laser cooling and building traps for neutral atoms (see, e.g., [4] and the references therein). This is why it took 70 years after Einstein's brilliant prediction for the experiments of Ketterle, Cornell, and Wieman and their coworkers (those among the most beautiful experiments of the 20th century) to observe Bose–Einstein condensation of cold atoms in a trap.[1]

In fact, because the BEC temperature is proportional to the particle mass, BEC could be realized at substantially higher temperatures, for example, with a positronium, or quasiparticles of Bose excitations in semiconductors — Wannier–Mott excitons (see [3, 6, 7] and the references therein) or polaritons in optical microcavities (see [8–12] and the references therein).

Estimates show that Bose condensation of excitons could be already obtained at temperatures of the order of several kelvins and the Bose condensation of polaritons at even higher temperatures. There is a difficulty here, however: quasiparticles have finite lifetimes due to their short recombination times (for excitons) and still shorter lifetimes (of the order of only ten picoseconds) of photons in an optical microcavity owing to its moderate quality (for polaritons).

For the Bose condensation to be produced, it is necessary that the time for a system of quasiparticles to reach thermal equilibrium and form the condensate be substantially shorter than the quasiparticle lifetime. This was one of the reasons why it was suggested rather long ago to use a system of excitons with spatially separated electrons (e) and holes (h) (see [13–15] and the references therein). Spatial separation in coupled quantum wells or in a single quantum well in a strong electric field reduces the recombination rate by several orders of magnitude. Furthermore, if the exciton concentration is not very high, repulsion between parallel electric dipoles occurring in response to spatial separation of electrons and holes prevents the standard coalescence of electrons and holes into metallic e–h-drops [16] and stabilizes the exciton phase in an isotropic (or nearly isotropic) electron–hole system. In the range of sufficiently low temperatures, we can expect to observe, as the concentration increases, a quantum crossover from the mode of BEC of dipole excitons [14] (or a local e–h pair in an equilibrium system) to the Bardeen–Cooper–Schrieffer (BCS) regime, i.e., to pairing of spatially separated electrons and holes (first discussed in the case of three-dimensional insulators by Keldysh and Kopaev [17] (see also [18])) such that the size of the Cooper pairs much exceeds the distance between them.[2] The spatial separation of electrons and holes plays another important role in the entire range of controlling parameters in which the coherent phase exists. First of all, in principle, it allows the observation of nondecaying *electric* currents associated with the superfluid motion of neutral excitons or Cooper e–h pairs as a whole. Second, the spatial separation suppresses tunneling and also phase fixation in an *equilibrium* e–h system, thus allowing superfluidity [15] (a three-dimensional equilibrium exciton dielectric has no superproperties). And finally, it permits observation of the Josephson effect between separately nonsuperconducting e- and h-layers [15].

A number of interesting optical effects, such as the stimulated light backscattering and other nonlinear optical effects, can be observed in a system of Bose-condensed dipole excitons [21].

However, Bose condensation is impossible in an extended two-dimensional system (of excitons) owing to the divergence of phase fluctuations in the Bose condensate even though superfluidity may arise in this system at a temperature below the Kosterlitz–Thouless transition point. BEC becomes possible in two-dimensional exciton traps created by nonuniform deformation [22], lithography, the nonuniform electric field of the tip of the scanning probe microscope or special-profile control electrode [23], or a 'natural' trap involving localization of excitons in a random potential due to impurities, boundary roughness, etc. [24].

We have calculated the properties of such traps and the distribution profile of excitons in them. Furthermore, we constructed a quasilocal generalization of the Kosterlitz–Thouless theory [25], which describes the transition to the superfluid state in an extended trap (e.g., produced by nonuniform strain).

As the concentration or the dipole moment of excitons increases, the role of correlation effects grows; in particular, they allow the formation of a liquid superfluid phase of excitons [14] and also of a new phase, the exciton crystal [26]. The results of our quantum Monte Carlo calculations [27] show that a crystal is formed in a system of dipole excitons at the Lindemann parameter equal to 0.23, which corresponds to a quantum phase transition at the dimensionless density of excitons $nr_0^2 = 290$, where n is the concentration of excitons, r_0 is a parameter of the dimension of length, $r_0 = md^2/(4\pi\hbar^2)$, and d is the exciton dipole moment. (Another scenario of quantum crystallization in a two-layer e–h system, stemming from the large difference between the effective masses of e and h, was studied in [28].)

In fact, fairly large deviations from the behavior typical of a weakly interacting electron gas are already detected for substantially lower parameters nr_0^2: the condensate is found to be significantly exhausted, a peak appears on the static structural factor that signifies the formation of a short-range order in the system of dipole excitons, the excitation spectrum deviates substantially from the Bogolyubov profile, and a roton minimum appears on the dispersion curve [29].

At present, serious progress is taking place in the experimental realization of a specific form of excitons [23, 24, 30]. It is interesting that the exciton systems currently being studied by experimenters are, as follows from our analysis [27, 29], rather strongly correlated.

[1] The spectacular success in this field was described, for instance, in [1, 2].

[2] No such crossover occurs in two-layer graphene in the absence of magnetic fields because excitons do not form in a band spectrum with a zero gap [19]. The regime produced in two-layer graphene in strong magnetic fields is the Bose condensation of dipole magnetoexcitons [20].

Strong magnetic fields offer an interesting possibility of controlling the effects of strong correlation of excitons and of generating a crystalline excitonic phase. The effective (magnetic) mass of excitons greatly increases in a strong magnetic field [31]; this increases the characteristic length parameter r_0, which in turn determines the controlling parameter of the quantum phase transition to the crystalline phase, i.e., the dimensionless exciton density nr_0^2. The result is the magnetic-field-induced quantum crystallization of excitons.

At the moment, the results of our quantum Monte Carlo simulation leave open the question of whether a supersolid phase in an extended dipole system is possible at all (crystal ordering and superfluidity are expected to coexist in the supersolid phase [32]). However, by using quantum Monte Carlo simulation, we were able to establish that supersolids can exist in mesoscopic systems of dipoles in traps [33]. It was simultaneously found that the concentration of the superconducting component decreases as the number of particles increases. If the phase of the exciton crystal is taken into account, the phase diagram of a two-layer system of electrons and holes with the interlayer distance d much greater than the effective Bohr radius a_0 must take the form shown in the figure (as d decreases, the existence range of the crystalline phase contracts and then disappears, and a liquid exciton phase appears at small $d \leqslant a_0$).

We consider a system of exciton polaritons, the one that is currently popular (see [8–11]) — an optical microcavity placed between two Bragg mirrors with one or several quantum wells placed in the cavity. In an optical cavity, photons with small longitudinal momenta (significant at low temperatures) have the dispersion law

$$\varepsilon_{\rm ph}(k_{||}) = c\sqrt{k_{||}^2 + \left(\frac{\pi N}{L}\right)^2} \approx E_0 + \frac{k_{||}^2}{2m_{\rm ph}}\,, \qquad (2)$$

where $m_{\rm ph} = (\pi N)^2/(cL^2)$ is a quantity that can be logically described as the effective longitudinal photon mass, $k_{||}$ is the longitudinal momentum, L is the transverse width of the microcavity, and E_0 is the ground-state energy; in what follows, we consider transverse quantization with $N = 1$. For the parameters used in the experiment, $m_{\rm ph}$ is of the order of $10^{-4} - 10^{-5}$ of the electron mass $m_{\rm e}$. The geometry of the system is selected such that at small momenta, the resulting dispersion curve of the photon in the cavity intersects the dispersion curve for quasi-two-dimensional excitons in the quantum well placed in an optical microcavity. As a result of the interaction between two types of bosons — cavity photons and excitons — Rabi splitting is produced in the intersecting dispersion curves and a new quasiparticle, the excitonic polariton, is generated, which is a superposition of the cavity photon and exciton and has two dispersion branches (the upper and the lower polaritons).

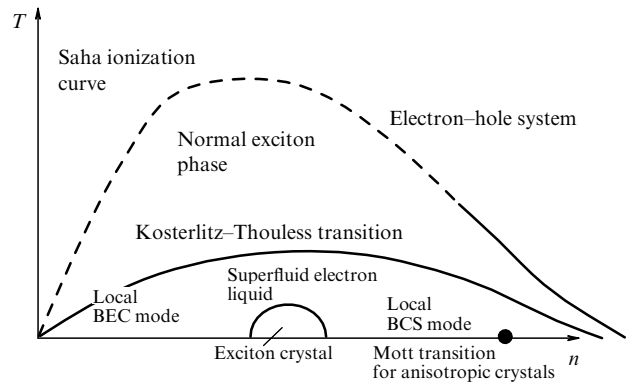

Figure. Phase diagram of a system of electrons and holes spatially separated in e- and h-layers at the interlayer separation d essentially larger than the effective Bohr radius a_0 (or in sufficiently strong magnetic fields H). As d (or H) decreases, the crystalline phase vanishes; liquid exciton phase emerges at $d \leqslant a_0$.

Because $m_{\rm eff}$ on the lower polariton branch must coincide with $m_{\rm ph} \sim (10^{-4} - 10^{-5})\, m_{\rm e}$, it follows that according to estimate (1), the Bose condensate temperature of polaritons should be very high at a sufficiently high level of pumping — up to room temperature!

It could be possible to observe the transition of polaritons (and of excitons) into a coherent state by observing the abrupt narrowing of the width of the photons emitted from the cavity and their statistics. The statistics of photons leaving the cavity would be those of the coherent phase of polaritons. If this were so, they would have the statistics of laser radiation, with no population inversion in the system. In this sense, the system is a laser without inversion.

Of course, Bose condensation is impossible in an extended two-dimensional system, but superfluidity of polaritons at temperatures below the Kosterlitz–Thouless temperature is possible, while this last must be fairly high owing to the polariton's small mass. However, the following interesting questions arise at this point:

1. How is polariton superfluidity to be observed?

2. How can the Kosterlitz–Thouless temperature in a system of polaritons be found?

Superfluidity could be established by observing unusual features in the behavior of the diffusion coefficient of polaritons and/or in the dependence of the effect of polariton entrainment by the two-dimensional gas of electrons located in the vicinity of a quantum well with excitons on polariton pumping. The electron current should entrain the exciton component of the polariton due to the interaction between the electron charge and the dipole moment induced by this charge in the excitons located in quantum wells (see also [34]), while the exciton component in turn entrains the photon component of the polariton. The result should be a change in the angular distribution of photons emitted from the cavity. The entrainment coefficient would manifest a singularity at the Kosterlitz–Thouless transition point.

As regards the calculation of the Kosterlitz–Thouless transition temperature in a system of polaritons, the following difficulty is obvious here, in contrast to a similar calculation for a system of exitons [14]: the polariton dispersion law resulting from the anti-intersection of two quadratic laws is highly nonquadratic. Furthermore, the effective interaction between polaritons also depends substantially on the momentum, as a result of 'entanglement' of excitons and photons in polaritons, which depends on the longitudinal momenta. Consequently, it becomes impossible to use the standard Landau recipe for calculating the superfluid density based on applying the Galilei transformation to the reference frame comoving with the superfluid component. The superfluid density thus has to be found using a more general formalism of linear response and applying sum rules [35]. This procedure is shown to be formally equivalent to calculating the flux by introducing a fictitious charge for the polariton placed in a gauge field. It was demonstrated in [35] that due to phase fixation, only one Kosterlitz–Thouless

phase transition occurs between (local) condensates of excitons and cavity photons in the system; the transition temperature depends on the control parameters, the cavity geometry and the polariton splitting (Rabi splitting).

Bose condensation of polaritons is possible in two-dimensional traps for polaritons. To localize the polariton gas, it suffices to localize just one of its components (photonic or excitonic). The following two methods are thus possible for implementing a polariton trap. The first is based on building photon confinement using a microcavity of a variable width or creating a dielectric permittivity inside the microcavity dependent on the longitudinal coordinates. The second method consists in building exciton confinement by applying an external potential to the quantum well with excitons or by nonuniformly deforming the system. This method was experimentally realized by Snoke and his group (see [22] and the references therein).

In view of this, we have theoretically investigated the properties of the Bose-condensed gas of polaritons in a two-dimensional trap [11, 36, 37]. A two-component analog of the Gross–Pitaevskii equation was studied in one of the approaches to describing Bose condensates of weakly interacting polaritons [36]. In this approach, the Bose condensate of polaritons is described as two connected condensates convertible into each other — a Bose condensate of excitons and another of microcavity photons.

The wave function of the polariton condensate has two components: the respective wave functions $\psi(r)$ and $\chi(r)$ of the photon and exciton condensate. It was assumed that practically all cavity photons and excitons in the quantum well are in the condensate state at $T=0$ and it would therefore be possible to obtain the two-component analog of the Gross–Pitaevskii equation.

The energy functional of a coupled system of exciton and cavity photon condensates has the form

$$E[\psi,\chi]=\int\left\{-\frac{1}{4\pi}\,\frac{\varepsilon}{\alpha}\,\psi^*\left(L(r)\,\frac{\partial^2}{\partial r^2}+\frac{\partial L(r)}{\partial r}\,\frac{\partial}{\partial r}+\frac{L(r)}{r}\,\frac{\partial}{\partial r}\right)\psi\right.$$
$$+\left(2\pi\,\frac{\varepsilon}{\alpha}\,\frac{1}{L(r)}-\mu\right)|\psi|^2-\frac{1}{2}\,\chi^*\left(\frac{\partial^2}{\partial r^2}+\frac{1}{r}\,\frac{\partial}{\partial r}\right)\chi$$
$$\left.+\left(V(r)-\mu\right)|\chi|^2+\frac{g}{2}\,|\chi|^4+\frac{\Omega}{2}\,(\psi^*\chi+\chi^*\psi)\right\}2\pi r\,\mathrm{d}r\,, \quad (3)$$

where V is the confining potential for excitons, Ω is the energy of polariton splitting, $\alpha=e^2/(\hbar c)=1/137$, ε is the dielectric permittivity of the medium in the cavity, μ is the chemical potential of the system, common for both subsystems, g is the exciton–exciton coupling constant, and L is the width of the optical microcavity, which depends on the cavity radius in general.

After varying the energy functional with respect to ψ^* and χ^*, we arrive at a system of coupled equations for the two-component condensate, which takes the following form in polar coordinates:

$$-\frac{1}{4\pi}\,\frac{\varepsilon}{\alpha}\left(L(r)\,\frac{\partial^2}{\partial r^2}+\frac{\partial L(r)}{\partial r}\,\frac{\partial}{\partial r}+\frac{L(r)}{r}\,\frac{\partial}{\partial r}\right)\psi(r)$$
$$+\left(\frac{2\pi}{L(r)}\,\frac{\varepsilon}{\alpha}-\mu\right)\psi(r)+\frac{\Omega}{2}\,\chi(r)=0\,,$$
$$-\frac{1}{2}\left(\frac{\partial^2}{\partial r^2}+\frac{1}{r}\,\frac{\partial}{\partial r}\right)\chi(r)+\left(V(r)-\mu\right)\chi(r)$$
$$+g\left|\chi(r)\right|^2\chi(r)+\frac{\Omega}{2}\,\psi(r)=0\,. \quad (4)$$

The range of values of the chemical potential of the system was determined in the Thomas–Fermi approximation, which allows the localization of the polariton gas. For the 'exciton' trap created by applying an external potential, this region is $\pi\varepsilon/(L\alpha)-\Omega/2<\mu<\pi\varepsilon/(L\alpha)$. For a photon trap in which localization is produced due to the symmetry of the microcavity, the chemical potential must fall in the interval $\pi\varepsilon/(L(0)\,\alpha)-\Omega/2<\mu<\pi\varepsilon/(L(\infty)\,\alpha)-\Omega/2$. As the chemical potential increases, not only the total number of particles but also the relative fraction of photons in the condensate increases.

We emphasize that we here assumed that the polariton system is in thermal equilibrium (this is also true for our papers [11, 37], in which a different approach was used for describing the polariton condensate in a trap). With real systems currently under study, the polariton lifetime in a cavity is so far too short to achieve thermal equilibrium, and hence the quality of the optical cavity needs essential improvement. Nevertheless, appreciable line narrowing is observed as pumping increases, plus the second-order time correlation function also changes greatly, which points to coherence emerging in the system. In view of this, it is very important to conduct a detailed and consistent analysis of the kinetics of the polariton condensate formation.

I express gratitude for support to the RFBR and RAS programs. I am deeply grateful to Yu V Kopaev, V B Timofeev, and the participants in the International Conference on Spontaneous Coherence of Excitons (Cambridge, 2008) for the useful discussions.

References

1. Pitaevskii L, Stringari S *Bose-Einstein Condensation* (Oxford: Clarendon Press, 2003); Pitaevskii L P *Usp. Fiz. Nauk* **176** 345 (2006); **168** 641 (1998) [*Phys. Usp.* **49** 333 (2006); **41** 569 (1998)]
2. Griffin A *Excitations in a Bose-condensed Liquid* (Cambridge: Cambridge Univ. Press, 2005); Griffin A, Nikuni T, Zaremba E *Bose-Condensed Gases at Finite Temperatures* (Cambridge: Cambridge Univ. Press, 2005)
3. Griffin A, Snoke D W, Stringari S (Eds) *Bose-Einstein Condensation* (Cambridge: Cambridge Univ. Press, 1995)
4. Metcalf H J, van der Straten P *Laser Cooling and Trapping* (New York: Springer, 1999); Minogin V G, Letokhov V S *Davlenie Lazernogo Izlucheniya na Atomy* (Laser Light Pressure on Atoms) (Moscow: Nauka, 1986) [Translated into English (New York: Gordon and Breach Sci. Publ., 1987)]
5. Ketterle W *Rev. Mod. Phys.* **74** 1131 (2002)
6. Keldysh L V, in *Bose-Einstein Condensation* (Eds A Griffin, D W Snoke, S Stringari) (Cambridge: Cambridge Univ. Press, 1995) p. 246
7. Moskalenko S A, Snoke D W *Bose–Einstein Condensation of Excitons and Biexcitons* (Cambridge: Cambridge Univ. Press, 2000)
8. Weisbuch C et al. *Phys. Rev. Lett.* **69** 3314 (1992); Imamoğlu A, Ram R J *Phys. Lett. A* **214** 193 (1996)
9. Kavokin A, Malpuech G *Cavity Polaritons* Vol. 32 *Thin Films and Nanostructures* (San Diego: Elsevier, 2003)
10. Gippius N A et al. *Usp. Fiz. Nauk* **175** 327 (2005) [*Phys. Usp.* **48** 306 (2005)]; Kylakovskii V D et al. *Usp. Fiz. Nauk* **173** 995 (2003) [*Phys. Usp.* **46** 967 (2003)]
11. Snoke D *Nature Phys.* **4** 673 (2008); *Science* **298** 1368 (2002); Balili R et al. *Science* **316** 1007 (2007)
12. Marchetti F M et al. *Phys. Rev. B* **77** 235313 (2008)
13. Lozovik Yu E, Yudson V I *Pis'ma Zh. Eksp. Teor. Fiz.* **22** 556 (1975) [*JETP Lett.* **22** 274 (1975)]; *Zh. Eksp. Teor. Fiz.* **71** 738 (1976) [*Sov. Phys. JETP* **44** 389 (1976)]; *Solid. State Commun.* **19** 391 (1976); Lozovik Yu E, in *Vsesoyuz. Soveshchanie po Dielektricheskoi Elektronike, Tashkent, 1973. Tezisy Dokladov* (Collected Papers of the USSR Conf. on Dielectric Electronics, Abstracts of Contributions) (Tashkent: FAN, 1973)

14. Lozovik Yu E, Berman O L *Pis'ma Zh. Eksp. Teor. Fiz.* **64** 526 (1996) [*JETP Lett.* **64** 573 (1996)]; *Zh. Eksp. Teor. Fiz.* **111** 1879 (1997) [*JETP* **84** 1027 (1997)]; Lozovik Yu E, Berman O L, Ruvinskii A M *Pis'ma Zh. Eksp. Teor. Fiz.* **69** 573 (1999) [*JETP Lett.* **69** 616 (1999)]
15. Lozovik Yu E, Yudson V I *Solid State Commun.* **22** 117 (1977); Klyuchnik A V, Lozovik Yu E *J. Phys. C: Solid State Phys.* **11** L483 (1978); Lozovik Yu E, Klyuchnik A V *J. Phys. Low Temp.* **38** 761 (1980); Shevchenko S I *Phys. Rev. Lett.* **72** 3242 (1994); Lozovik Yu E, Poushnov A V *Phys. Lett. A* **228** 399 (1997)
16. Keldysh L V, in *Electron-Hole Liquid* (Amsterdam: North-Holland, 1986)
17. Keldysh L V, Kopaev Yu V *Fiz. Tver. Tela* **6** 2791 (1964) [*Sov. Phys. Solid State* **6** 2219 (1965)]
18. Kozlov A N, Maksimov L A *Zh. Eksp. Teor. Fiz.* **48** 1184 (1965) [*Sov. Phys. JETP* **21** 790 (1965)]; Halperin B I, Rice T M *Solid State Phys.* **21** 115 (1968); Guseinov R R, Keldysh L V *Zh. Eksp. Teor. Fiz.* **63** 2255 (1972) [*Sov. Phys. JETP* **36** 1193 (1973)]
19. Lozovik Yu E, Merkulova S P, Sokolik A A *Usp. Fiz. Nauk* **178** 757 (2008) [*Phys. Usp.* **51** 727 (2008)]; Lozovik Yu E, Sokolik A A *Pis'ma Zh. Eksp. Teor. Fiz.* **87** 61 (2008) [*JETP Lett.* **87** 55 (2008)]
20. Berman O L, Lozovik Yu E, Gumbs G *Phys. Rev. B* **77** 155433 (2008)
21. Lozovik Yu E, Poushnov A V *Phys. Rev. B* **58** 6608 (1998); Lozovik Yu E, Pushnov A V *Zh. Eksp. Teor. Fiz.* **115** 1353 (1999) [*JETP* **88** 747 (1999)]; Lozovik Yu E, Ovchinnikov I V *Phys. Rev. B* **66** 075124 (2002); Lozovik Yu E, Kurbakov I L, Ovchinnikov I V *Solid State Commun.* **126** 269 (2003); Lozovik Yu E, Ovchinnikov I V, Sharapov V A *Zh. Eksp. Teor. Fiz.* **125** 659 (2004) [*JETP* **98** 582 (2004)]
22. Balili R B et al. *Appl. Phys. Lett.* **88** 031110 (2006); Berman O L, Lozovik Yu E, Snoke D W *Phys. Status Solidi C* **3** 3373 (2006)
23. Gorbunov A V, Timofeev V B *Usp. Fiz. Nauk* **176** 651 (2006) [*Phys. Usp.* **49** 629 (2006)]; Timofeev V B, Gorbunov A V *Pis'ma Zh. Eksp. Teor. Fiz.* **83** 178 (2006) [*JETP Lett.* **83** 146 (2006)]
24. Butov L V *J. Phys. Condens. Matter* **19** 295202 (2007)
25. Lozovik Yu E, Kurbakov I L, Willander M *Phys. Lett. A* **366** 487 (2007)
26. Lozovik Yu E, Berman O L *Phys. Scripta* **58** 86 (1998); Kulakovskii D V, Lozovik Yu E, Chaplik A V *Zh. Eksp. Teor. Fiz.* **126** 979 (2004) [*JETP* **99** 850 (2004)]
27. Astrakharchik G E, Boronat J, Kurbakov I L, Lozovik Yu E *Phys. Rev. Lett.* **98** 060405 (2007); Ludwig P, Filinov A, Lozovik Yu E, Stolz H, Bonitz M *Contrib. Plasma Phys.* **47** 335 (2007)
28. Lozovik Yu E et al. *Zh. Eksp. Teor. Fiz.* **133** 348 (2008) [*JETP* **106** 296 (2008)]; Astrakharchik G E et al. *Phys. Rev. A* **75** 063630 (2007)
29. Vörös Z et al. *Phys. Rev. Lett.* **97** 016803 (2006)
30. Lozovik Yu E, Ruvinsky A M *Phys. Lett. A* **227** 271 (1997); Lozovik Yu E et al. *Phys. Rev. B* **65** 235304 (2002); Butov L V et. al. *Phys. Rev. Lett.* **87** 216804 (2001)
31. Andreev A F, Lifshits I M *Zh. Eksp. Teor. Fiz.* **56** 2057 (1969) [*Sov. Phys. JETP* **29** 1107 (1969)]; Chester G V *Phys. Rev. A* **2** 256 (1970)
32. Lozovik Yu E, Volkov S Y, Willander M *Pis'ma Zh. Eksp. Teor. Fiz.* **79** 585 (2004) [*JETP Lett.* **79** 473 (2004)]
33. Lozovik Yu E, Nikitkov M V *Zh. Eksp. Teor. Fiz.* **111** 1107 (1997); **116** 1440 (1999) [*JETP* **84** 612 (1997); **89** 775 (1999)]
34. Lozovik Yu E, Semenov A G *Pis'ma Zh. Eksp. Teor. Fiz.* **86** 30 (2007); *Theor. Mat. Fiz.***154** 372 (2008) [*JETP Lett.* **86** 28 (2007); *Theor. Math. Phys.* **154** 319 (2008)]; see Lozovik Yu E, Semenov A G, Willander M *Pis'ma Zh. Eksp. Teor. Fiz.* **84** 176 (2006) [*JETP Lett.* **84** 146 (2006)]
35. Voronova N S, Lozovik Yu E *Fiz. Tver. Tela* **50** 1496 (2008) [*Phys. Solid State* **50** 1555 (2008)]
36. Berman O L, Lozovik Yu E, Snoke D W *Phys. Rev. B* **77** 155317 (2008)
37. Deng H et al. *Science* **298** 199 (2002)

PACS numbers: **63.20.–e**, **63.50.–x**, **78.30.–j**
DOI: 10.3367/UFNe.0179.200903l.0313

Inverted optical phonons in ion-covalent crystals

E A Vinogradov, B N Mavrin,
N N Novikova, V A Yakovlev

1. Introduction

In this report, we discuss additional optical phonons, considered excess from the standpoint of selection rules, discovered in the majority of crystals with ion-covalent interatomic bonds, including their solid solutions. These 'excess' phonons are located inside the transverse–longitudinal splitting of the main phonons, where the real part of the crystal permittivity is negative, and are split by the crystal field into transverse optical (TO) and longitudinal optical (LO) phonons, the frequencies of 'excess' LO phonons turning out to be lower than those of 'excess' TO phonons.

Solid solution systems like $Zn_{1-x}Cd_xS$, $Zn_{1-x}Cd_xSe$, and $ZnSe_xS_{1-x}$ hold much promise for practical applications, in particular in optoelectronics, due to their unusual physical properties. Structures with quantum wells [1] and quantum dots [2] based on thin layers of these materials, which are candidates for light sources in the blue spectral region, were formed and investigated. Chromium-doped crystals of these materials have proven to show promise for making femtosecond lasers in the near-infrared (IR) region ($\lambda \approx 2.5-3.5$ μm) [3, 4].

The compositional disorder of a solid solution modifies the structural, vibrational, and optical properties of polar crystals. These changes give rise to special features in the lattice dynamics of ternary solid solutions of the substitution type (single-mode, two-mode, or intermediate behavior of the transverse ω_{TO} and longitudinal ω_{LO} vibration frequencies of the system [5]) as well as to the emergence of new modes (local, gap, or resonance (quasiresonance) excitations) and to the defect-induced density of phonon states [6].

In the rigid-ion model [7], for a diatomic crystal of the ZnS type, the phonon frequencies ω_{TO} and ω_{LO} are given by [8]

$$\omega_{TO}^2 = \omega_0^2 - \frac{4\pi}{3}\,\frac{e_B^2(m_1+m_2)}{\sigma m_1 m_2}\,, \tag{1}$$

$$\omega_{LO}^2 = \omega_0^2 + \frac{8\pi}{3}\,\frac{e_B^2(m_1+m_2)}{\sigma m_1 m_2}\,, \tag{2}$$

$$\omega_0^2 = -\frac{m_1+m_2}{m_1 m_2}\sum_l \Phi^N\begin{pmatrix} l \\ +- \end{pmatrix}, \tag{3}$$

where m_1 and m_2 are the positive- and negative-ion masses, l is the cell number, σ is the elementary cell volume, ω_0 is the frequency of triply degenerate atomic vibrations, neglecting long-range Coulomb forces, Φ^N are short-range force constants, which are independent of the ion position relative to the crystal surface, and e_B is the Born effective charge of an ion. The long-range Coulomb ion field in single crystals partly removes the triple degeneracy of a vibration with the frequency ω_0, splitting it into a doubly degenerate vibration (ω_{TO}) and a nondegenerate one (ω_{LO}); the symmetry of atomic vibrations remains unaltered in this case.

As follows from formulas (1) and (2), the frequencies of longitudinal optical phonons should always exceed the transverse phonon frequencies:

$$\omega_{\mathrm{LO}}^2 - \omega_{\mathrm{TO}}^2 = \frac{4\pi e_{\mathrm{B}}^2}{\sigma\mu}\,, \quad e_{\mathrm{B}} = \frac{\varepsilon_\infty + 2}{3}\, e_{\mathrm{S}}^*\,, \tag{4}$$

where μ is the reduced dipole mass, ε_∞ is the crystal permittivity at frequencies much higher than the phonon frequencies, and e_{S}^* is the microscopic Szigeti charge [9] used to describe the crystal lattice dynamics in the rigid-ion model [7, 8].

This clear and coherent picture is disturbed by the existence of special features in the IR reflection spectra of crystals with ion and ion-covalent atomic bonds. Observed in the majority of such crystals, especially in their ternary solid solutions of the $A_{1-x}B_xC$ type where atoms A and B belong to the same group of the periodic table, are excess (additional with respect to the selection rules) optical phonons at the center of the Brillouin zone with inverted frequencies of the longitudinal $\omega_{\mathrm{LO}}^{\mathrm{add}}$ and transverse optical $\omega_{\mathrm{TO}}^{\mathrm{add}}$ phonons: $\omega_{\mathrm{LO}}^{\mathrm{add}} < \omega_{\mathrm{TO}}^{\mathrm{add}}$. In the solid solutions of the polar compounds of the $A_{1-x}B_xC$ type, unlike in the extreme compounds AC and BC, an elementary cell contains not only the base dipoles $A-C$ and $B-C$ but also the $A-B$ dipole, which is an order of magnitude weaker than the base ones [10–18]. Our report is concerned with the investigation of these additional dipoles and their related optical phonons, as well as with an attempt to explain their nature by the example of the monocrystals of $Zn_{1-x}Cd_xS$, $Zn_{1-x}Cd_xSe$, and $ZnSe_xS_{1-x}$ solid solutions.

2. Experiment

The main parameters of the crystal lattice dynamics (the frequencies ω_{TO} and ω_{LO} of optical phonons at the center of the Brillouin zone ($\mathbf{k} \approx 0$), their lifetimes, oscillator strengths, etc.) are derived from the measurements of IR reflection spectra and Raman scattering (RS) spectra [19, 20]. The crystal permittivity, which is related to the majority of the desired parameters, is recovered from the reflection spectrum:

$$\varepsilon(\omega) = \varepsilon_\infty + \sum_{j=1}^{n} \frac{4\pi\rho_{\mathrm{TO},j}\,\omega_{\mathrm{TO},j}^2}{\omega_{\mathrm{TO},j}^2 - \omega^2 - \mathrm{i}\gamma_{\mathrm{TO},j}\,\omega}\,, \tag{5}$$

where $\omega_{\mathrm{TO},j}$, $4\pi\rho_{\mathrm{TO},j}$, and $\gamma_{\mathrm{TO},j}$ are the frequency, the oscillation strength, and the damping constant of the jth transverse mode and ε_∞ is the high-frequency permittivity due to interband electron transitions. In the quasiharmonic approximation, when $\gamma_{\mathrm{TO},j} \ll \omega_{\mathrm{TO},j}$, it is possible to show the validity of the formula [21]

$$\varepsilon^{-1}(\omega) = \varepsilon_\infty^{-1} - \sum_{j=1}^{n} \frac{4\pi\rho_{\mathrm{LO},j}\,\omega_{\mathrm{LO},j}^2}{\omega_{\mathrm{LO},j}^2 - \omega^2 - \mathrm{i}\gamma_{\mathrm{LO},j}\,\omega}\,, \tag{6}$$

where $\omega_{\mathrm{LO},j}$, $4\pi\rho_{\mathrm{LO},j}$, and $\gamma_{\mathrm{LO},j}$ are the frequencies, the oscillation strengths, and the damping constants of the longitudinal optical vibrations (phonons).

The spectral dependences of $\mathrm{Im}\,\varepsilon(\omega)$ and $\mathrm{Im}(-\varepsilon^{-1}(\omega))$ with $\varepsilon(\omega)$ in the form of expressions (5) and (6) each have j peaks at the respective frequencies $\omega_{\mathrm{TO},j}$ and $\omega_{\mathrm{LO},j}$. The width of each peak is equal to the corresponding damping constant: $\gamma_{\mathrm{TO},j}$ or $\gamma_{\mathrm{LO},j}$. In this case, the oscillator strengths of the transverse and longitudinal vibration modes, under the condition that their damping is weak and $\gamma_{\mathrm{TO},j}$, $\gamma_{\mathrm{LO},j} \ll \omega_{\mathrm{TO},j}$, are expressed by the formulas [20]

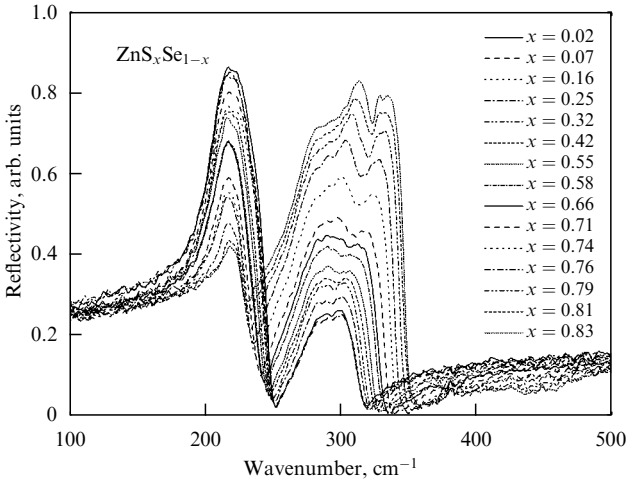

Figure 1. Reflection spectra of a family of $ZnSe_xS_{1-x}$ crystals for a near-normal incidence of radiation [17].

$$4\pi\rho_{\mathrm{TO},j} = \frac{\gamma_{\mathrm{TO},j}}{\omega_{\mathrm{TO},j}}\ \mathrm{Im}\,\varepsilon(\omega_{\mathrm{TO},j})\,, \tag{7}$$

$$4\pi\rho_{\mathrm{LO},j} = \frac{\gamma_{\mathrm{LO},j}}{\omega_{\mathrm{LO},j}}\ \mathrm{Im}\big(-\varepsilon^{-1}(\omega_{\mathrm{LO},j})\big)\,. \tag{8}$$

The crystal permittivity $\varepsilon(\omega)$ may be recovered from the experimental reflection spectrum $R(\omega)$ by means of the integral Kramers–Kronig relations. The parameters ε_∞, $\omega_{\mathrm{TO},j}$, $4\pi\rho_{\mathrm{TO},j}$, and $\gamma_{\mathrm{TO},j}$ may be determined from the measured reflection spectrum of a specimen by selecting them in such a way as to minimize the misfit between the calculated reflection spectrum and the measured one.

For example, Fig. 1 shows the reflection spectra of a family of $ZnSe_xS_{1-x}$ crystals. A feature in the form of a small dip is observed in the high-frequency band of the residual rays (in the ZnS-like modes). In the frequency range between the frequencies ω_{TO} and ω_{LO} of the ZnS-like modes, two additional modes were discovered, one of which (~ 300 cm^{-1}), well visible in the spectra of RS and enhanced due to a Fermi resonance, is attributed to the second-order line, and the other (near 325 cm^{-1}) is attributed to the quasiresonance mode of the atomic Se impurity in ZnS for small x [16, 17].

Figure 2 shows the optical phonon frequencies recovered from IR reflection spectra [16, 17]. The dependence of the ZnS- and ZnSe-like TO and LO modes on the composition of solid solutions is unambiguously interpreted as the double-mode behavior of optical phonons and is in good agreement with the results of previous investigations of optical phonons in $ZnSe_xS_{1-x}$. The additional mode at a frequency close to 325 cm^{-1} has an inverted TO–LO doublet. To verify the possibility that such an impurity vibrational mode exists, the vibration frequencies of an atomic Se impurity in a ZnS crystal were calculated based on the microscopic dynamic theory of a crystal lattice with a low impurity density, developed in [22].

3. Discussion

The vibration frequencies of impurity atoms (in the mass defect approximation) are rather well described by Vinogra-

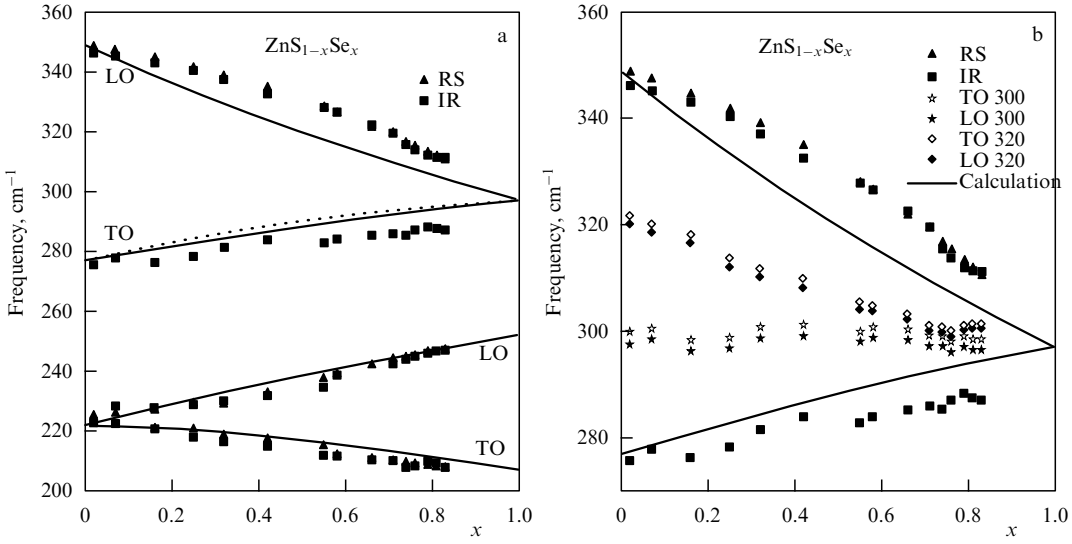

Figure 2. Density dependence of the optical phonon frequencies of $ZnSe_xS_{1-x}$ single crystals derived from IR reflection and RS spectra [16, 17]: (a) main ZnS- and ZnSe-like optical phonons, (b) additional optical phonons inside the LO – TO splitting of the main ZnS-like phonons; between them are two branches of inverted phonons, which converge to the local vibration frequency of sulfur atoms in ZnSe.

dov's theory [22] at densities $x < 0.3$ and $1 - x < 0.3$ [9 – 13, 18] if the optical phonon density-of-state function and the atomic vibration amplitudes of the impurity-free crystal are known. As shown in Ref. [13], in the system of solid solution $Zn_{1-x}Cd_xS$, calculations based on the theory in [22] with the use of the phonon density-of-state function in ZnS from Ref. [23] described the experimental data in Ref. [12] unexpectedly well, without recourse to fitting parameters, throughout the density range, including the frequencies of additional (inverted) phonons. Additional phonons in $Zn_{1-x}Cd_xS$ were attributed to the quasilocal vibrations of Cd atoms in ZnS. These quasilocal vibrations fall within the quasigap in the optical phonon density of states of ZnS [23].

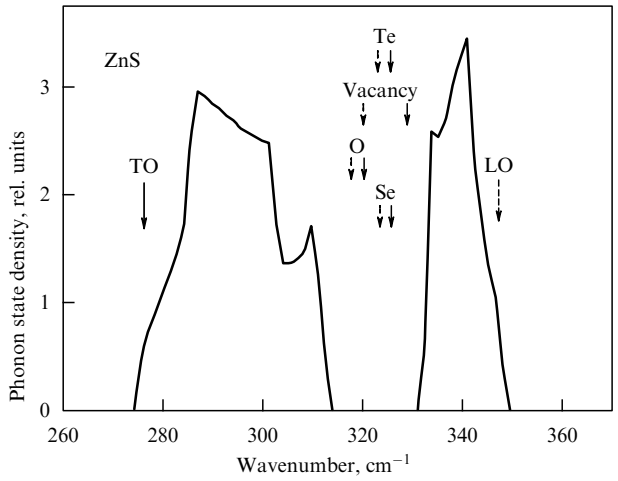

Figure 3. Density of optical phonon states for a cubic ZnS monocrystal [23]. The optical phonon frequencies are $\omega_{TO} = 276$ cm^{-1} and $\omega_{LO} = 350$ cm^{-1}. The vibration frequencies of impurity atoms that replace sulfur atoms, as well as the vibration frequencies of atomic sulfur vacancies, which fall within the quasigap in the density of optical phonon states, are indicated by arrows: solid arrows correspond to transverse vibrations and dashed arrows correspond to the longitudinal vibrations of impurity atoms with a density of 20%.

Figure 3 shows the results of a solution of Vinogradov's equation for impurity atoms of a mass m^*, which replace sulfur atoms in ZnS, with $m^* = 0$ (a sulfur vacancy), $m^* = 16$ (oxygen), $m^* = 79$ (selenium), and $m^* = 127.6$ (tellurium).

An analysis of the known data on the phonon dispersion and phonon density-of-state function in ion-covalent crystals showed that the optical phonon density of states has a dip at frequencies between the LO and TO phonons at the center of the Brillouin zone for virtually all crystals of A^1B^7 and A^2B^6 compounds, as well as for several A^3B^5 crystals. In ZnS, this dip (quasigap), as it were, divides the density of optical phonon states into two parts: transverse optical phonons prevail in the low-frequency part and the longitudinal ones prevail in the high-frequency part. As follows from formula (4), the magnitude of the LO – TO splitting at the center of the Brillouin zone is proportional to the square of the ion charge. The higher the degree of ionicity of a compound, the greater is this splitting. The results of calculation of the optical phonon dispersion throughout the Brillouin zone [23] suggest that the LO–TO splitting at the center of the Brillouin zone may be comparable to (or even exceed) the dispersion of optical phonons over the Brillouin zone for many ionic and ion-covalent crystals, giving rise to a quasigap in the density of optical phonon states.

As follows from formula (4), experimental data allow determining the value of the effective microscopic ion charge e_S^*, which was previously measured for A^2B^6 compounds with an uncertainty of $\pm 0.02e$ [24]: $e_S^*(ZnS) = 0.88\,e$; $e_S^*(ZnSe) = 0.72\,e$; $e_S^*(ZnTe) = 0.65\,e$; $e_S^*(CdS) = 0.87\,e$; $e_S^*(CdSe) = 0.83\,e$; $e_S^*(CdTe) = 0.74\,e$. For a $ZnSe_xS_{1-x}$ alloy, in particular, the difference in the charges of sulfur and selenium ions on substitution of selenium for sulfur atoms is equal to 0.16 of the electron charge. This implies that for a total electroneutrality of a cell of the solid solution crystal, there must be an S – Se dipole with the oscillator strength 10 times lower than for the Zn – S and Zn – Se dipoles, because its charges amount to $\pm 0.08\,e$ rather than to about $\pm 0.8\,e$ as in the extreme compounds. Jahne [18] hypothesized that in the solid solutions of $A_{1-x}B_xC$ com-

pounds, unlike in the binary extreme compounds AC and BC, an A^2B^6 dipole may be present in an elementary cell along with the $A-C$ and $B-C$ dipoles. As is clear from the experimental values of the ion charges of $A-B$ compounds outlined above, an S – Se dipole may exist in the solid solution $ZnSe_xS_{1-x}$.

In the system of $Zn_{1-x}Cd_xSe$ solid solutions, additional inverted phonons were also discovered in the frequency range where the real part of the crystal permittivity is negative: between the principal frequencies of TO and LO phonons [14]. In Ref. [14], the normal vibrations of atoms were also found theoretically in the framework of the isodisplacement model [18, 25], which takes the interaction of ZnSe- and CdSe-like vibrations into account. The main assumption underlying this model is that the anions and cations of the ZnSe (CdSe) groups oscillate in phase with the same amplitude and that every ions experiences forces statistically averaged over all its neighbors. Calculated for $Zn_{1-x}Cd_xSe$ were the density dependences of the optical mode frequencies and oscillator strengths, which were seen to agree with the experimental ones quite well. The amplitudes of atomic displacements were also calculated. It was shown that apart from vibrations related to the Zn – Se and Cd – Se dipoles, there are vibrations under which Se atoms are virtually immobile, while Zn and Cd atoms oscillate relative to each other to make up a weak Zn – Cd dipole.

For $x = 0$, Zn and Se atoms in the principal mode vibrate in antiphase, which is well known for the optical mode in the ZnSe crystal. With increasing x, Cd atoms begin to participate in this vibration, to oscillate in phase with Zn atoms, and their amplitude increases, while the amplitude of atomic Zn vibrations decreases. In this case, the amplitude of atomic Se vibrations depends on the solid solution composition only slightly.

In the quasiresonance mode with inverted LO and TO phonon frequencies, Cd and Zn atoms vibrate in antiphase, while Se atoms are hardly involved in this mode [14]. With increasing x, the amplitude of atomic Cd displacements decreases, but the displacement amplitude of Zn atoms, which vibrate in antiphase to Cd atoms, increases. The dipole moment emerging in these vibrations is defined by the difference between the atomic charges of Zn and Cd ions. This difference is moderate, and the dipole moment of the Zn – Cd vibrations is nearly 10 times smaller than the dipole moment of the principal modes (Zn – Se or Cd – Se). This implies the low oscillator strengths of the Zn – Cd vibrations and the low magnitudes of the RS peaks and the functions $\mathrm{Im}\,\varepsilon(\omega)$ and $\mathrm{Im}(-\varepsilon^{-1}(\omega))$ for the Zn – Cd mode [14, 15].

4. Summary

Because of the different degrees of ionicity of binary solution pairs (the difference in Szigeti charges), there emerge additional weak Zn – Cd dipoles related to relative ion vibrations in the solid solutions $Zn_{1-x}Cd_xS$, $Zn_{1-x}Cd_xSe$, and $Zn_{1-x}Cd_xTe$, and weak S – Se dipoles in $ZnSe_xS_{1-x}$. In the binary solid solutions of $A_{1-x}B_xC$ compounds, unlike in the extreme binary compounds AC and BC, an elementary cell contains not only the base dipoles $A-C$ and $B-C$ but also the $A-B$ dipole, which is an order of magnitude weaker than the base ones. This removes the contradiction related to the initially apparent violation of selection rules.

Additional inverted phonons emerge due to the high degree of ionicity of A^2B^6 compounds, and the magnitude of the transverse–longitudinal splitting of phonons at the center of the Brillouin zone turns out to be sufficiently large in comparison with the phonon dispersion over the entire Brillouin zone. That is why a quasigap, within which the vibrations of impurity atoms fall, emerges in the density of optical phonon states. The vibrations of impurity atoms in the quasigap should be considered quasilocal or quasiresonance, depending on the parameters of the quasigap (its width and depth). In the quasigap region, the real part of the crystal permittivity is negative: the transverse–longitudinal splitting of the quasilocal or quasigap vibrations of impurity atoms turns out to be inverted, i.e., the longitudinal vibrations of impurity atoms are lower in frequency than the transverse ones.

We also note that IR reflection spectra are always recorded from the crystal surface, and the surface layer typically contains numerous stacking faults like vacancies, changes in interatomic distances, and other defects arising from contamination of the crystal surface by adsorbed atoms and molecules. It can be seen from Fig. 3 that the vibration of vacancies may fall within the quasigap in the density of optical phonon states to produce the spectral reflectivity feature under discussion.

References

1. Giugno P et al. *Phys. Rev. B* **54** 16934 (1996)
2. Gasser C et al. *Appl. Phys. Lett.* **72** 972 (1998)
3. Sorokin E, Naumov S, Sorokina I T *IEEE J. Selected Topics Quantum Electron.* **11** 690 (2005)
4. Sorokina I T et al. *OSA Trends Optics Photonics* **98** 263 (2005)
5. Genzel L, Martin T P, Perry C H *Phys. Status Solidi B* **62** 83 (1974)
6. Hayes W, Loudon R *Scattering of Light by Crystals* (New York: Willey, 1978)
7. Kellermann E W *Philos. Tans. R. Soc. London A* **238** 513 (1940)
8. Balkanski M, in *Proc. Intern. Conf. on II–VI Semiconducting Compounds* (Rhode Islands: Flammarion, 1963) p. 1007
9. Szigeti B *Trans. Faraday Soc.* **45** 155 (1949)
10. Vodop'yanov L K, Vinogradov E A, Vinogradov V S *Fiz. Tverd. Tela* **16** 849 (1974) [*Sov. Phys. Solid State* **16** 545 (1974)]
11. Vodopyanov L K, Vinogradov E A *Cryst. Lattice Defects* **5** 125 (1974)
12. Mityagin Yu A, Vodop'yanov L K, Vinogradov E A *Fiz. Tverd. Tela* **17** 2054 (1975) [*Sov. Phys. Solid State* **17** 1341 (1975)]
13. Vinogradov E A, Mityagin Yu A *Fiz. Tverd. Tela* **20** 3162 (1978) [*Sov. Phys. Solid State* **20** 1825 (1978)]
14. Vinogradov E A, Mavrin B N, Vodop'yanov L K *Zh. Eksp. Teor. Fiz.* **126** 866 (2004) [*JETP* **99** 749 (2004)]
15. Vodopyanov L K et al. *Phys. Status Solidi C* **1** 3162 (2004)
16. Vinogradov E A, Mavrin B N, Novikova N N, Yakovlev V A *Fiz. Tverd. Tela* **48** 1826 (2006) [*Phys. Solid State* **48** 1940 (2006)]
17. Vinogradov E A et al. *Laser Phys.* **19** (2) 162 (2009)
18. Jahne E *Phys. Status Solidi B* **74** 275 (1976); **75** 221 (1976)
19. Born M, Huang Kun *Dynamic Theory of Crystal Lattices* (Oxford: Clarendon Press, 1954) [Translated into Russian (Moscow: IL, 1958)]
20. Vinogradov E A, Khammadov I I *Spektroskopiya Ob"emnykh i Poverkhnostnykh Fononov Kristallov* (Spectroscopy of Bulk and Surface Phonons in Crystals) (Tashkent: FAN, 1989)
21. Belousov M V *Fiz. Tverd. Tela* **15** 1206 (1973) [*Sov. Phys. Solid State* **15** 813 (1973)]
22. Vinogradov V S *Fiz. Tverd. Tela* **11** 2062 (1969) [*Sov. Phys. Solid State* **11** 1666 (1969)]
23. Bilz H, Kress W *Phonon Dispersion Relations in Insulators* (Berlin: Springer-Verlag, 1979)
24. Vinogradov E A, Author's Abstract of Thesis for Candidate's Degree (Dolgoprudnyi: MFTI, 1973)
25. Peterson D L et al. *Phys. Rev. B* **33** 1160 (1986)

PACS numbers: 05.30.Jp, **33.20.–t**, **36.40.–c**, 67.25.dw
DOI: 10.3367/UFNe.0179.200903m.0317

Spectroscopy of small helium clusters and 'nanoscopic' superfluidity: He_N–CO, $N = 2–20$...

B S Dumesh, A V Potapov, L A Surin

1. Introduction

Studies of clusters attract considerable attention of researchers, because they allow building bridges between the quantum microcosm and the thermodynamic macrocosm. In recent years, much success has been achieved in the study of small clusters consisting of several atoms or molecules bound by van der Waals forces. Such clusters can be comparatively easily produced in the expansion of a supersonic gas jet into a vacuum. It is significant that their spectroscopic research can be conducted in the region of the wide expansion of the jet, where atomic collisions are very rare and the spectral linewidth approaches the Doppler limit. Consequently, the lines of different clusters can be easily resolved, thus permitting tracing the dependence of different physical properties of clusters on their size or composition.

Spectroscopic studies of small helium clusters with an embedded molecule of a chromophore have been developed quite actively in the last few decades. These studies are based on direct measurements of spectra, both purely rotational and vibrational–rotational, in the region of some fundamental vibration of the chromophore, which are then used to determine the effective moment of inertia of the embedded molecule and its virbration frequency shift caused by the interaction with surrounding helium atoms. To date, systems such as He_N–X, where X is a molecule of OCS [1], CO_2 [2], N_2O [3, 4], CO [5–7], or HC_3N [8] and N smoothly varies from 2 to ≈ 70, have been studied. These clusters are formed at a finite temperature of the helium jet as low as 0.3–0.1 K. Because the binding energy of all the above molecules — chromophores with helium clusters — is sufficiently small, the resultant clusters are not solid but liquid, and a nonmonotonic dependence of the effective moment of inertia on the number of attached helium atoms is observed for all these molecules. This means that for the number of helium atoms larger than a certain value N, the chromophore rotation with part of the attached helium atoms relative to the remaining helium environment proceeds with sliding. This sliding motion seems to be essentially dissipation-free, because no additional broadening of spectral lines is observed and their widths are such that the molecule appears to accomplish at least 10^5 revolutions without any signs of dissipation. This phenomenon strongly resembles superfluidity and it is this feature that caused a great interest in these investigations. A review of the early experiments was published in [9].

On the other hand, numerous spectral measurements of chromophore molecules in helium droplets [10, 11] (nanodroplets, which contain more than a thousand helium atoms at the temperature ≈ 0.35 K) have been carried out recently. Under these conditions, ^{4}He is certainly in a superfluid state and the results obtained give the limiting values of the spectroscopic parameters as the cluster size increases. The most spectacular feature that distinguishes superfluid helium from other liquids is the well-resolved rotational structure in the spectra of molecules embedded into it. As a rule, the measured moment of inertia is several times larger than the moment of inertia in the gas phase. This means that the rotating molecules become covered with a significant helium 'coat' during rotation.

An exception is given by light molecules such as HCN and CO, whose moment of inertia increases by only about 20% and the effective size of the 'coat' is less than one helium atom. It is significant that in droplets consisting of ^{3}He with the temperature ≈ 0.15 K, the vibrational lines of the embedded molecules are sufficiently wide and the rotational structure is completely 'washed out.' In the experiments with helium droplets consisting of a mixture of ^{3}He and ^{4}He, a thermodynamic limit for the appearance of superfluidity was also established, i.e., the minimum number of ^{4}He atoms ($N_{\min} \approx 60$) necessary for the separation of the isotope solution was evaluated [12].

The properties of small clusters, naturally, depend on the parameters of the interaction between helium and the chromophore molecule, and the nearer their binding energy to the chemical potential of liquid helium (7.5 K), the less the disturbance of the helium environment caused by the molecule. From this standpoint, a unique species is the CO molecule, with its binding energy with helium equal to 9 K; already in the He–CO binary complex, the CO molecule rotates almost freely [13, 14]. At present, the He_N–CO system is the only one in which two types of rotation of the embedded molecule are observed: almost free within the cluster; and together with the surrounding helium. The presence of two types of rotation, in addition to being very interesting by itself, allows obtaining additional information on the properties of clusters.

Studying He_N–CO clusters is also important for the problem of hydrogen superfluidity. In 1972, Ginzburg and Sobyanin showed theoretically that liquid parahydrogen could pass into a superfluid state at $T \approx 6$ K if it did not become solid at $T \approx 13.6$ K [15]. After this, searches began for metastable states of liquid parahydrogen with sufficiently low solidification points. It is known that the freezing point is strongly reduced in small clusters; indeed, experiments showed that hydrogen clusters with the number of hydrogen molecules $N < 50$ formed in a supersonic gas jet are liquid rather than solid [16]. In clusters of $(paraH_2)_N$ – CO with $N = 7–17$, a dissipation-free sliding upon the rotation of CO molecules was discovered [17], which indicates a common nature of phenomena observed in these clusters and in small helium systems.

In this report, we consider spectral studies of small He_N–CO clusters. Because sufficiently low temperatures are required for obtaining such clusters, only the lowest rotational level of the molecule with an angular momentum $J = 0$ proves to be populated and only transitions from this level, i.e., $J = 1–0$, are observed. The frequency of one of these transitions lies near the free rotation frequency of CO (115 GHz); the other transition in small clusters lies in the range of centimeter wavelengths. Two analogous transitions are observed near the fundamental vibration of the CO molecule (in the region of 2100 cm^{-1}). Specifically, it was these transitions that were first investigated in these clusters [5, 6]. Unfortunately, it is impossible to independently determine two rotational constants and the fundamental vibration frequency of CO in the cluster from the positions of these two measured transitions. Therefore, the very interesting results of these works have rather a qualitative

nature, while direct measurements of frequencies of the rotational transitions are necessary for obtaining quantitative characteristics.

2. Experimental methods

As was already mentioned above, helium clusters are formed in a cold supersonic gas jet. To obtain such a jet, a mixture of gaseous helium with a small admixture of chromophore molecules (0.01%) is directed through a supersonic nozzle with a characteristic diameter of the opening of 0.5 – 1 mm into a vacuum chamber, where the jet expands adiabatically. At a sufficiently large rate of evacuation of the chamber, which ensures the residual gas pressure of the order of 10^{-3} Torr, the efficiency of cooling is mainly determined by the initial pressure and temperature. At the initial pressure 50 atm and the nozzle kept at room temperature, the final temperature of the helium jet reaches 0.3 K, and when cooling the nozzle by liquid-nitrogen vapors, even 0.1 K [5]. To ensure a combination of the necessary fluxes of the gas in the jet with reasonable pumping rates of the vacuum chamber, the nozzle works in the regime of short pulses. For this purpose, a magnetic valve is established before the nozzle entrance; is opened to admit the flow of gas for a period of the order of 1 ms. An oil booster pump with the pumping rate 1000 l s^{-1} creates the necessary vacuum in the chamber at the pulse repetition frequency of the order of 1 Hz.

The spectral studies of helium clusters and binary complexes have been conducted in the infrared (IR) range (McKellar's group, Ottawa), in the centimeter range (Jäger's group, Edmonton), and in the millimeter-wave range (Russian – German group, Troitsk – Cologne) of wavelengths. Because the spectral linewidths in the supersonic jet are close to the Doppler limit, all the measurements have been carried out on spectrometers with coherent radiation sources and high spectral resolution.

A more complicated problem is to reach a sensitivity for registration of weak lines necessary for such experiments. To obtain the necessary temperatures, the content of a chromophore in helium must be low, and the concentration of the formed clusters must be less than 0.1% from that of the chromophore. The sensitivity of the usual single-pass spectrometers is too low for detecting such weak signals; schemes with a multiple pass of radiation through the supersonic jet must be used. In the IR range, a spectrometer based on diode lasers with a toroidal system of mirrors is employed, which ensures more than a hundred passages of the laser beam through the jet [18]. In the millimeter and centimeter ranges, such multipass schemes are unrealistic because of the long wavelength of the radiation, and the only method to achieve the required sensitivity is to pass the jet through a radiation-filled high-Q open resonator. Highly sensitive pulsed Fourier spectrometers in the centimeter range have been developed, which are combined well with open resonators. The installation used in Jäger's group belongs to this type, in particular [19].

Unfortunately, these spectrometers are ineffective in the millimeter-wave range because sufficiently powerful radiation sources with a large frequency tuning are absent at present. In our group, we have developed an intracavity spectrometer [20] based on a domestic wide-range oscillator in the millimeter range, the so-called orotron [21]. The spectrometer developed has its own radiation-frequency-driving open resonator, through which the gas to be investigated can be passed. As a result, about hundred effective passages of radiation through the jet can be obtained, which ensures a sufficiently high spectrometer sensitivity.

Owing to the high spectral resolution, the spectral lines that refer to different clusters do not overlap and can be analyzed separately. Furthermore, it is very important that the optimum temperature of cluster formation monotonically decrease with increasing the cluster size. Therefore, the intensities of spectral lines pass through a maximum with decreasing the temperature (with increasing the initial pressure of the gas and/or cooling of the nozzle). Based on the position of this maximum, a given spectral line can be referred to a cluster of specific composition.

Of great service in the identification of complex spectra is the double-resonance method. If one of the two transitions in a three-level system is saturated, the populations of all levels change and, correspondingly, the intensity of radiation absorbed in another transition also changes. Consequently, by tuning the spectrometer to the second transition, it is possible to detect the absorption of radiation from an additional source at the first transition based on a change in the signal of the spectrometer. Along with the selection of the pairs of transitions that relate to three-level systems, the double-resonance method allows effectively extending the relevant spectral range and recording transitions from levels whose thermal population is too low to be observed directly. An orotron-spectrometer-based setup for observing double resonance is described in [22].

3. Experimental results

The frequencies of purely rotational $J = 1-0$ transitions in $^4He_N - CO$ clusters are given in Fig. 1. All the high-frequency lines have been measured using the orotron spectrometer, and the low-frequency lines in clusters with $N \leqslant 7$ were measured

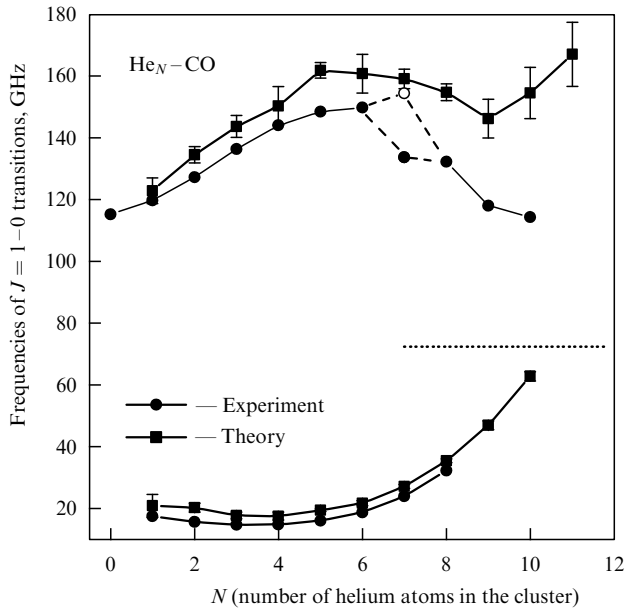

Figure 1. Measured (•) and calculated (■) [23] frequencies of $J = 1-0$ transitions in $He_N - CO$ clusters. The frequency of the upper component in the $He_7 - CO$ cluster (○) was determined from the IR data [5] with allowance for the shift of the CO vibration obtained in [7]. The dotted line shows the value of $2B$ in helium droplets [24].

using the pulsed Fourier spectrometer. The corresponding line in $^4He_8-CO$ that lies higher than the Fourier spectrometer range is registered on the orotron spectrometer using the double-resonance technique. The low-frequency transitions correspond to the rotation of a molecule together with a helium coat, and their frequency is inversely proportional to the moment of inertia of CO with the attached helium coat. The moment of inertia increases upon attaching up to three helium atoms to the molecule, and then begins decreasing; hence, the sliding upon the rotation of the molecule begins in a $^4He_N-CO$ cluster that contains four helium atoms. Subsequently, the transition frequency increases smoothly and at $N \geqslant 6$ exceeds its value in ^4He-CO. This means that in clusters with $N \geqslant 6$, the effective size of the coat is less than one helium atom.

The frequency of high-frequency transitions first increases with increasing the cluster size, passes through a maximum at $N = 6$, 7, and then decreases. In a cluster with $N = 7$, the transition line in the IR spectrum splits into two components. We could register only one line, but its proximity to the position of the lower component predicted on the basis of IR data suggests that the splitting also exists in the fundamental vibrational state of $^4He_7-CO$.

For describing the observed rotations of a CO molecule in helium clusters, the following qualitative model can be suggested. Because the interaction potential is independent of the azimuthal angle, a helium cluster has an almost cylindrical symmetry. The rotation axis of CO is parallel to the cylinder axis during low-frequency rotations and is perpendicular to it in high-frequency rotations. Because the helium atoms are attracted predominantly to the oxygen end of the molecule [13], the helium environment is deformed near this end; this deformation accompanies the low-frequency rotation of CO and makes a contribution to the measured moment of inertia. As the number of helium atoms increases, the cluster becomes more rigid and its deformation decreases. The transition frequency increases until the first coordination shell is filled up, which is indeed observed in the IR range [5].

In a high-frequency rotation, the role of the helium environment reduces to increasing the anisotropy of the potential of interaction with CO, which leads to an increasing transition frequency. This phenomenon can be described in the framework of the perturbation theory developed for ^4He-CO in [13] using realistic values of the relevant constants. However, in clusters with a filled coordination shell, the difference between the two rotations disappears and their frequencies must be close. Therefore, as the number of helium atoms in a cluster approaches $N \approx 13$, 14, the frequency of the high-frequency transition is reduced.

Figure 1 also gives the results of the calculations of excitations in the $^4He_N-CO$ system obtained by the diffusion Monte Carlo method [23]. The results of calculations satisfactorily describe the behavior of the low-frequency branch, although the calculated values are somewhat overstated. Things are worse in the case of the high-frequency branch. The experimental frequencies in clusters with $N = 8-10$ decrease monotonically, whereas the theory predicts their increase in this region. The fundamental question here is whether the transition frequencies in large clusters remain sufficiently high, as the calculations predict, or both rotation branches merge. As an experimental indication of the possibility of the second scenario, we note a doubling of the line of the $J = 1-0$ transition in the $^4He_{15}-CO$ cluster observed in the IR range [5].

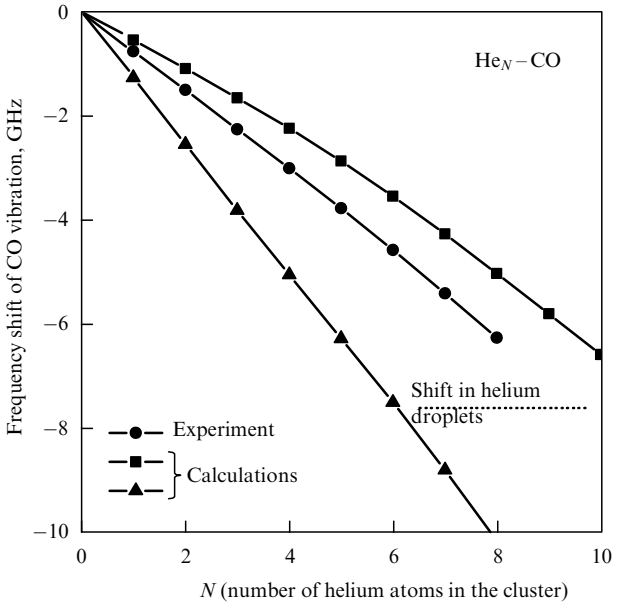

Figure 2. (•) Experimentally determined frequency shift of CO vibration in He_N-CO clusters. The results of the theoretical calculations of the shift (■, ▲) are taken from Ref. [23]. The dotted line shows the value of the shift in helium droplets [24].

From a comparison of the microwave and IR spectral data, it is possible to determine the frequency shift of the fundamental vibration of CO in the helium clusters; the data obtained are given in Fig. 2 together with the results of calculations based on different interaction potentials for ^4He-CO [23]. The dependence of the frequency shift on the number of helium atoms in a cluster is almost linear, in contrast to that in helium clusters based on CO_2, N_2O, and OCS [1–4]. In the latest systems, a change is observed in the sign of the frequency shift at $N = 5$, which is ascribed to the filling of the rigid ring with helium on the equator of these molecules and by the arrangement of the other helium atoms on the periphery of the chromophore molecules. The monotonic character of the shift of the vibration frequency in the clusters based on CO indicates the diffuse nature of the cluster structure, with no essential differences in the arrangement of different atoms. The experimental results are described by the theory qualitatively well, but obtaining a quantitative correspondence requires refining the ^4He-CO interaction potential.

Figure 2 also shows the shift in the frequency of the fundamental vibration of CO in helium droplets that was obtained in [24]. This shift proved to be very small; it approximately corresponds to the value obtained by the extrapolation of our data to the case of $^4He_{10}-CO$. Because there are no reasons for the change in the nature of the dependence of the frequency shift on the number of helium atoms until the first coordination shell is filled, the shift in these clusters is larger (in absolute value) than in droplets. Therefore, we should either expect a change in the sign of the dependence of the frequency shift on the number of helium atoms in large clusters or suppose that the procedure for determining it used in [24] is not entirely correct.

Figure 3 depicts the dependences of the effective rotational constant B (inverse of the moment of inertia of a molecule with a helium coat) on the number of helium atoms in the cluster for all the $^4He_N-X$ systems investigated to date, where X is OCS [1], CO_2 [2], N_2O [3], CO, or HC_3N [8]. The

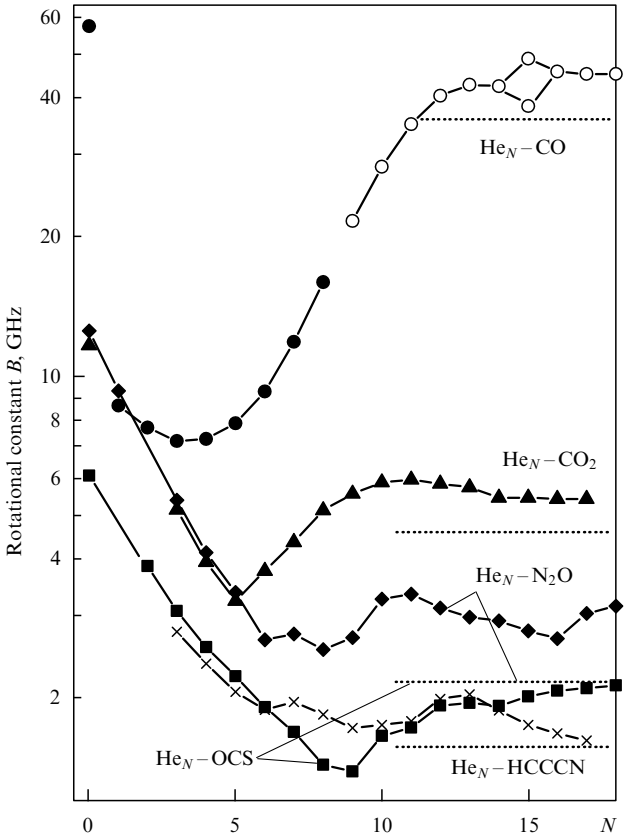

Figure 3. Dependence of the effective rotational constant B of different chromophore molecules on the number N of helium atoms in a cluster. The dotted lines show the limit values of B found in helium droplets.

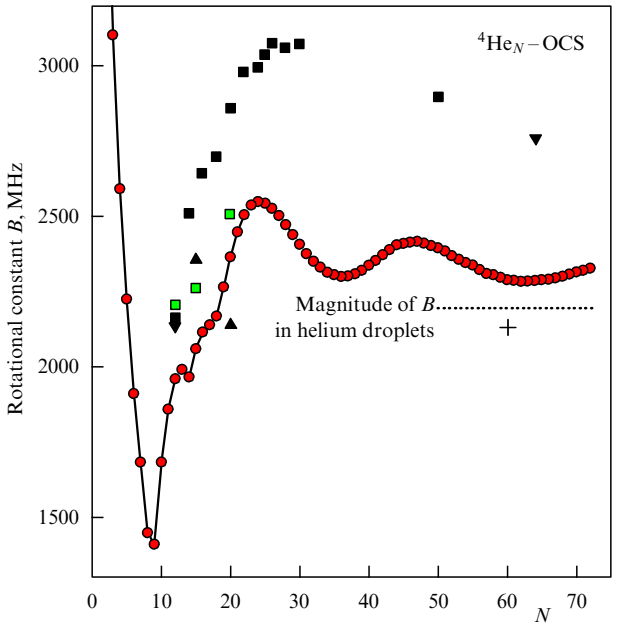

Figure 4. Dependence of the rotational constant B of an OCS molecule on N for ^4He_N clusters [1].

data for $^4He_N-CO$ with $N \leqslant 8$ have been obtained from the frequencies of the low-frequency rotational transitions [7] and those with $N > 8$, by extrapolation [5] under the assumption of the linearity of the frequency shift of the CO vibration obtained in [7]. In all the systems with the number of helium atoms exceeding a certain value, an increase in the rotational constant (a decrease in the moment of inertia) is observed; this phenomenon appears the earlier, the less the binding energy of helium with the molecule. The 'record holder' is the $^4He_N-CO$ system, in which the decrease in the moment of inertia begins at $N = 4$, and the effective size of the coat, beginning from $N = 6$, becomes less than one helium atom. At the same time, it can be supposed that other molecules can have a 'coat' consisting of several helium atoms and that such a relatively rigid formation rotates inside the remaining helium cluster.

A decrease in the momentum of inertia with increasing the cluster size resembles the Andronikashvili effect [25], consisting in a nonentrainment of superfluid helium with bodies that move in it. It is also significant that with a further increase in the cluster size, the frequency of rotation of chromophore molecules smoothly tends to a limit characteristic of superfluid helium in droplets, which is demonstrated in Fig. 4 using the He_N-OCS system with $N = 2-70$ as an example [1]. A natural question arises regarding the relation of the phenomena observed in small helium clusters to superfluidity. By its properties, helium in a cluster resembles a quantum liquid in which single-particle excitations that can lead to relaxation are absent. Otherwise, an additional broadening of spectral lines would be observed. At the same time, around ten atoms is certainly insufficient for the formation of a quasi-continuous spectrum of the Bose type, and the absence of relaxation is most probably related to the discrete character of the spectrum of excitations of a small cluster. Therefore, the phenomena observed in small clusters can be treated in terms of 'nanoscopic superfluidity,' which substantially differs from classical superfluidity. Analogous remarks also refer to 'hydrogen superfluidity,' which is observed in $(paraH_2)_N-CO$ clusters at $N = 7-17$ [17]. Nevertheless, in a number of works [26, 27], the properties of small helium clusters are treated in terms of fractions of the normal and superfluid helium components, which is unjustified in our opinion.

4. Conclusions

Ya B Zel'dovich once formulated a question: "How many helium atoms are necessary for a droplet to arise?"

It seems that there is no unambiguous answer to this question, and the differences that characterize the physical properties of a droplet begin to manifest themselves at different numbers of atoms. Thus, according to estimations, for a quasicontinuous spectrum of elementary excitations to form, the number of atoms required is of the order of 100, while for the development of sliding upon rotation of a chromophore molecule, only four atoms suffice.

One more question arises: whether analogous dissipation-free sliding upon rotation of a chromophore molecule also exists in fermionic clusters as long as they are so small that excitations of the particle–hole type that can impede the superfluidity are absent. We believe that the answer to this question can be found in the studies of rotational spectra in $^3He_N-CO$ clusters. We plan to perform these studies in the near future.

This work was supported in part by the Russian Foundation for Basic Research grants Nos 06-02-16035 and 08-02-91966 and Deutsche Forschungsgemeinschaft grants Nos 436 RUS 113/946/0-1 and SU 579/1-1. A.V.P also is grateful to the Russian Science Support Foundation (a grant for Candidates of Science of the Russian Academy of Sciences).

References

1. McKellar A R W, Xu Y, Jäger W *J. Phys. Chem. A* **111** 7329 (2007)
2. McKellar A R W *J. Chem. Phys.* **128** 044308 (2008)
3. Xu Y, Blinov N, Jäger W, Roy P-N *J. Chem. Phys.* **124** 081101 (2006)
4. McKellar A R W *J. Chem. Phys.* **127** 044315 (2007)
5. Tang J, McKellar A R W *J. Chem. Phys.* **119** 754 (2003)
6. McKellar A R W *J. Chem. Phys.* **125** 164328 (2006)
7. Surin L A et al. *Phys. Rev. Lett.* **101** 233401 (2008)
8. Topic W et al. *J. Chem. Phys.* **125** 144310 (2006)
9. Dumesh B S, Surin L A *Usp. Fiz. Nauk* **176** 1137 (2006) [*Phys. Usp.* **49** 1113 (2006)]
10. Toennies J P, Vilesov A F *Angew. Chem. Int. Ed.* **43** 2622 (2004)
11. Makarov G N *Usp. Fiz. Nauk* **174** 225 (2004) [*Phys. Usp.* **47** 217 (2004)]
12. Grebenev S, Toennies J P, Vilesov A F *Science* **279** 2083 (1998)
13. Chuaqui C E, Le Roy R J, McKellar A R W *J. Chem. Phys.* **101** 39 (1994)
14. Surin L A et al. *J. Chem. Phys.* **112** 4064 (2000); "Errata" *J. Chem. Phys.* **112** 9190 (2000)
15. Ginzburg V L, Sobyanin A A *Pis'ma Zh. Eksp. Teor. Fiz.* **15** 343 (1972) [*JETP Lett.* **15** 242 (1972)]
16. Tejeda G et al. *Phys. Rev. Lett.* **92** 223401 (2004)
17. Moroni S et al. *J. Chem. Phys.* **122** 094314 (2005)
18. Brookes M D et al. *Spectrochim. Acta A* **60** 3235 (2004)
19. Xu Y, Jäger W *J. Chem. Phys.* **106** 7968 (1997)
20. Surin L A et al. *Rev. Sci. Instrum.* **72** 2535 (2001)
21. Rusin F S, Bogomolov G D *Pis'ma Zh. Eksp. Teor. Fiz.* **4** 236 (1966) [*JETP Lett.* **4** 160 (1966)]
22. Surin L A et al. *J. Mol. Spectrosc.* **222** 93 (2003)
23. Škrbić T, Moroni S, Baroni S *J. Phys. Chem. A* **111** 7640 (2007)
24. von Haeften K et al. *Phys. Rev. B* **73** 054502 (2006)
25. Andronikashvili E L *Zh. Eksp. Teor. Fiz.* **16** 780 (1946); **18** 424 (1948)
26. Paesani F, Kwon Y, Whaley K B *Phys. Rev. Lett.* **94** 153401 (2005)
27. Paesani F et al. *J. Chem. Phys.* **122** 181106 (2005)

PACS numbers: **61.43.–j**, **78.47.–p**, **78.55.–m**
DOI: 10.3367/UFNe.0179.200903n.0322

Single molecules as spectral nanoprobes for the diagnostics of dynamic processes in solid media

A V Naumov, Yu G Vainer

In this report, we briefly review the results of works directed at the development and use of the method of single-molecule spectroscopy (SMS) for investigating dynamic processes in disordered solid-state media.

The first optical experiments on the detection of single-quantum systems were carried out in the mid-1970s in the gas phase with rarefied atomic beams and single ions in electromagnetic traps [1]. An important step in the way of recording spectra of single molecules (SMs) in condensed media was the development of methods of selective laser spectroscopy of impurity centers, i.e., the method of the excitation of fine-structure fluorescence spectra and of burning-out stable spectral holes [2]. We note that both these scientific avenues were developed for the first time at the Institute of Spectroscopy, Russian Academy of Sciences (ISAN).

The first experimental electronic absorption spectra of single chromophore molecules introduced into a solid-state matrix were observed by Moerner and Kador in 1989 [3]. Soon after this, in 1990, Orrit and Bernard [4] showed that when recording individual spectra of SMs by the method of excitation of fluorescence spectra in the optical range, the signal-to-noise ratio radically increases in comparison with the case of absorption spectra [4]. The possibility of the direct measurement of optical spectra of SMs in solid-state matrices opened the way to setting up various experiments. Since that time, systematic studies of condensed media with the application of the SMS method (see [5] and the references therein) have begun. This area of studies is being vigorously developed now. According to the Web of Science (database of the Institute of Scientific Information, USA), the number of scientific publications devoted to this field in the journals analyzed by the Web of Science was more than 1300 in 2007 alone.

One of the most promising avenues of the SMS method in studies of the properties of condensed media is the use of isolated impurity molecules as spectral nanoprobes for obtaining information on dynamic processes in the local environment of these molecules. The main idea of this approach is that the parameters of an electron transition of an impurity chromophore molecule embedded into a solid-state matrix are very sensitive to the parameters of the local environment of the molecule. The inertialess nature of this spectral probe allows conducting studies with a maximally high time resolution (up to several femtoseconds), and the smallness of the probe dimensions allows obtaining information about the medium on a nanoscopic scale. As a consequence, the optical spectra of impurity molecules contain unique data on the local structure of the matrix and, most importantly, on dynamic processes that occur in the nearest vicinity of such molecules.

The most important advantage of the SMS method is that it allows completely removing the effect of ensemble averaging over a large number of impurity centers, which is inherent in conventional methods of selective laser spectroscopy. Moreover, in contrast to the known methods of investigating the dynamics of solid-state media (based on acoustic or thermodynamic measurements, or on the registration of Raman spectra, inelastic neutron scattering, etc.), the SMS method allows investigating dynamic processes at the level of single molecules and, thus, almost completely removing the averaging over the volume of the sample investigated. This advantage plays a fundamentally important role in the investigations of strongly disordered solid-state media (glass, polymers, polycrystals, nanostructured objects, biological media, and other complex systems), because in such media, as a result of the significant microscopic inhomogeneity of the substance, the parameters and the nature of the local dynamics can differ radically at different points of a sample.

We consider the basic ideas of the low-temperature dynamics of disordered solid-state media in more detail. Numerous studies have demonstrated that at low temperatures, the dynamic characteristics of such media differ significantly from the appropriate properties of crystals. It has also been proved that the observed anomalous properties of disordered media have a universal nature and are practically independent of the concrete structure and chemical composition of the substance. In the specialized literature, diverse disordered media frequently are therefore simply called glasses.

In 1971 [6, 7], a fruitful idea was proposed on the existence of specific elementary low-energy excitations in such disordered solid-state media, namely, of so-called tunneling

two-level systems (TLSs). According to the model suggested in these works, which was called the standard model of low-temperature glasses, the jumps in the TLSs (the tunneling transitions initiated by phonons of groups of atoms or molecules between two lower levels in double-well energy potentials) make the basic contribution to the dynamics of glass at temperatures $T < 1$ K.

The model of TLSs allows describing the majority of dynamic phenomena in glasses observed at temperatures $T < 2-3$ K. The anomalous dynamic properties of glass that are manifested at higher temperatures (up to several tens of kelvins) are usually ascribed to the presence of *quasi-localized low-frequency vibrational modes* (LFMs) in disordered solid-state media (see, e.g., [8–12]), the modes that can be regarded as vibrations of groups of atoms or molecules in a single-well potential.

The soft-potential model (SPM) describes the TLSs and LFMs in the framework of a common approach [13, 14] and can be considered a generalization of the TLS and LFM models. The soft-potential model allows describing the dynamics of glasses in a wider temperature range than the standard model of glasses. However, this model, which is finding ever increasing acceptance among researchers, just like the TLS model, is purely phenomenological and cannot describe all dynamic phenomena observed in glass.

To describe the effect of jumps in a TLS on the electronic transition frequency (and therefore on the optical spectrum) of an impurity molecule a very simple model called the *stochastic random-jump model* is widely used [15]. For a more rigorous analysis of a TLS–chromophore-molecule interaction, some authors use the dynamic approach (see, e.g., [16]). In the stochastic model, the transitions in a TLS adjacent to the chromophore molecule lead to sharp changes in the frequency of the electron transition of this molecule. The transition frequency of a single molecule at an instant t is determined by the totality of *independent* transitions in all TLSs surrounding this molecule:

$$\omega(t) = \omega_0 + \sum_j \zeta_j(t)\, \upsilon_j \,, \tag{1}$$

where the stochastic variable $\zeta_j(t) = 0$ ($\zeta_j(t) = 1$) if the jth TLS at the instant t is in the ground (excited) state and ω_0 is the frequency of the 0–0 transition of the SM under the condition that all TLSs that interact with the SM are in the ground state. In the case of a dipole–dipole type of the TLS–chromophore-molecule interaction, the quantity υ_j is expressed as

$$\upsilon_j \sim \frac{\Delta\mathbf{M}_j\, \Delta\mathbf{M}_{\mathrm{OM}}}{r_j^3} = 2\pi\Lambda\, \frac{A_j\, \varepsilon_j}{E_j\, r_j^3} \,, \tag{2}$$

where $\Delta\mathbf{M}_j$ is the change in the dipole moment of the TLS caused by its jump, $\Delta\mathbf{M}_{\mathrm{OM}}$ is the change in the dipole moment of the impurity molecule caused by its transition from the ground to the excited state, r_j is the distance between the TLS and impurity molecule, Λ is the constant of the TLS–chromophore interaction, ε_j is the orientational parameter, A_j is the parameter of asymmetry of the TLS, and E_j is the energy splitting of the TLS.

In the experiment, the interaction between an SM and an active TLS is manifested (depending on the relation between the characteristic frequency of jumps and the time of measurement) as spectral jumps or a broadening of spectral lines, as well as in the form of spectrum splitting.

The observed width of a separate spectral peak is determined by the interaction of the chromophore with vibration-type excitations (LFMs and acoustic phonons) and with a large quantity of remote TLSs. A quadratic electron–phonon interaction of the chromophore with the LFM leads to a uniform broadening Γ and a frequency shift of spectral peaks in the spectrum of the SM. The broadening Γ is usually described by a formula [16] that is valid in the case of a weak LFM–chromophore coupling,

$$\Gamma = \frac{w \exp(-\Delta E/kT)}{\left[1 - \exp(-\Delta E/kT)\right]^2} \,, \tag{3}$$

where ΔE is the energy of the LFM, w is the constant of the quadratic LFM–chromophore interaction, and k is the Boltzmann constant. Thus, the spectrum shape of the impurity molecule, as well as the temperature and time dependences of its characteristics, contains information on the parameters of elementary excitations in the local environment of this molecule and on the interaction of these excitations with this molecule.

In spite of the significant effort expended in the study of the low-temperature dynamics of glass, the majority of fundamental questions in this field remain open. First of all, this concerns the microscopic nature of the dynamic processes that occur in such media (in particular, the microscopic nature of TLSs and LFMs). The problems of the applicability limits of the models suggested (the overwhelming majority of which are purely phenomenological); the problems of phenomena observed in some experiments that cannot be described in the framework of these models; and the problem of the connection between the local dynamics of glass and the concrete structure and chemical composition of the medium studied remain unsolved.

Single-molecule spectroscopy revealed unique possibilities to achieve essential progress in resolving these problems, because this method allows investigating the dynamics of the medium at the level of single molecules (up to the measurement of the individual parameters of single elementary excitations). The first measurements [17] of spectra of SMs in an amorphous polymer carried out in 1994 already afforded the first direct experimental proof of the existence of tunneling TLSs in such media.

Unfortunately, the development of the SMS as the method of studying the dynamics of complex disordered solid-state systems met with a number of essential difficulties, namely, the low value of the signal-to-noise ratio realizable in such measurements, which is determined by the smallness of the light signals coming from one molecule; the presence of the incidental radiation of the matrix; the presence of phonon wings in the individual spectra of molecules; and, as a result, quite a long time necessary for the reliable registration of the signal. Some difficulties were also related to the limited number of impurity systems in which it was possible to register the spectra of SMs. Significant problems appeared upon analysis and interpretation of the spectra. In particular, serious problems appeared in attempts at a correct statistical processing of the experimental spectra of SMs because of an insufficient elaboration of the corresponding procedures.

In the series of works performed in 2000–2008 that are discussed in this report, we substantially developed the procedure for registering SM spectra and a whole series of techniques for analysis of the data obtained, including the

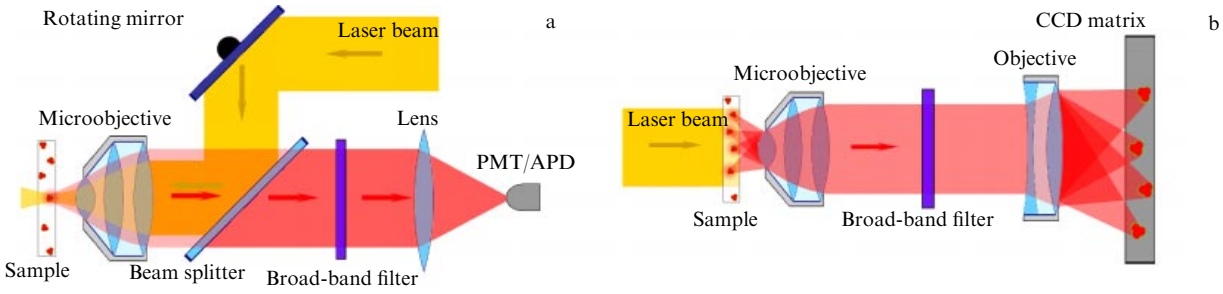

Figure 1. Schemes for the registration of the excitation spectra of SM fluorescence: (a) single-channel scheme with the use of a photomultiplier (PMT) or an avalanche photodiode (APD); and (b) multichannel scheme with a highly sensitive matrix photodetector based on a cooled CCD matrix (CCD: charge-coupled device).

procedure for the multichannel registration of the excitation spectra of the fluorescence of SMs and for the computer processing of the images of these molecules, as well as the procedure for statistical analysis of the parameters of a large number of SM spectra. This allowed eliminating many important problems of using SMS for studying the dynamics of impurity solid-state media and thus allowed achieving significant progress in the study of the fundamental laws that govern the low-temperature dynamics in disordered solid-state media (organic glasses and polymers).

Until recently, schemes of registration of signals with a single-channel photodetector [18] (photomultiplier or avalanche photodiode) were typically used for the experimental registration of the fluorescence excitation spectra of SMs in solid-state media. In recent years, experimental SMS installations for measurements at low temperatures have been constructed based on a confocal microscope. A typical setup with single-channel photodetection in a confocal regime is outlined in Fig. 1a. For the excitation of a fluorescence spectrum, a single-frequency tunable laser whose beam is focused on the sample by means of a high-aperture microobjective is typically used. The fluorescent radiation is collected with the same microobjective and is directed to the photodetection system. Broad-band interference filters and/or cutting-off light filters reject the scattered laser radiation with the nonshifted frequency and transmit the Stokes component of the fluorescence spectrum of the detected molecules. Then the radiation is directed onto the photosensitive surface of the single-channel photodetector.

Usually, *the excitation spectra of SM fluorescence* (the dependence of the integrated intensity of the SM fluorescence on the frequency of the exciting laser radiation) are recorded in experiments; these spectra can be considered the equivalent of the absorption spectrum. Retuning to provide measurements in another region of the sample in this scheme is achieved by a displacement of the sample or with the aid of a scanning mirror.

The spectra of SMs in amorphous media at low temperatures can consist of several peaks and vary randomly in time. The complex and mainly random shape of the SM spectra is caused by transitions in nearest TLSs and by any other structural rearrangements in the matrix in the local environment of an SM. A much more informative and more convenient method of measurement of such spectra is the use of a technique of a frequently repeated registration of the excitation spectra of SM fluorescence in a selected spectral range [19]. The results of such measurements are usually represented in the form of a two-dimensional pattern (2D plot), a kind of 'time topograph' of the measured spectra (Fig. 2).

An analysis of such a two-dimensional picture allows unambiguously identifying spectral peaks that belong to different SMs [20–22]. Indeed, a transition in one TLS sufficiently 'strongly coupled' to a given SM manifests itself in the form of simultaneous and identical jumps in all spectral peaks that belong to the spectrum of this SM. At the same time, this transition either is not practically manifested in the spectra of other molecules, because they are typically located sufficiently far from the TLS in question, or is manifested in the form of shifts that differ from the above-mentioned one in terms of the amount of the displacement. Thus, in the two-dimensional picture, a *spectral trail* can be distinguished, which is frequently also called a *spectral trajectory*, corresponding to the time evolution of the individual spectrum of the chosen molecule.

An analysis of spectral trajectories gives important information on the processes in the matrix and changes in its parameters in the *local environment* of the observed chromophore molecule. For instance, as was shown in [20–22], the time evolution (broadening, frequency jumps, splitting of spectral lines) of the observed spectral trajectories of impurity molecules of tetra-*tert*-butylterrylene (TBT) introduced into amorphous polyisobutylene (PIB) is described well by the standard model of glasses. Namely, the splitting or the frequency jumps of the observed spectral lines of the SM between 2^N spectral positions (see Fig. 2) can be explained by the coupling of the observed molecule to N nearby TLSs (with the transitions in them leading to appropriate changes in the frequency of the spectral line). In turn, the observed broadening of spectral lines can be explained by the coupling of the impurity molecule to the vibrational excitations of the matrix and to a large number of TLSs located far from the impurity molecule (this coupling leads to only insignificant spectral jumps in comparison with the observed width).

The spectral trajectories of SMs observed in low-temperature experiments in disordered media can demonstrate a complex behavior, which may not always be explained in the framework of the standard model of glasses. For instance, in [22], cases were observed where an SM interacts with two TLSs, which, in turn, interact with each other. In some cases, spectral trails have been registered that indicate the existence of three-level systems in disordered solid-state media, as well as spectral trails that manifest themselves in a continuous frequency drift in the SM spectrum.

An unprecedented source of information about the local dynamics of the matrix can be the temperature dependence of

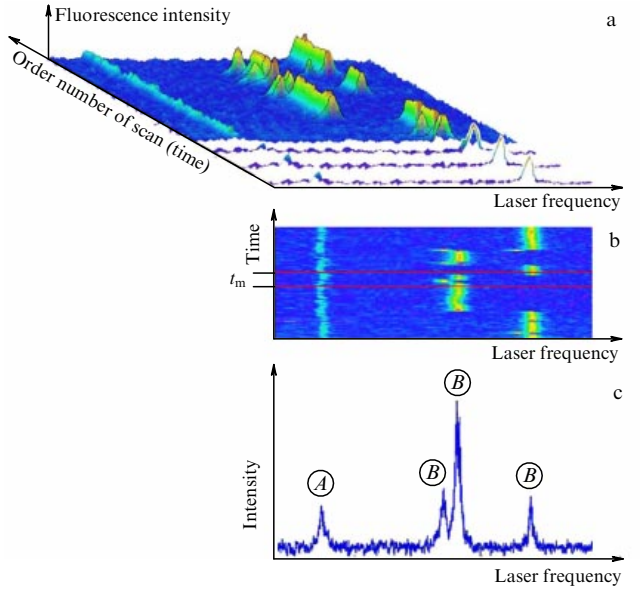

Figure 2. (a, b) Temporal evolution of single-molecule spectra of TBT embedded in PIB recorded repeatedly at $T = 2$ K. The results of measurements are presented in the form of (a) three-dimensional and (b) two-dimensional images. The color (gray) scales in (a) and (b) correspond to the intensity of fluorescence. The spectrum of molecule A does not reveal pronounced jumps during the time of observation. The spectrum of molecule B exhibits 'jumps' between four spectral positions (interaction with two nearby active TLSs). (c) The resulting integral spectrum, which is the sum of all spectra taken in the time interval $t_m = 120$ s (shown in Fig. 1b by horizontal lines). The total spectrum corresponds to two molecules: A (singlet) and B (triplet).

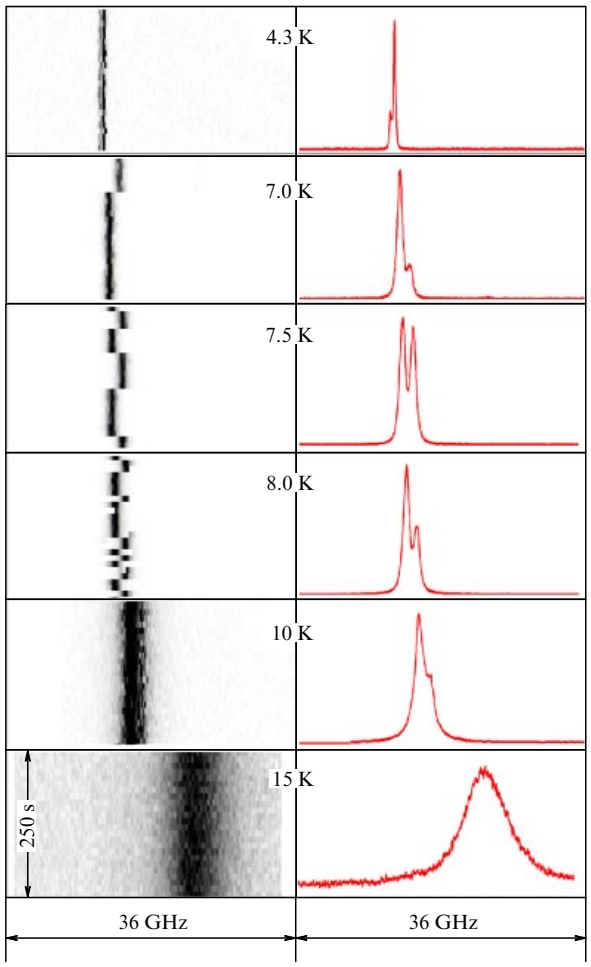

Figure 3. Spectral trails (left panel) and the corresponding total spectra (right panel) of the same single molecule of TBT embedded in PIB at various temperatures (borrowed from [25]).

the parameters of SM spectra. Figure 3 shows examples of spectral trails and the corresponding integrated spectra of the same SM measured at different temperatures. At $T = 7$ K, transitions in TLSs are activated that cause significant jumps of the spectrum between its two positions. In the range between 7 and 8 K, the characteristic rate of such jumps increases considerably. With a further increase in temperature, the jumps of spectral lines are masked with a strong broadening caused by the coupling of the SM to the LFMs. A shift of the SM spectrum with increasing the temperature is also observed.

As shown in [23–26], an analysis of the temperature dependence of the parameters of the SM spectra allows determining not only the local but also the individual parameters of single elementary excitations of a disordered medium. For instance, in [23], an analysis of the temperature dependence of the ratio of the intensities of two spectral components in the SM spectrum (which is split as a result of coupling of the selected SM to a TLS that suffered rapid jumps, in comparison with the time of measurement) allowed determining the asymmetry of this TLS (energy difference between the ground and excited states). It was also found that TLSs exist in which the populations of the energy levels do not obey the Boltzmann statistics. An analysis of the influence of an external electric field on the spectrum of an SM coupled to a TLS [27] allowed measuring the complete set of individual parameters of a single TLS, i.e., the tunneling parameter, the asymmetry, and the electric dipole moment.

An analysis of the individual temperature dependences of the widths $\Gamma(T)$ of peaks of the SM spectrum [24–26] permitted us to obtain data on the local parameters of LFMs in the nearest environment of impurity TBT molecules in amorphous PIB. We measured the $\Gamma(T)$ dependences in the temperature range from a few to several tens of kelvins, in which the predominant contribution to the processes of broadening of the SM spectra comes from the coupling to LFMs. The local parameters (the frequency of an LFM and the quadratic coupling constant of this mode to a given molecule) were determined by approximating each $\Gamma(T)$ dependence using formula (3). It was found that the frequencies of the LFM in this system have a significant dispersion, which can be regarded as a consequence of the localized nature of the LFM in this medium.

As can be seen from the above examples, the use of the SMS for measuring local parameters of solid-state media offers unique possibilities for the direct observation of dynamic processes in such media on the microlevel (up to the detection of elementary quantum mechanical events). Such measurements, undoubtedly, are of great interest from both the scientific and practical standpoints. They are especially important in the case of media characterized by strong local inhomogeneity.

To correctly relate the experimentally measured local parameters of a solid-state medium to its macroscopic (functional) characteristics, structure, and chemical composition and to correctly compare the results of the measurements

of such parameters with theoretical estimations, the averaged values of these parameters must be known. Wide opportunities for determining these values are given by a statistical analysis of data on the parameters of SM spectra obtained from a large number of such spectra. This idea was first realized in a series of our works [20, 21, 28 – 31]. We developed an approach based on the use of moments and related derivative functions, (cumulants) for a quantitative description of the complex shapes of SM spectra in disordered solid-state media at low temperatures.

In [20, 21], we measured and calculated the distributions of the first four moments of SM spectra (spectral shifts, generalized width, asymmetry, and peakedness of the spectra). The distributions obtained were compared with the distributions of the moments of model SM spectra for the same system calculated in the framework of the stochastic theory of SM spectra in low-temperature glasses [32]. This allowed estimating the minimum distance between the impurity molecule and a TLS and thus to obtain information on the minimal size of a TLS in the system. Furthermore, the analysis carried out allowed determining the dispersion parameters of the TLS – SM coupling constant.

It was shown in Refs [28 – 30] that the distributions of the first two cumulants of the SM spectra in the impurity system of TBT in PIB at $T = 2$ K are satisfactorily described in the framework of the Lévy statistics (Lorenz and Smirnov functions for the respective distributions of the first and second cumulants). As was shown in theoretical work [33], this indicates the validity of the basic concepts of the standard TLS model assuming the dipole – dipole nature of the chromophore – TLS coupling and also the uniform distribution of TLSs. The original method of the analysis of distributions of the SM-spectrum moments that was developed and realized in [31] allowed us to determine (based on the example of an amorphous system of TBT in PIB, at $T = 2$ K) the characteristic distances (zone) where the coupling of a TLS to an impurity molecule mainly leads either to a splitting or to a broadening of the spectrum, and also the distance beyond which this coupling is practically unrevealed.

We note that in all studies related to the statistical analysis of the parameters of SM spectra, a problem of the statistical confidence of the results occurs [34]. This problem is especially acute when using the conventional single-channel detection scheme (Fig. 1a), in which the measurement of a statistically reliable number of spectra of different SMs requires an enormous amount of time, which is not always realizable. Furthermore, in such measurements, passing from one point of the sample to another requires a certain time, which prevents simultaneous observations of local dynamic characteristics at different points of the sample. These problems can be solved by using a multichannel measuring method, based on the scheme of a fluorescence microscope with a multichannel photodetector (Fig. 1b). In this case, the images of all SMs that fall into the field of view of the microobjective are recorded simultaneously with the aid of a matrix detector. This scheme permits implementing a parallel synchronous control over the spectral characteristics of all SMs whose electronic transition frequencies lie in the chosen frequency range of measurements.

The multichannel registration of SM spectra in solid-state media was first realized in works performed in 1998 – 2000 at the Swiss Federal Institute of Technology Zurich (ETH Zürich) [35]. However, the use of this equipment in practice was hindered for a number of reasons: (a) the matrix detectors at that time had low ultimate sensitivity and high noise; (b) the electronic and computer equipment did not allows ensuring a reasonable time resolution of experiments; (c) the registration of a significant number of SM spectra required a large disk space (several tens of gigabits); and (d) the processing of the measurement results took too long, even when using specialized electronic computing work stations. All these problems were acquiring a catastrophic scale in attempted measurements of the spectral trails of a large number of SMs in solid-state media. As a consequence, the procedure developed and the equipment designed did not receive wide acceptance.

The appearance of highly sensitive CCD cameras with internal electron multiplication and low noise, a significant increase in the efficiency of computers, the possibility of rapid writing/processing of significant arrays of data, and, most importantly, the development of original algorithms of the automated recognition of fluorescent images of SMs allowed us to realize a technique of multichannel detection of spectral trails of SMs with the aid of a fluorescence microscope at a qualitatively new level. The technique developed opened up new possibilities and allowed us to obtain a number of fundamentally new results, which are discussed below. In Refs [36 – 38], a technique of measurements of the frequency spectrum of LFMs (vibrational density of states, or VDOS) was proposed and developed in solid-state media from the spectra of SMs embedded in the medium to be studied. The technique was based on measurements and analysis of individual temperature dependences of the widths of separate spectral peaks of a large number of impurity molecules.

At each temperature, fluorescent images of the detected SMs were recorded synchronously with a retuning of the laser source frequency in the selected spectral range in the form of a sequence of video frames from a CCD camera. The digitized video frames were saved in the permanent memory of a computer in the form of a block of data, which were used for further analysis. The individual fluorescence excitation spectra of SMs observed in the field of view of the microobjective with a sufficiently high signal-to-noise ratio were extracted from the saved data using a specially developed computer program. It is significant that this procedure was automated. The program determined the positions of groups of adjacent pixels of the CCD matrix whose signals gave a spike at a certain frequency of the laser excitation, which could be interpreted as a spectral peak at this frequency (Fig. 4). Each such group of pixels was correlated with a luminescent image of a certain (ith) SM. The dependence of the intensity of fluorescence signals detected by a given group of pixels on the number of a frame (i.e., at the excitation frequency) is interpreted by the program as a fluorescence excitation spectrum of a given SM. The coordinates of the image of this SM, x_i, y_i, on the CCD matrix are determined as the coordinates of the centers of gravity of pixels in a given group (Fig. 4a). The approximation of separate spectral peaks in the measured SM spectrum by a Lorenz function allowed determining the width of the spectral line Γ_i of a given SM (Fig. 4b).

To obtain the temperature dependence of the widths of spectral lines of the observed SMs, the measurements were repeated at various temperatures in the range from 8 – 10 to 30 – 40 K, where the contribution from LFMs to the broadening of the spectral lines of SMs predominates over the contributions of other processes. In the course of measurements, a special control was performed of the constancy of the

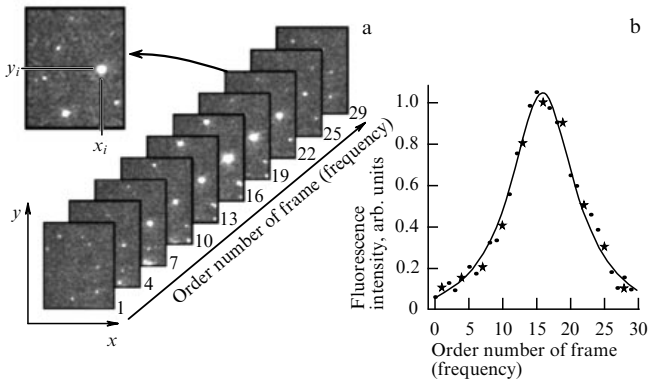

Figure 4. The procedure of extracting the SM spectrum from a sequence of video frames (schematic): (a) identification of luminescent images of the same single molecule upon scanning of the spectrum; and (b) the fluorescence excitation spectrum of a selected ith molecule with coordinates x_i, y_i (points) and its approximation by a Lorenz function (solid line). The asterisks correspond to the video frames shown in Fig. 4a (borrowed from [37]).

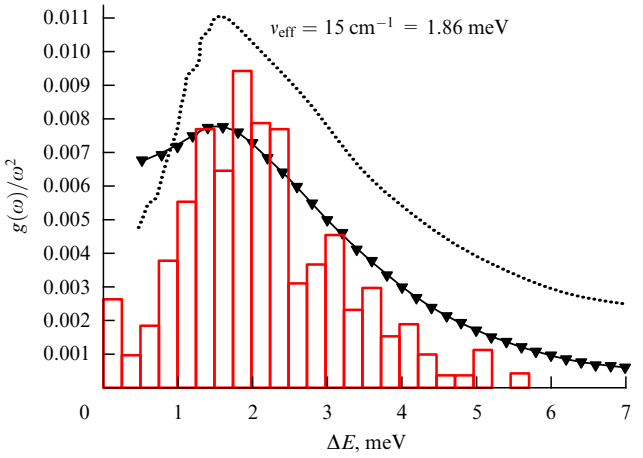

Figure 5. Energy spectrum of LFMs and the boson peak in frozen toluene measured using three experimental methods. Histograms represent the spectrum of LFMs in frozen toluene doped with TBT (measured by the SMS method). Triangles correspond to the spectrum of the density of vibrational states (VDOS, or the boson peak) measured for solid toluene doped with molecules of ferrocene (nuclear scattering method). The dotted line shows the VDOS spectrum measured in the undoped toluene at $T = 7$ K (Raman scattering). The arrow indicates the effective (averaged) energy of LFMs measured (by the photon-echo method) for solid toluene doped with molecules of zinc octaethylporphyrine.

coordinates of the molecules depending on temperature. The approximation of each measured temperature dependence using formula (3) allowed determining the local parameters of an LFM, such as the energy ΔE_i and the quadratic coupling constant w_i in the nearest nanovicinity of the ith SM.

Using the procedure developed, we measured the energy spectra of LFMs for amorphous PIB and frozen toluene doped with TBT molecules [36–38]. In [38], the measured energy spectra of LFMs were compared with the data on the VDOS (which is frequently called a boson peak in the literature) measured for pure PIB and toluene by inelastic neutron scattering, Raman scattering, and inelastic nuclear scattering. The measured LFM spectrum in [38] was also compared with the effective values of the LFM energy measured for the same matrices using the photon echo method.

A sufficiently good agreement of the parameters of the experimental spectrum of LFMs with the data on VDOS (Fig. 5) obtained by different methods allows formulating two important conclusions:

(1) the LFMs that cause the experimentally observed broadening of the spectral lines of isolated molecules of TBT embedded into PIB and toluene have the same microscopic nature as the vibrational excitations that determine the shape of the boson peak in impurity-free PIB and toluene;

(2) the introduction of small concentrations of TBT into PIB and toluene does not lead to noticeable changes in the vibrational dynamics observed in the matrix under investigation.

The technique of rapid multichannel detection of SM spectra and the equipment designed for this method allowed solving one more important and complex problem, namely, to significantly facilitate the search for new impurity matrix systems suitable for recording the excitation spectra of SM fluorescence at low temperatures. It should be remembered that in using a single-channel registration scheme, a serious problem exists in searching for an SM in both the coordinate in the field of view of the microobjective and the frequency within a wide inhomogeneous absorption contour. The multichannel detection scheme of fluorescent images substantially facilitates this problem, because in this case the need is eliminated in the spatial search for SMs in various regions of the sample. This opens up fundamentally new possibilities in investigations of the spectral dynamics of impurity solid-state media using SM spectra.

In [34, 39], we for the first time detected SM spectra in low-molecular glass (frozen solutions of TBT molecules in conventional and deuterated toluene) and obtained an unexpected result: we found that on the microscopic level, the dynamic processes in low-molecular glasses at $T < 2$ K, in contrast to the processes in amorphous polymers, cannot be adequately described by the standard model of glasses. We found an additional contribution to the spectral dynamics, which manifested itself in the form of continuous drifts and frequency-unrepeatable random jumps of the spectra of the SMs under consideration (Fig. 6). It is probably these effects that prevented the experimental detection of SM spectra in these liquids. It may be supposed that the unsuccessful attempts to measure SM spectra in other low-molecular liquids are also related to the same effects.

An analysis of the influence of the deuteration degree of toluene molecules (isotope effect) on the distribution of the widths of the spectral lines of SMs and on the energy spectrum of LFMs showed that the dynamics of this matrix at $T = 2$ K is determined by the excitations of the tunneling type, whereas at $T > 7$ K, the observed dynamics is determined by excitations of the vibrational type.

To summarize, we can conclude that single-molecule spectroscopy is a powerful tool for investigations of the dynamics of disordered solid-state media at a local level. The suggested technique of fast multichannel detection of SM spectra and the equipment design permitting the realization of the original methods of automated computer-aided processing of fluorescent SM images, as well as the related methods of statistical analysis of individual parameters of a large number of experimental spectra of SMs, open up qualitatively new opportunities for the investigation of the principal features and microscopic nature of dynamic processes in solids.

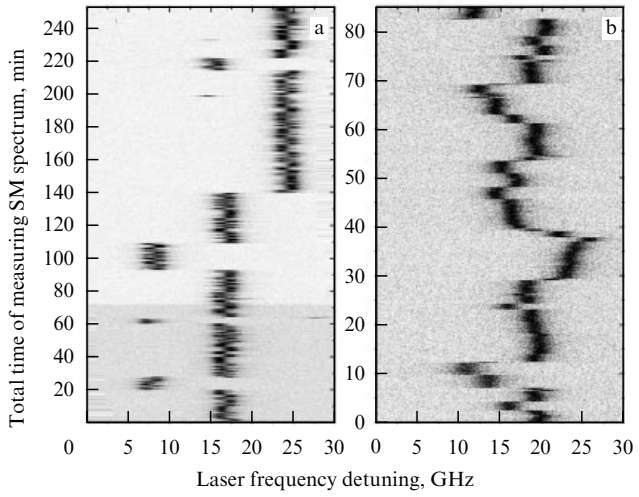

Figure 6. Spectral trails of single TBT molecules introduced into amorphous PIB (a) and a frozen solution of toluene (b), measured at $T = 7$ K (according to the data in [38]).

We are grateful to L Kador and M Bauer for their fruitful cooperation in the investigations performed in this work. This work was supported in part by the Russian Foundation for Basic Research grants Nos 07-02-00206 and 08-02-00147 and by the Deutsche Forschungsgemeinschaft, Sonderforschungsbereich. A.V.N. also appreciates the support from the Ministry of Education and Science of the Russian Federation and from the U.S. Civilian Research and Development Foundation (Basic Research and Higher Education Project), and also support from the Grant of the President of the Russian Federation (MK-239.2007.2).

References

1. Balykin V I et al. *Pis'ma Zh. Eksp. Teor. Fiz.* **26** 492 (1977) [*JETP Lett.* **26** 357 (1977)]
2. Personov R I, Al'shits E I, Bykovskaya L A *Pis'ma Zh. Eksp. Teor. Fiz.* **15** 609 (1972) [*JETP Lett.* **15** 431 (1972)]; Gorokhovskii A A, Kaarli R K, Rebane L A *Pis'ma Zh. Eksp. Teor. Fiz.* **20** 474 (1974) [*JETP Lett.* **20** 216 (1974)]; Kharlamov V M, Personov R I, Bykovskaya L A *Opt. Commun.* **12** 191 (1974)
3. Moerner W E, Kador L *Phys. Rev. Lett.* **62** 2535 (1989)
4. Orrit M, Bernard J *Phys. Rev. Lett.* **65** 2716 (1990)
5. Kulzer F, Orrit M *Annu. Rev. Phys. Chem.* **55** 585 (2004)
6. Anderson P W, Halperin B I, Varma C M *Philos. Mag.* **25** 1 (1972)
7. Philips W A *J. Low Temp. Phys.* **7** 351 (1972)
8. Elliott S R *Europhys. Lett.* **19** 201 (1992)
9. Laird B B, Schober H R *Phys. Rev. Lett.* **66** 636 (1991)
10. Schirmacher W, Diezemann G, Ganter C *Phys. Rev. Lett.* **81** 136 (1998)
11. Taraskin S N et al. *Phys. Rev. Lett.* **86** 1255 (2001)
12. Gurevich V L et al. *Pis'ma Zh. Eksp. Teor. Fiz.* **76** 650 (2002) [*JETP Lett.* **76** 553 (2002)]
13. Karpov V G, Klinger M I, Ignat'ev F N *Zh. Eksp. Teor. Fiz.* **84** 760 (1983) [*Sov. Phys. JETP* **57** 439 (1983)]
14. Parshin D A *Fiz. Tverd. Tela* **36** 1809 (1994) [*Phys. Solid State* **36** 1811 (1994)]
15. Klauder J R, Anderson P W *Phys. Rev.* **125** 912 (1962); Reinecke T L *Solid. State Commun.* **32** 1103 (1979)
16. Osad'ko I S *Selektivnaya Spektroskopiya Odinochnykh Molekul* (Selective Spectroscopy of Single Molecules) (Moscow: Fizmatlit, 2000) [Translated into English (Berlin: Springer, 2003)]
17. Kettner R et al. *J. Phys. Chem.* **98** 6671 (1994)
18. Tamarat Ph et al. *J. Phys. Chem. A* **104** 1 (2000)
19. Ambrose W P, Moerner W E *Nature* **349** 225 (1991)
20. Naumov A V et al. *Phys. Rev. B* **63** 212302 (2001)
21. Naumov A V, Vainer Yu G, Bauer M, Kador L *J. Chem. Phys.* **116** 8132 (2002)
22. Vainer Yu G, Naumov A V, Bauer M, Kador L *Opt. Spektrosk.* **94** 936 (2003) [*Opt. Spectrosc.* **94** 873 (2003)]
23. Bauer M, Kador L, Naumov A V, Vainer Yu G *J. Chem. Phys.* **119** 3836 (2003)
24. Naumov A V, Vainer Yu G, Bauer M, Kador L *Phys. Status Solidi B* **241** 3487 (2004)
25. Vainer Yu G, Naumov A V, Bauer M, Kador L *J. Chem. Phys.* **122** 244705 (2005)
26. Naumov A V, Vainer Yu G *Izv. Ross. Akad. Nauk, Ser. Fiz.* **70** 470 (2006) [*Bull. Russ. Acad. Sci.: Phys.* **70** 532 (2006)]
27. Bauer M, Kador L *J. Chem. Phys.* **118** 9069 (2003)
28. Barkai E et al. *Phys. Rev. Lett.* **91** 075502 (2003)
29. Barkai E et al. *J. Lumin.* **107** 21 (2004)
30. Vainer Yu G et al. *Opt. Spektrosk.* **98** 806 (2005) [*Opt. Spectrosc.* **98** 740 (2005)]
31. Vainer Yu G, Naumov A V *Opt. Spektrosk.* **98** 814 (2005) [*Opt. Spectrosc.* **98** 747 (2005)]
32. Geva E, Skinner J L *J. Phys. Chem. B* **101** 8920 (1997)
33. Barkai E, Silbey R, Zumofen G *Phys. Rev. Lett.* **84** 5339 (2000)
34. Vainer Yu G, Naumov A V, Bauer M, Kador L *J. Lumin.* **127** 213 (2007)
35. Bach H et al. *Opt. Mater.* **9** 376 (1999); Donley E A et al. *J. Phys. Chem. A* **103** 2282 (1999)
36. Vainer Yu G, Naumov A V, Bauer M, Kador L *Phys. Rev. Lett.* **97** 185501 (2006)
37. Naumov A V, Vainer Yu G *Izv. Ross. Akad. Nauk, Ser. Fiz.* **72** 748 (2008) [*Bull. Russ. Acad. Sci.: Phys.* **72** 708 (2008)]
38. Vainer Yu G, Naumov A V, Kador L *Phys. Rev. B* **77** 224202 (2008)
39. Naumov A V, Vainer Yu G, Kador L *Phys. Rev. Lett.* **98** 145501 (2007)

PACS numbers: **07.07.–a**, **87.64.–t**, 87.85.fk
DOI: 10.3367/UFNe.0179.200903o.0329

Optical biosensors of genotoxicants based on DNA nanoconstructions and portable dichrometers

O N Kompanets, Yu M Yevdokimov

1. Introduction

In this report, we briefly review results obtained in the last five years in the field of the development and practical use of biosensor methods and devices for the rapid determination of genotoxicants in liquids. Special attention is given to the nanobiotechnological approach developed in the Engelhardt Institute of Molecular Biology (IMB), Russian Academy of Sciences, with the instrumental support of the Institute of Spectroscopy, Russian Academy of Sciences (ISAN), which suggests the use, as integral biosensing units, of nanoconstructions that consist of double-stranded DNA molecules immobilized in optically transparent isotropic hydrogels having the property of abnormal optical activity, and of portable dichrometers as the recorders and transducers of circular dichroism.

Progressively increasing anthropogenic environmental pollution dictates the need for developing methods and devices for medical and ecological diagnostics, and also methods for controlling the quality of food products and medicinal preparations to ensure highly sensitive and rapid determination of the presence in them of toxicants that are hazardous to health and whose 'target' is the genetic material of cells. Such toxicants include some antibiotics and other

medicines, heavy metals, pesticides, dioxins, proteins, and other biologically active compounds (BACs), which are always present in physiological liquids (blood, blood plasma, urine, water, etc.).

For the determination of the overwhelming majority of biologically active and toxic compounds, traditional analytical techniques can be used, such as chemical analysis, as well as numerous methods with the application of biochemical analyzers, liquid and gas chromatographs, mass spectrometers, and other analytical instrumentation. An alternative to traditional methods is the so-called biosensor methods of analysis, which use sensing elements (biosensors) that have a specific sensitivity to the compounds to be determined, in combination with various transducers and converters. Biosensor technologies are by no means necessarily better than nonbiosensor methods, but an intimate combination of the production of a signal and its detection and the possibility of the miniaturization of equipment are opening newer and newer areas of measurements. In medicine, this can be the use of medical monitoring in situ, directly near a patient; in pharmacology and the food industry, rapid (online) control of the quality of pharmaceutical preparations and food products; in the biotechnological industry, the control and optimization of technological processes; and in environmental monitoring, the immediate detection of toxic substances, without the transfer of samples into the laboratory.

A promising trend in the solution to these problems that is very important for the protection of human life and health is the nanobiotechnological approach rapidly developed in the last few years, which implies the use of 'structured' biomaterials, devices, and systems with properties that are connected with the geometrical dimensions or specific physicochemical features of nanostructures, such as molecular constructions based on DNA [1]. Nanoconstructing on the basis of double-stranded DNA (dsDNA) molecules represents a purposeful creation of three-dimensional constructions (nanostructures, nanoconstructions (NaCs), nanobiomaterials), whose 'building blocks' are dsDNA molecules or their complexes [2]. The most important problem with such nanoconstructing is the creation of three-dimensional constructions with controlled properties, which contain built-in molecules of various compounds ('guests'), which can be targets for BACs, i.e., the creation of biosensors on the basis of NaCs for the determination of BACs that recognize guest molecules [3 – 5].

In the literature, several approaches to the creation of biosensors on the basis of NaCs of nucleic acids have been described. These approaches can be conditionally divided into two groups. Following one hybridization strategy — the strategy of sequential construction [6] — the nanostructures are formed consecutively, using single dsDNA molecules as building blocks, which entails large expenditures due to the need to obtain fragments of DNA with the necessary sequences of nitrogen bases and an entire 'arsenal' of ferments for splitting and 'sewing' DNA fragments, the separation of specific structures from the reaction mixture, and the use of modern methods of control (such as atomic force microscopy) at all stages of nanoconstructing. For this reason, the problem of the practical application of NaCs on the basis of single dsDNA molecules remains unsolved to a considerable degree.

Another, fundamentally different, strategy of nanoconstructing, which was developed at IMB RAS [7], is based not on the use of single dsDNA molecules (or complexes of dsDNA molecules) but on the use of ordered spatial structures spontaneously arising upon the 'phase exclusion' (condensation) of these molecules from aqueous salt solutions of polymers. As a result of phase exclusion, rigid dsDNA molecules with a low molecular weight ($< 10^6$ Da) become ordered and form particles ~ 0.5 μm on size, which are characterized by a liquid-crystalline mode of packing of adjacent DNA molecules into layers with an approximately parallel orientation of molecules in each layer and a change (twist) in this orientation in passing to other layers [8].

The transition into an ordered cholesteric liquid-crystalline state is accompanied by the appearance of an abnormal band in the spectrum of circular dichroism (CD) located in the absorption area of the nitrogen bases of DNA ($\lambda \sim 270$ nm). The liquid-crystal state does not disrupt the reactivity of the molecules, i.e., their capacity for molecular 'recognition' and specific addressing of chemical substances and BACs. For example, the interaction of colored antitumor antibiotics with the DNA molecules that form the particles of cholesteric liquid-crystal dispersions of DNA (DNA CLCDs) is accompanied by the appearance of an additional abnormal band in the CD spectrum in the absorption region of these compounds. The abnormal CD signal allows following even the smallest changes in the properties of the dsDNA molecules, i.e., the DNA CLCD particles act as miniature optical biosensing units, which change their characteristics in response to the action of a BAC from the liquid being investigated. The spectral features of this signal (the sign, height, and position of the maximum) recorded by a portable CD spectrometer (dichrometer) are used as an analytical criterion that allows not only determining the presence and concentration of a BAC in the sample analyzed but also establishing the method of its interaction with the dsDNA molecules. A liquid sample to be probed (of a 'test-tube' form) is prepared by mixing the solution of the probed biological liquid in the polymer with a solution of the dsDNA in the polymer, i.e., with the dsDNA CLCD (biosensor).

2. Biosensor analytical system

The practical problem of determining BACs with the help of biosensing units on the basis of DNA CLCDs was solved together with the Institute of Spectroscopy RAS (ISAN), which developed a prototype of a portable polyfunctional dichrometer (SKD-2) and manufactured first samples of these analyzers for the operating range 250 – 750 nm [9]. In 2004, the Experimental Plant of Scientific Instrumentation (EZNP), Russian Academy of Sciences (Chernogolovka, Moscow region), based on the documentation of ISAN, manufactured a small batch of ten SKD-2 dichrometers (No. 26900-04 in the Federal Agency on Technical Regulation and Metrology on the Manufacturing and Repair of Means of Measurement). Although the overall dimensions of the dichrometer were three times less than those of the commercial dichrometers of well-known firms and the weight was 5 – 7 times less, the detecting ability of the SKD-2 portable dichrometer ($\sim 10^{-6}\,\Delta A/A$, where A is the absorption in the sample) proved to be 2 – 3 times better. A biosensor analytical system based on DNA biosensing units and the SKD-2 dichrometer has no analogs in the world as regards its operating principle; it is characterized by a high sensitivity (10^{-7} to 10^{-14} M l^{-1}), low operational expenditures (1.5 dollars per hour), low prime cost of a single test (0.5 dollars), the possibility of conducting straight rapid analysis of liquids containing BACs, and in all these

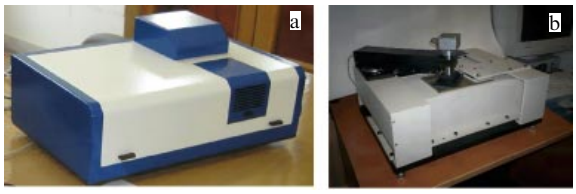

Figure 1. Polyfunctional portable dichrometers: (a) SKD-2M and (b) SKD-3.

characteristics it considerably exceeds the foreign analytical systems of analogous designation. The novelty of the development is confirmed by patents by Russia, the USA, the EU, Germany, and Japan, the gold medals at the 50th World Exhibition of Innovation (Brussels, Eureka, 2001) and of the Presidium of the Russian Academy of Sciences (2002), as well as the Grand-Prix and Prize for Victory in the 2nd Competition of Russian Innovations (2003).

In 2005 – 2007, the SKD-2 dichrometer was modernized with the purpose of expanding the range of working wavelengths to 200 nm and increasing the reliability of operation on the whole. In the improved version of the device (SKD-2M, Fig. 1), a virtually ozone-free temperature regime of the illuminator was realized with a twofold increase in the output of ultraviolet (UV) emission near $\lambda = 200$ nm; a higher stability of the modulator of the circular polarization with respect to external actions; a decrease in the value of the residual CD signal caused by stresses in the windows of the cuvette; an increase in the accuracy of installation of the sample temperature; a decrease in the overall dimensions of the device; the use of modern components in the electronic units and functional modules; the possibility of connecting both external and built-in computers through a USB interface.

In the same period, the developed bioanalytical system was used at IMB RAS to demonstrate the possibility of detection in physiological liquids of a large number (> 50) of compounds that enter into antitumor compounds, a number of polyaminoacids, polypeptides and proteins, cellular metabolites, organophosphorus compounds, and ascorbic acid, and a number of phytogenous genotoxicants.

3. Biosensing units based on DNA nanoconstructions

The significant distance between DNA molecules (from 2.5 to 5.0 nm), the liquid-like nature of the packing of these molecules, and their high concentration (~ 400 mg ml^{-1}) in quasinematic layers of particles of their CLCDs provide conditions for the rapid diffusion of molecules of many compounds both between DNA molecules in the same layer and between DNA molecules in adjacent layers of such particles. In view of the preservation of reactivity of the DNA molecules in the structure of CLCD particles, the genotoxicants from physiological liquids can easily penetrate inside such particles and modify the secondary structure of the dsDNA molecules or intercalate between the pairs of dsDNA bases without damaging the character of ordering of the molecules. In addition, the new chemical groups on the surface of the DNA molecules offer the possibility of forming 'bridges' between adjacent DNA molecules.

For the formation of the bridges, it is necessary that, places where they 'begin' and 'end' must exist on the surface of the DNA molecules (the ions of metal connected with a nitrogen base or the molecules of a ligand additionally introduced into the system, for instance, can serve as such places). In view of the spatial arrangement of reactive groups (in particular, N-7 nitrogen atoms of the purine bases) in the spatial structure of the DNA molecules, the connection between two adjacent DNA molecules is possible only if the spatial orientation of these molecules is coordinated, i.e., if a kind of 'phasing' of the positions of the adjacent DNA molecules is provided. This means that the formation of nanobridges is a delicate process, which is realized only if several conditions are satisfied. This problem was solved by the creation of nanobridges [7] from alternating molecules of an anthracycline antibiotic and copper ions, which connect adjacent DNA molecules in each of the quasinematic layers and DNA molecules of the adjacent layers of CLCD particles. This led to the appearance of a rigid spatial structure of such particles (Fig. 2b), which were called nanoconstructions, and to dramatic changes in their properties.

The basic factor in the stabilization of NaCs is now the number and 'strength' of nanobridges rather than the osmotic pressure of the aqueous solution, in contrast to the initial CLCD particles. The liquid-crystalline nature of the packing of the adjacent DNA molecules in NaCs and the diffusion mobility of the DNA molecules disappear, and the particle acquires the properties of a solid material (Fig. 2b). In the composition of an NaC, not only is a high local concentration of DNA molecules preserved but also a high concentration of the antitumor antibiotic daunomycin (DAU) appears.

Characteristic for a DNA NaC are both abnormal optical activity, which manifests itself in the appearance of an intense band in the CD spectrum in the absorption region of the DNA (~ 270 nm), and additional anomalous optical activity in the absorption region of the antibiotic chromophores (~ 520 nm). The abnormal optical activity allows controlling the change in the secondary structure of the initial DNA molecules, the appearance in the NaC structure of molecules that form nanobridges, and the integrity of the nanobridges themselves. The decrease in the activity (up to its complete disappearance), which accompanies the destruction of nano-

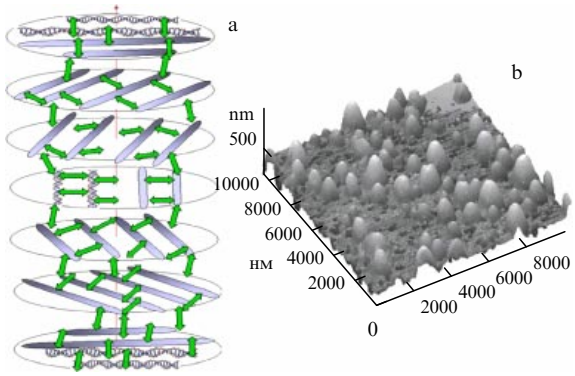

Figure 2. (a) Hypothetical scheme of a three-dimensional rigid nanoconstruction based on dsDNA molecules fixed in the spatial structure of a CLCD particle and 'sewn' by nanobridges. The DNA molecules in adjacent layers are shown in the form of rods; each subsequent layer is turned through a certain angle with respect to the preceding layer; arrows show nanobridges. (b) A three-dimensional scheme of NaCs immobilized on the surface of a nuclear membrane filter.

bridges under the action of genotoxicants (BACs), can under certain conditions be directly connected with the concentration of the agent that destroys the nanobridge; this gives the possibility of using DNA NaCs as optical biosensors for the detection (in biological tests) of the presence and concentration of BACs whose 'targets' are the nanobridges, which are, in fact, nanosensors. The optical signal generated by such biosensors can easily be recorded using a portable dichrometer.

Based on the determination of model substances, in particular, ascorbic acid [10] and bovine serum albumin (BSA) [11], which change the valence state of Cu^{2+} ions or 'extract' them from the composition of the nanobridge, the respective limits of detection of analytes at a level of 10^{-7} to 10^{-8} M were achieved, which are comparable with the limits of their determination by classical chemical (biochemical) methods.

Biosensors of this type were also used also for the detection and selection of phytogenic pharmaceutical substances, which have clearly pronounced complex-generating properties with respect to Cu^{2+} ions. When a biosensor is treated with hiporamin (an antiviral and antimicrobial preparation of the All-Russia Research Institute of Medicinal and Aromatic Plants (VILAR), Russian Academy of Agricultural Sciences (RASKhN)), the destruction of nanobridges and, correspondingly, the decrease in the anomalous optical activity (Fig. 3) is also caused by the 'extraction' of Cu^{2+} ions from the nanobridge and by the formation of a more stable complex between hiporamin and Cu^{2+} ions as a result of secondary complex generation. It was also shown that at a fixed time of treatment of NaC by hiporamin (10 min), the amplitude of the band in the CD spectrum of DNA NaC is directly proportional to the concentration of a phytopreparation (in the range up to 4 μg ml^{-1}); this linear dependence can be used as a calibration line when determining low ($\sim$ 0.5 μg ml^{-1}) concentrations of hiporamin in the sample analyzed. Analogous data were obtained for donelvin, hamenerin, chanerol, and eucalyminum [12].

Thus, the development of integral biosensors on the basis of NaCs with a sufficiently long-time stability of optical properties, which are independent of the osmotic pressure of the aqueous solution, has substantially increased the number of BACs that can be detected in liquids with the aid of the biosensor technology proposed.

With the development of the technology of obtaining DNA nanoconstructions, which can include a large fraction of guest molecules, a new type of biomaterial with controllable properties has, in essence, been created. This technology is not yet completed and can be improved by selecting other components of nanobridges or the DNA molecules themselves, including their complexes with various polymers.

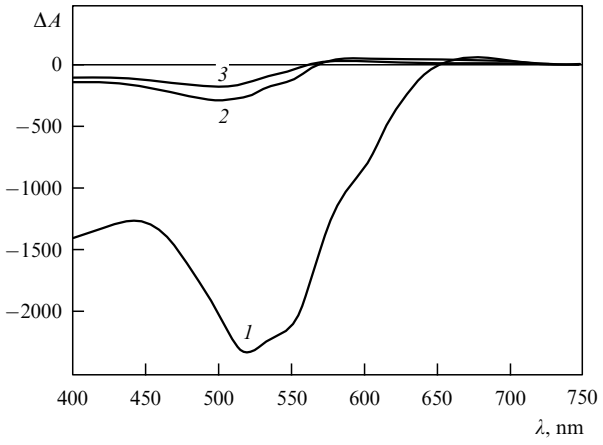

Figure 3. CD spectra of DNA nanoconstructions (*1*) before treatment with hiporamin (HP) ($c_{HP} = 0$) and (*2*) after treatment with hiporamin ($c_{HP} = 3.953$ μg ml^{-1} a $c_{DNA} \sim 5.6$ μg ml^{-1}. Curve *3* corresponds to the CD spectra of a CLCD complex (DNA – DAU), $\Delta A = (A_L - A_R) \times 10^{-6}$ optical units; A_L and A_R are the light absorption in samples with left and right circular polarization.

4. Stabilization of the physicochemical properties of biosensing units based on DNA nanoconstructions

An essential disadvantage of biosensing units based on DNA NaCs from the standpoint of their practical application is the instability of optical properties caused by a gradual sedimentation of DNA NaC particles when using their test-tube form. This shortage, which can easily be removed by agitation of the test tube, is allowable while conducting biochemical studies and analyses on small scales, but is completely unacceptable when carrying out mass analyses, decentralized measurements, 'personified' medicine, or technological online control. For eliminating this disadvantage, a new approach to the creation of stabilized forms of biosensing units based on DNA NaCs and, correspondingly, a new construction of a dichrometer were required.

The problem of the stabilization of the physicochemical properties of biosensing units was solved by creating a hydrogel containing NaC particles. Together with the elimination of sedimentation of the DNA NaC particles, the hydrogel allows preserving the abnormal optical properties of the biosensing unit even upon swelling. In this case, the biosensing unit represents a synthetic polymeric matrix (SPM), which contains spaced-apart single particles of DNA NaCs (Fig. 4), and in its operational principle is analogous to film-type indicators [13].

Based on the technology developed at IMB RAS, elastic polymeric hydrogels have been created with a low toxicity and biodegradation, optically isotropic, with a high transparency in the wavelength range between 230 and 750 nm, chemically and biologically inert with respect to dsDNA molecules and to other BACs. The parameters of the spatial organization of

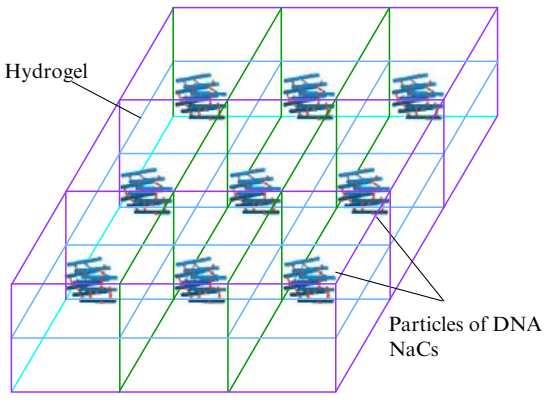

Figure 4. Schematic of a hydrogel containing particles of DNA nanoconstructions that are spaced apart.

a hydrogel and its physicomechanical characteristics ensure the fixation of DNA NaC particles without the disturbance of their spatial structure, the reactivity of the 'building' blocks of these structures, and the condition for the diffusion of BACs on a realtime scale (from 30 min to 3 h, depending on the molecular weight of the analyte). The gel biosensors containing particles of DNA NaCs preserve the abnormal optical activity for a long period (more than a year).

The immobilization of the DNA NaC particles in the hydrogel does not substantially influence the shape and amplitude of the related anomalous bands, whose maxima are located in the ultraviolet (~ 270 nm) and visible (~ 520 nm) ranges of the CD spectrum. At DNA concentrations ~ 20 μg ml^{-1}, the amplitude of the band in the visible range of the spectrum, which is generated by a gel biosensing unit approximately 3 mm thick, is no less than 1200×10^{-6} optical units.

In the experiment, we used homocysteine (HC) as an analyte capable of diffusing into the hydrogel and destroying DNA NaC particles contained in it. The homocysteine is formed in the human body as a result of the metabolism of methionine; in the case of disturbance of the process of reverse transformation into the methionine, it begins to enter the bloodstream, which leads to the appearance of hyperhomocysteinemia i [14] and related diseases (thrombovascular disease, atherosclerosis, pregnancy pathologies, etc.). The determination of HC in blood plasma using highly efficient liquid chromatography is a lengthy and expensive process that requires the use of expensive equipment and highly skilled personnel. This means that the development of an inexpensive, high-precision, and simple procedure for determining HC is an urgent problem of contemporary biomedicine.

Figure 5 shows the CD spectra (registered through different time intervals) of a hydrogel placed in a solution containing HC, which, diffusing into the hydrogel, causes a decrease in the anomalous CD band up to its complete disappearance. This means that after HC penetrates into the hydrogel, it 'extracts' Cu^{2+} ions from the nanobridges and causes the destruction of the DNA NaCs. This clearly shows that the DNA NaCs immobilized in the hydrogel easily 'responds' to the presence of HC in the solution.

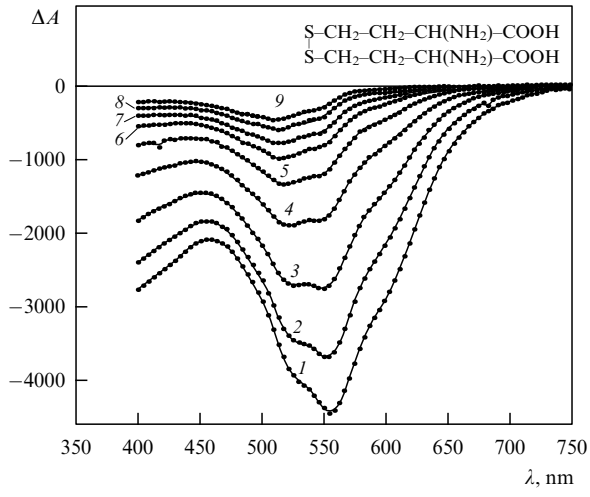

Figure 5. CD spectra of DNA NaCs in the composition of a hydrogel placed in a homocysteine-containing aqueous-salt solution of polyethylene glycol (PEG) recorded after various times: (*1*) 0, (*2*) 15, (*3*) 25, (*4*) 35, (*5*) 45, (*6*) 55, (*7*) 65, (*8*) 85, and (*9*) 115 min; $c_{DNA} = 19.92$ μg ml^{-1}; $c_{PEG} = 120$ mg ml^{-1}; $c_{HC} - 39.22$ μg ml^{-1}.

The nanobiomaterial obtained, which contains the DNA NaC particles, was also used in biosensors for controlling the quality of phytopreparations (alpisarinum, hiporhamin, chamaenerin, chanaerol) in the VILAR Center of Biomedical Technologies.

The gel-like nature of the DNA biosensing units and their specific features, such as the diffusion permeability for analytes, light scattering in the biomaterial, and small length of light interaction with the sample, required the development of a new polyfunctional dichrometer (SKD-3, Fig. 1b) with a scheme of a vertical formation of an optical ray and illumination of the gel sample on a small area (0.6×0.6 mm). The gel samples of the biosensing units can be placed in special cells of a UV microtablet, where they interact with the liquid sample to be analyzed. To expand the working range of the device into the ultraviolet region of the spectrum (to 190 nm), the dichrometer provides a hermetic sealing of the optical block and the possibility of filling it with gaseous nitrogen to eliminate losses of UV radiation because of its absorption by ozone that can form if working in air [15].

5. Optical biosensing units based on DNA nanoconstructions and a single-wave dichrometer

As was shown in Section 4, biosensors based on DNA NaCs that are spaced apart and immobilized in a hydrogel preserve inherent abnormal optical activity in the absorption band of DNA (~ 270 nm) and also manifest new optical activity in the absorption band (~ 520 nm) of the components of the nanobridges of DNA NaCs.

The abnormal optical activity of biosensing units based on DNA NaCs in the band near $\lambda \sim 520$ nm remains constant for a long period and can decrease (up to complete disappearance) under the effect of BACs, whose 'targets' are the structural elements of nanobridges. This circumstance determined the direction of the development of a new, even more compact and cheaper biosensor device. Such a device, in contrast to the broadband systems of the SKD-2M and SKD-3 type, would not need a large-dimensional wide-band (including ultraviolet range) lamp radiation source with a high-voltage power source and a monochromator with a device for wavelength tuning; they are replaced by a miniature diode emitter operating only in one of the above-indicated bands in the visible spectrum range. Simultaneously, such a device can be used for measuring diffusion rates of different liquids in gel or film nanobiomaterials.

At the turn of 2007 – 2008, a simple prototype of a new biosensor system with the use of gel DNA biosensors, a diode radiation source, and some units borrowed from the SKD-2 dichrometer was successfully tested at ISAN [16]. At present, a base model of a compact specialized single-wave dichrometer and an analytical system based on it are being developed. This system can be extensively applied in medical centers in which direct determination of concrete BACs or other significant chemical compounds in liquids should be conducted.

6. Competitive position of optical biosensors

It is assumed that biosensors based on DNA NaCs and the dichrometers of the new type with the procedures for their

application must compose the basis of newly developed biosensor technology and biosensor devices for the direct determination in liquids of various BACs that are dangerous to human health and life or have a therapeutic function. These devices should have a high sensitivity, no fast, and have a low prime cost of analysis. The main fields of application of such portable biosensor analytical complexes (optical biosensors) are medical clinical diagnostics, biochemical analysis, pharmacology, the biotechnological and food industries, ecological control, and scientific research.

The possibility of the commercialization of the biosensors of the new type and related devices is fortified by the presence of both the priority of Russian scientists in this field and of the incorporeal rights with respect to the developed nanobiomaterials, technologies, and devices. As follows from an analysis of the market for biosensor systems, the project developments of scientists of the Russian Academy of Sciences in the field of biosensor analytical devices with the use of DNA biosensors are in a very advantageous position on the world market for biotests in the basic competition characteristics (the cost of equipment, the price of tests, and the degree of universality of the equipment as regards its applicability). Full-featured analogs of these developments do not exist elsewhere in the world and, judging from the publications, cannot be anticipated in the next several years. In view of the cost of the competing equipment (from 70–250 US dollars for devices for individual application from firms such as Bayer, LifeScan, Roche/Boerhinger, Medisense to 130 thousand dollars for biosensors from the Affymetrix firm, with the price of one measurement on it being about 250 dollars) and the degree of the universality of the equipment proposed on the market, the optical biosensors under consideration occupy a position that is completely accessible to users based on both the overall cost (25 thousand dollars) and an extremely advantageous price of one measurement (0.5 dollars), not to mention their suitability for the determination of the majority of BACs. We note that an ordinary clinical laboratory assistant will be able to learn now to operate the analytical complex of domestic development in 3–5 days, whereas in the case of foreign polyfunctional analogs, this requires much more extended training. These estimations are valid even to a greater degree for the latest developments, whose main advantages are the long-time stability of gel (film) DNA biosensors, the low price and compactness of the single-wave dichrometer, and the possibility of conducting direct rapid analyses of liquids.

The above features of optical biosensors make them potentially attractive for many groups of users, but most of all they are necessary in those fields where measurements by traditional methods either cannot be made (new tasks) or prove to be too expensive and/or prolonged (the field of mass biochemical analyses, decentralized measurements, 'personified' medicine (including new fields), technological online control, etc.).

The newly developed biosensor analytical systems have already been used in ten biomedical establishments for conducting scientific and applied research, including IMB RAS, for the development of new types of nanobiosensing units based on dsDNA molecules and the analytical procedures with their use, for determining antitumor preparations in patient tissues (in collaboration with the Hertsen Moscow Research Oncological Institute), for controlling the quality of the new-type of carriers of gadolinium for the neutron-trapping therapy of malignant tumors (together with the Institute of Nuclear Research, RAS), for detecting phytogenotoxicants and controlling the quality of phytopreparations (at the VILAR Center of Biomedical Technologies, RAMS), and also at the Institute of Laser and Information Technologies, RAS, at the Semenov Institute of Chemical Physics, RAS, and at the Institute of Theoretical and Experimental Biophysics, RAS.

This work was supported in part by the Presidium of the Russian Academy of Sciences (in the framework of the program for basic research, Fundamental Sciences for Medicine) and by the Federal Agency on Science and Innovations (Federal project Nos 02.512.11.2006 and 02.512.11.2217).

References

1. Yevdokimov Yu M, Sytchev V V *Usp. Khim.* **77** 194 (2008) [*Russ. Chem. Rev.* **77** 193 (2008)]
2. Yevdokimov Yu M et al. *Int. J. Biol. Macromol.* **36** 103 (2005)
3. Star A et al. *Proc. Natl. Acad. Sci. USA* **103** 921 (2006)
4. Hahm J, Lieber C M *Nano Lett.* **4** 51 (2004)
5. Tang X et al. *Nano Lett.* **6** 1632 (2006)
6. Seeman N C *Sci. Am.* **290** (6) 64 (2004)
7. Evdokimov Yu M et al. *Zhidkokristallicheskie Dispersii i Nanokonstruktsii DNK* (Liquid-Crystal Dispersions and DNA Nanoconstructions) (Ed. Yu M Evdokimov) (Moscow: Radiotekhnika, 2008)
8. Goldar A, Thomson H, Seddon J M *J. Phys. Condens. Matter* **20** 035102 (2008)
9. Kompanets O N *Usp. Fiz. Nauk* **174** 686 (2004) [*Phys. Usp.* **47** 630 (2004)]
10. Evdokimov Yu M et al. *Mol. Biol.* **37** 340 (2003) [*Mol. Biol.* **37** 293 (2003)]
11. Evdokimov Yu M et al. *Sensorn. Sistemy* **13** 82 (1999) [*Sensory Syst.* **13** 81 (1999)]
12. Skuridin S G et al. *Tekhnol. Zhiv. Sistem* (3) 3 (2006)
13. Turner A P F, Karube I, Wilson G S (Eds) *Biosensors: Fundamenals and Applications* (Oxford: Oxford Univ. Press, 1987) [Translated into Russian (Moscow: Mir, 1992)]
14. Fonseca V, Guba S C, Fink L M *Endocrine Rev.* **20** 738 (1999)
15. Gusev V M et al. *Al'manakh Klinich. Medits.* **XVII** (2) 308 (2008)
16. Gusev V M et al. *Al'manakh Klinich. Medits.* **XVII** (2) 311 (2008)